INFORMATION TO USERS

This material was produced from a microfilm copy of the original document. While the most advanced technological means to photograph and reproduce this document have been used, the quality is heavily dependent upon the quality of the original submitted.

The following explanation of techniques is provided to help you understand markings or patterns which may appear on this reproduction.

1. The sign or "target" for pages apparently lacking from the document photographed is "Missing Page(s)". If it was possible to obtain the missing page(s) or section, they are spliced into the film along with adjacent pages. This may have necessitated cutting thru an image and duplicating adjacent pages to insure you complete continuity.
2. When an image on the film is obliterated with a large round black mark, it is an indication that the photographer suspected that the copy may have moved during exposure and thus cause a blurred image. You will find a good image of the page in the adjacent frame.
3. When a map, drawing or chart, etc., was part of the material being photographed the photographer followed a definite method in "sectioning" the material. It is customary to begin photoing at the upper left hand corner of a large sheet and to continue photoing from left to right in equal sections with a small overlap. If necessary, sectioning is continued again – beginning below the first row and continuing on until complete.
4. The majority of users indicate that the textual content is of greatest value, however, a somewhat higher quality reproduction could be made from "photographs" if essential to the understanding of the dissertation. Silver prints of "photographs" may be ordered at additional charge by writing the Order Department, giving the catalog number, title, author and specific pages you wish reproduced.
5. PLEASE NOTE: Some pages may have indistinct print. Filmed as received.

Xerox University Microfilms
300 North Zeeb Road
Ann Arbor, Michigan 48106

73-31,478

KALBACK, Walter Martin, 1943-
THE THERMAL DECOMPOSITION OF NITROUS OXIDE
ON GOLD AT ELEVATED PRESSURES.

The University of Oklahoma, Ph.D., 1973
Engineering, chemical

University Microfilms, A XEROX Company, Ann Arbor, Michigan

THE UNIVERSITY OF OKLAHOMA

GRADUATE COLLEGE

THE THERMAL DECOMPOSITION OF NITROUS OXIDE ON GOLD AT ELEVATED PRESSURES

A DISSERTATION

SUBMITTED TO THE GRADUATE FACULTY

in partial fulfillment of the requirements for the

degree of

DOCTOR OF PHILOSOPHY

BY

WALTER MARTIN KALBACK

Norman, Oklahoma

1973

THE THERMAL DECOMPOSITION OF NITROUS OXIDE ON GOLD AT ELEVATED PRESSURES

APPROVED BY

C. M. Sliepcevich

David W. Johnson

K. E. Starling

DISSERTATION COMMITTEE

ABSTRACT

The thermal decomposition of nitrous oxide to nitrogen and oxygen was studied in the pressure range from 2 to 70 atmospheres and a temperature range of 445° to 605°C. Kinetic data were obtained for the reaction in a continuous flow system using a tubular gold-lined reactor. The reactor coil was kept at constant temperature by immersion in a bath of fluidized sand heated with a pressurized propane burner. The burning propane-air mixture served as a heating source and a means for fluidizing the sand in the bath. Residence times varied from 2.6 to 17.4 minutes and product conversions varied from 0.23 to 25.80 percent. Reactor inlet and outlet concentrations were obtained by gas chromatography.

The decomposition reaction on gold was found to occur by simultaneous heterogeneous and homogeneous kinetics. Both the homogeneous and the surface reaction were found to be first-order for the conditions employed in this investigation. Suitable selection of low temperatures in conjunction with pressure provided surface rate constants in the absence of homogeneous effects. Heterogeneous and homogeneous rate constants were determined for each of the temperatures studied.

Activation energies for the heterogeneous and homogeneous reactions compared favorably with those found in the literature.

The unimolecular theories of Kassel, Rice and Ramsperger, and Slater predicting that the unimolecular rate constant should increase with pressure until a high pressure limiting rate constant was reached were found to be inapplicable. The rate constant at high pressures was shown to decrease with increasing pressure after passing through a maximum value. An explanation based upon a modification of the absolute reaction rate theory has been proposed to account for this observed behavior.

ACKNOWLEDGMENTS

The author expresses his grateful appreciation to his advisory committee, Dr. C. M. Sliepcevich, Dr. A. W. Aldag, Dr. S. D. Christian, Dr. D. W. Johnson, Dr. K. E. Starling, and Dr. J. A. Christenson for their interest and assistance provided during this graduate program.

The efforts of Ms. Bobbie Everidge and Mrs. Carlotta Wood who typed the manuscript, and Mr. Steve Presson who handled a portion of the graphical work are greatly appreciated. Thanks is also due to Dr. Jerry Lott, who assisted in the editing of this dissertation, and to Dr. William Talley whose comments and assistance were of value in the analysis of the experimental data.

The author also wishes to thank Gulf Research and Development Company of Pittsburgh, Pennsylvania, for providing two of the chromatographic columns used in this investigation, and Mr. George Williams who prepared these columns.

This investigation was primarily sponsored by the National Science Foundation through a Graduate Traineeship. Additional support was provided by a Texaco, Inc., Fellowship and a grant from University Engineers, Inc.

I also acknowledge the support and assistance of my wife, Faith, through this period of graduate studies.

Walter M. Kalback

TABLE OF CONTENTS

LIST OF TABLES

LIST OF ILLUSTRATIONS

Figure Page

CHAPTER I

INTRODUCTION

The study of the variation of unimolecular rate constants with pressure permits one to test the statistical mechanical theories of kinetics using a class of reactions for which accurate data may be obtained. While the absolute value of the reaction rate cannot be predicted solely from statistical mechanical developments, the fact that these methods can predict the pressure trends of the rate constants is of significant value. Within the general class of unimolecular reactions, there are many materials represented with molecules of varying degrees of complexity. Therefore, in any study of unimolecular reactions it would be advantageous for the investigator to choose a molecule with as little complexity as possible. The results obtained could then be later applied to studies of more complex members of the unimolecular reaction class. A molecule matching this criterion **is** nitrous oxide, which is the simplest molecule capable of undergoing a unimolecular decomposition.

The variation in the rate constant with pressure for the thermal decomposition of nitrous oxide has been rather extensively studied at pressures below and to one atmosphere; only one study exists at significantly higher pressures. The existing low pressure studies have substantiated the theories of Kassel, Rice and Ramsperger, and Slater, which predict a decline in the rate constant with decreasing pressure. The only study of the thermal decomposition of nitrous oxide made at pressures substantially above atmospheric pressure indicated that the value of the rate constant was leveling off with increasing pressure.

The objectives of this investigation were

1. To obtain rate data in the previously unexplored region from 2 to 70 atmospheres pressure.
2. To show the feasibility of using a pressurized flow system in obtaining kinetic data.
3. To determine the effect of gold as a catalyst in the decomposition reaction.
4. To determine the exact behavior of the rate constant at high pressures and thereby obtain an experimental high pressure value for the rate constant.

The reaction study was conducted in a gold-lined, tubular reactor immersed in a constant temperature bath of fluidized sand. Reaction rate data were taken at temperatures ranging from 445°C to 605°C and at pressures from 2 to 70 atmospheres.

CHAPTER II

THEORETICAL BACKGROUND

General Reaction Kinetics Principles

In order to discuss the reaction rate of a particular process, it is necessary to have a clear definition of what is meant by the rate of a reaction. Reaction rate refers to the rate of change with time in the number of moles of a particular component, expressed in terms of unit volume. This definition may be represented by

$$-r_j = \frac{1}{V}\frac{dn_j}{dt} \qquad \text{(II-1)}$$

with n being the number of moles, V representing the system volume, and the subscript j referring to the j^{th} component in the system. Equation II-1 can be applied to both batch and continuous flow processes, although, in this work, we will be concerned only with continuous flow processes. In the batch process, V is a fixed system volume. In a flow process, V is the volume related to a fixed mass, and will usually be a function of time. Generally, the reaction rate may be expressed as

$$r_j = k_c\, f(c_1, c_2, c_3, \ldots, c_n) \qquad \text{(II-2)}$$

or $$r_j = k_a\ f(a_1, a_2, a_3, \ldots, a_n) \qquad \text{(II-3)}$$

with the rate constant k_c expressed in terms of concentrations and k_a expressed in terms of activities. In Equation II-2 the rate constant is multiplied by a function of the individual component concentrations, while in Equation II-3, the rate constant is multiplied by a function of the individual component activities. The rate expression has been presented in terms of concentrations in this investigation.

General Chemical Reaction Theories

Among the earliest contributions to the understanding of the factors which affect the rate of a chemical reaction was the "Law of Mass Action," presented by Guldberg and Waage in 1879. Their law can be related to the following basic equation:

$$A + B \underset{k_r}{\overset{k_f}{\rightleftharpoons}} C + D \qquad \text{(II-4)}$$

where k_f is the forward rate constant and k_r the reverse reaction rate constant. The rate of the forward and reverse reactions can be given by, respectively,

$$r_f = k_f\ [A][B] \qquad \text{(II-5)}$$

$$r_r = k_r\ [C][D] \qquad \text{(II-6)}$$

The bracketed quantities, which are usually interpreted as molar concentrations, were termed "active masses" by Guldberg and Waage. Their law simply states that the rates of reactions of the type expressed by Equations II-5 and II-6 are proportional to the product of the concentrations of the reacting species, with k_f and k_r being the constants of proportionality.

Soon after Guldberg and Waag's concept was presented, another significant advancement in chemical kinetic theory was reported by Arrhenius in 1889. Arrhenius was aware of the van't Hoff relationship between the equilibrium constant K and internal energy change ΔE of a reaction, namely

$$\left(\frac{\partial \ln K}{\partial T}\right)_V = \frac{\Delta E}{RT^2} \qquad \text{(II-7)}$$

Using this relationship together with Guldberg and Waage's expression for the equilibrium constant, $K = k_f/k_r$, the following relationship develops:

$$\left(\frac{\partial \ln k_f}{\partial T}\right)_V - \left(\frac{\partial \ln k_r}{\partial T}\right)_V = \frac{\Delta E}{RT^2} \qquad \text{(II-8)}$$

In Equation II-8, ΔE can be expressed as the difference between the energies of activation of the forward and reverse reactions $(E_o^f - E_o^r)$ as well as the difference between the internal energies of the products and reactants. From a mathematical rearrangement, it follows that

$$\left(\frac{\partial \ln k_f}{\partial T}\right)_V - \frac{E_o^f}{RT^2} = \left(\frac{\partial \ln k_r}{\partial T}\right)_V - \frac{E_o^r}{RT^2} = \alpha \qquad \text{(II-9)}$$

Arrhenius found experimentally that plots of ln k versus 1/T were linear over the temperature ranges studied, so he concluded that the constant α was very small, if not zero. Therefore, Arrhenius developed an integrated form of Equation II-9 for the temperature dependence of the specific rate constant, which was

$$k_c = A \exp(-E_o/RT) \qquad \text{(II-10)}$$

In Equation II-10, k_c is the specific rate constant, E_o is the energy of activation, R the gas constant, T the absolute temperature, and A the temperature-independent constant of integration, usually known as the "frequency factor," but otherwise undefined in the Arrhenius theory.

Arrhenius' most significant contribution to kinetic theory was the definition of the "activated state," but his theory did not provide a detailed concept of the nature of this state. Arrhenius' proposal that an equilibrium exists between ordinary molecules and "activated" molecules which have sufficient energy to react includes two ideas which are fundamental to both the collision theory and the absolute reaction rate theory:

1. Equilibrium between ordinary and activated molecules, and
2. The presence of an activated state.

In the collision theory, the reaction is assumed to occur following a collision of molecules, provided that the reactant molecules possess a certain minimum activation energy,

E_o. The number of collisions occurring per unit time can be approximated by the kinetic theory equation for collision between a pair of molecules, A and B.

$$N = c_A \, c_B \, \sigma_{AB}{}^2 \sqrt{\frac{8\pi RT(M_A + M_B)}{M_A M_B}} \qquad \text{(II-11)}$$

with M_A and M_B the respective molecular weights, R the gas constant, T the absolute temperature, and $\sigma_{AB}{}^2$ the effective collision diameter.

At ambient temperatures and atmospheric pressure, N is a very large number on the order of 10^{28}/ml-sec. However, since reactions do not occur this fast, not every collision is capable of producing a reaction. It is assumed, therefore, that only molecules possessing a certain minimum amount of energy, E_o, are capable of reacting upon collision. The fraction of molecules that possess an energy in excess of E_o is given by the expression:

$$f(E_o) = \exp(-E_o/RT) \qquad \text{(II-12)}$$

The specific reaction rate can then be determined from the product of the number of collisions per unit time and the fraction of these collisions with energy in excess of E_o. This rate is

$$r = f(E_o) \, N \qquad \text{(II-13)}$$

Substituting Equation II-12 for $f(E_o)$ gives

$$r = N \exp(-E_o/RT) \qquad \text{(II-14)}$$

This expression is somewhat simplified but it is useful for predicting the reaction rate of simple molecules.

The transition state theory assumes that reaction occurs when an "activated complex" capable of reacting ultimately decomposes into products. It is assumed that an equilibrium exists between the activated complex and the reactants and products, as

$$A + B \rightleftarrows X^{\neq} \longrightarrow C + D \qquad \text{(II-15)}$$

where $X^{\neq}$ is the activated complex. Using this assumption and a detailed statistical mechanical development, the specific reaction rate constant can be represented by the following:

$$k = \eta \frac{k_B T}{h} K_C^{*} = \eta \frac{k_B T}{h} \left[\frac{F_x^{\neq}}{F_A F_B}\right] \exp(-E_o/RT) \qquad \text{(II-16)}$$

where k_B = Boltzman constant

h = Plank's constant

K_C^{*} = equilibrium constant for the reactants and activated complex in terms of concentrations

$F_x^{\neq}$ = partition function for the activated complex with one vibrational degree of freedom removed

F_A, F_B = partition functions of A and B

η = transmission coefficient

The transmission coefficient in Equation II-16 is used to account for the fact that, in many reactions, not every activated molecule becomes a product.

Unimolecular Reaction Theories

Unimolecular reactions are a class of reactions which proceed through a transition state consisting of a single, activated molecule. The reactant molecule has gained the necessary energy of activation by collisions with other molecules. Unimolecular reactions may either be isomerizations or decompositions. Most decompositions, of which the decomposition of nitrous oxide is an example, do not occur in a single step but by a series of steps making up the mechanism; the first step, however, is generally a unimolecular decomposition.

When first discovered, unimolecular reactions were not at all understood. The first-order behavior at certain pressures could not be explained using a second-order collision process. In 1919, Perrin (48) tried to show that the activation was caused by absorption of a given quantity of radiation. His theory was discredited when later experimental work showed that many unimolecular reactions became second-order at low pressures. In 1922, Lindemann (42) proposed a mechanism for unimolecular reactions which was compatible with both experimental results and collision theory. His theory is the basis of all modern theories of unimolecular reactions, although a number of important modifications have been made to it.

According to Lindemann's theory, reactant molecules may receive energy by collisions, whereby the molecules possess energy in excess of that needed for reaction. The energy gained by a reactant molecule is attained at the expense of its collision partner, which may be another like reactant molecule or any inert foreign molecule. A reactant molecule that contains sufficient energy to enable it to become a product molecule without the necessity of acquiring any additional energy is said to be energized. If the conversion of energized molecules into products is slow compared to the rate at which they are deenergized by collision, an equilibrium concentration of the energized molecules will be built up and their concentration will be proportional to the concentration of the reactant molecules. The rate of reaction will be proportional to the concentration of energized molecules, and consequently, will also be proportional to the concentration of reactant molecules. The reaction would be considered first-order. At sufficiently low pressures, by contrast, the collisions cannot maintain a sufficient supply of energized molecules. The rate of the reaction then depends upon the rate of energization, and is therefore proportional to the square of the concentration of reacting molecules, which is a second-order reaction.

The mechanism for the Lindemann theory can be expressed as

$$A + A \xrightarrow{k_1} A^* + A \qquad \text{(II-17)}$$

$$A + A^* \xrightarrow{k_{-1}} A + A \qquad \text{(II-18)}$$

$$A^* \xrightarrow{k_2} B \text{ (products)} \qquad \text{(II-19)}$$

with A representing a normal reactant molecule and A* an energized molecule. Application of a steady-state analysis to [A*] produces the equation

$$d[A^*]/dt = k_1[A]^2 - k_{-1}[A^*][A] - k_2[A^*] = 0 \qquad \text{(II-20)}$$

Since the net rate of reaction is:

$$r_A = k_2[A^*] \qquad \text{(II-21)}$$

the quantity [A*] may be eliminated from Equations II-20 and II-21 to give the following expression in terms of [A] alone:

$$r_A = \frac{k_1 k_2 \; [A]^2}{k_2 + k_{-1}[A]} \qquad \text{(II-22)}$$

At sufficiently high pressures, $k_{-1}[A] >> k_2$, and the rate may be expressed by

$$r_A + \frac{k_1 k_2}{k_{-1}} [A] = k^\infty [A] \qquad \text{(II-23)}$$

This reaction is seen to be first-order. The term k^∞ has traditionally been defined as the first-order rate constant at high pressures. At low pressures, on the other hand, $k_{-1}[A] << k_2$, and $k_{-1}[A]$ can be neglected. The rate equation then reduces to

$$r_A = k_1[A]^2 \qquad \text{(II-24)}$$

so that the reaction is now second-order.

Lindemann's theory gives a satisfactory qualitative interpretation of unimolecular reactions, but quantitatively it is not completely satisfactory. This shortcoming may be seen in the following development.

A first-order rate coefficient k^1 may be given by the equation

$$r_A = k^1[A] \tag{II-25}$$

Equations II-22 and II-25 produce the following

$$k^1 = \frac{k^\infty}{1 + k_2/k_{-1}[A]} \tag{II-26}$$

A plot of k^1 against [A] (or against pressure) gives a curve of the form shown in Figure 1. It is apparent that the coefficient k^1 is constant in the higher pressure region, but falls to zero at lower pressures. From the relationship of the rate constants, it can be shown that the concentration $[A]_{1/2}$ at which k^1 should become equal to $k^\infty/2$ is given by k^∞/k_1. The value of k^∞, the first-order rate constant at high pressures, can be found from experiments if data are taken at high enough pressures. According to the simple collision theory, k_1 should be equal to $Z_1e^{-E_o/RT}$, where E_o is the energy of activation. In all observed cases, the procedure given above for testing the Lindemann theory leads to the prediction that the first-order rate constant should fall off at a much higher pressure than is actually observed. If one can obtain an

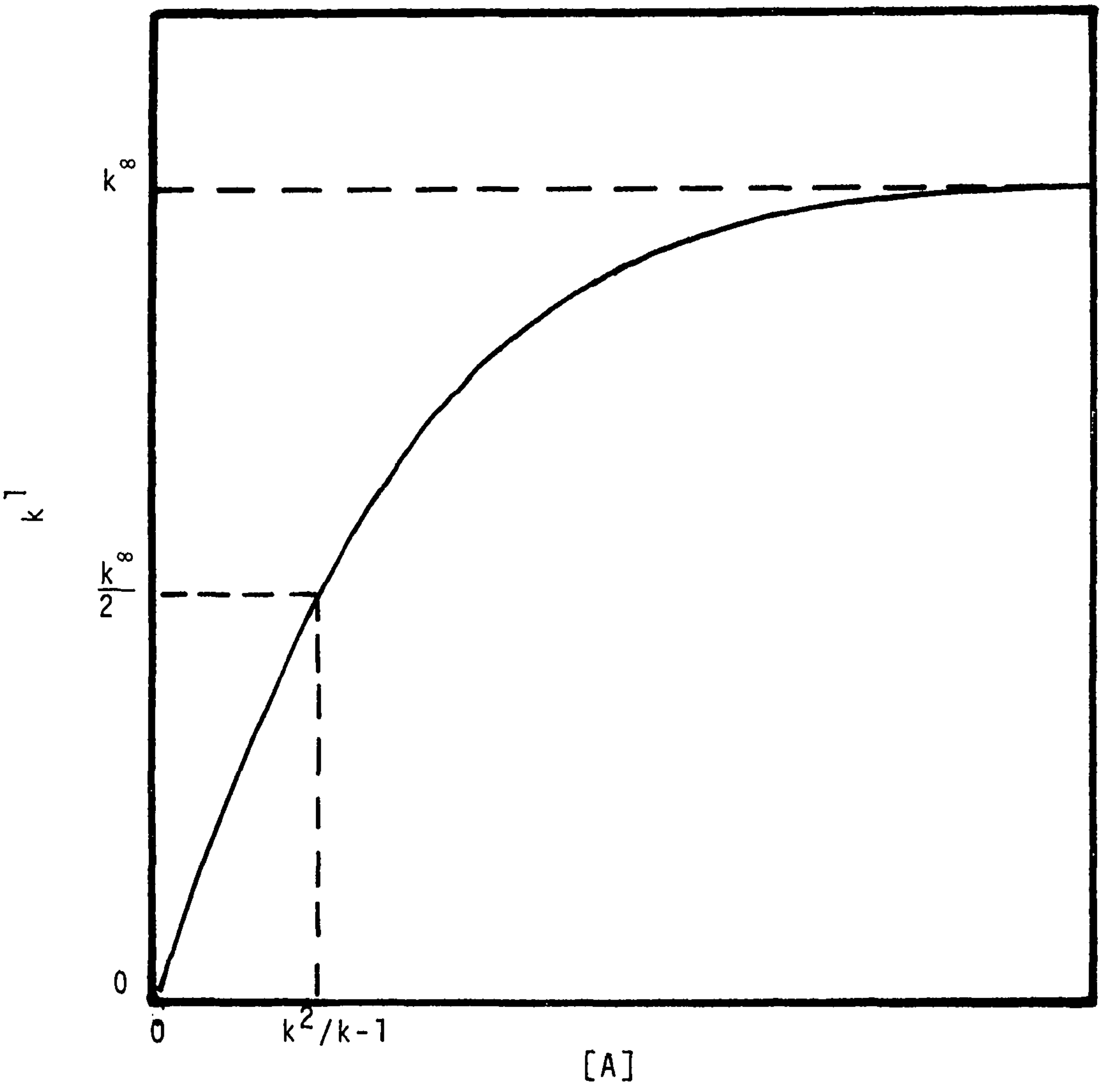

Figure 1. First-Order Specific Rate Constant as a Function of Concentration.

experimental value for k^{∞} at sufficiently high pressures, then the error present must therefore be in the estimation of k_1. Thus, it becomes necessary for the collision theory to be modified in such a manner as to give larger values for k_1.

Another difficulty with the Lindemann theory becomes apparent from consideration of a second point of view. Equation II-26 may be written as

$$\frac{1}{k^1} = \frac{k_{-1}}{k_1 k_2} + \frac{1}{k_1 [A]} \qquad \text{(II-27)}$$

and a plot of $1/k^1$ against the reciprocal of the concentration should give a straight line. However, for many substances, deviations from linearity are found of the type shown schematically in Figure 2.

An explanation for the fact that the first-order rates are maintained down to lower concentrations than those permitted by the Lindemann theory was first given by Hinshelwood (25) in 1927. The basis of his modification to the earlier Lindemann theory is that the rate constant for the energization process, k_1, may be much greater for a complex molecule than for a simple molecule. This fact is possible because the energy possessed by a complex molecule may be distributed among a considerable number of degrees of vibrational freedom.

Using a statistical mechanical treatment, Hinshelwood derived an expression for k_1. If the collision frequency corresponding to k_2 is written as Z_2, the expression for k_1 is

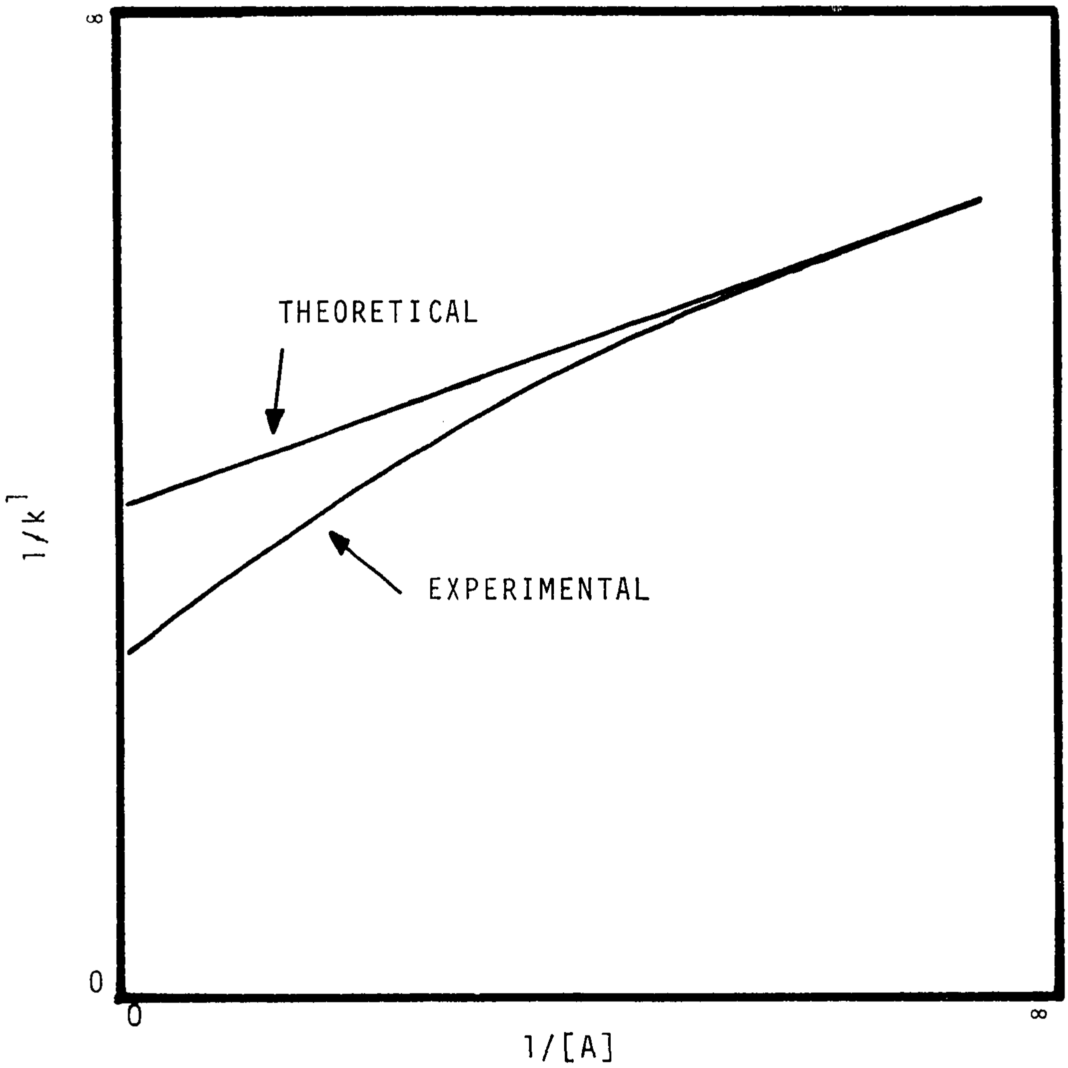

Figure 2. Reciprocal First-Order Rate Constant as a Function of Reciprocal Concentration.

$$k_1 = Z_2 \frac{1}{(s-1)!} \left(\frac{\varepsilon^*}{k_B T}\right)^{s-1} e^{-\varepsilon^*/k_B T} \qquad \text{(II-28)}$$

which can be compared to the expression

$$k_1 = Z_1 \, e^{-\varepsilon^*/k_B T} \qquad \text{(II-29)}$$

In Equation II-28, s equals the number of individual degrees of freedom and ε^* is the minimum energy that the molecule must possess in order for it to decompose into products. Equation II-29 is the expression originally developed on the basis of the simple collision theory. In employing Equation II-28, one must note that, whereas in Equation II-29, the quantity ε^* is the experimental energy of activation per molecule, the ε^* in Equation II-28 differs from the experimental value ε_{exp} by the following

$$\varepsilon^* = \varepsilon_{exp} + (s + 3/2)\, k_B T \qquad \text{(II-30)}$$

The Hinshelwood theory will predict that the first-order rate constant will begin to fall off at pressures lower than those predicted by the Lindemann theory. In practice, s is usually found by trial and error, and it is usually possible to explain the results using a value of s that is equal to, or less than, the total number of normal modes of vibration in the molecule. Usually, s is found to be about one-half the total number of normal modes, possibly because of the fact that the energy required for activation comes from only a portion of the total normal modes and not from all of them.

Hinshelwood's treatment, and the other modifications to Lindemann's theory that follow, are to be considered in terms of the following scheme of reactions

$$A + A \underset{k_{-1}}{\overset{k_1}{\rightleftharpoons}} A^* + A \qquad \text{(II-31)}$$

$$A^* \xrightarrow{k_3} A^{\neq} \qquad \text{(II-32)}$$

$$A^{\neq} \xrightarrow{k^{\neq}} B \text{ (products)} \qquad \text{(II-33)}$$

At this point, a distinction is made between an activated complex, represented by the symbol $A^{\neq}$, and an energized molecule, represented by A^*. The activated complex is such that it will pass smoothly into the product state. An energized molecule is one that has sufficient energy to become an activated molecule without acquiring additional energy. However, it must undergo vibrational changes before it can become an activated complex, where energy has become localized in the particular bond or bonds that are to be broken during the reaction. According to the Hinshelwood treatment, the molecules may be energized much more readily than was predicted by the simple collision theory. However, a long period of time may elapse before the energized molecule becomes an activated molecule. Hinshelwood's theory predicts a very large value for k_1, and k_3 is correspondingly low to compensate for this fact. The theories presented below also postulate a large value for k_1, but they consider that k_3 becomes larger with an increase in the amount of energy that is possessed by the energized molecule. The theories of Rice and Ramsperger and of Kassel (RRK), on the one hand, and of Slater (S), on the other, represent two alternative ways of attacking this problem.

In order to explain the fall-off in reaction rate with a decrease in pressure, Rice and Ramsperger (53) in 1927 and Kassel (35) in 1928 modified and improved the Hinshelwood theory. The statistical RRK theory is based on the assumption that k_3 will be a function of the energy possessed by the energized molecule A*. According to this theory, a molecule is assumed to be a system of loosely coupled oscillators; these oscillators are conveniently thought to be equivalent to the normal modes of vibration of the molecule. Alternatively, they may be regarded as individual vibrating bonds. The postulate that the oscillators are loosely coupled is introduced in order to allow a flow of energy between the normal modes without destroying the separateness of the normal modes in the process. The oscillators are regarded as all having the same frequency of vibration.

In the RRK theories the rate constant k_3 for the decomposition of the active molecule is regarded as increasing with the energy possessed by the molecule in its various degrees of freedom. The larger the energy possessed by the energized molecule, the greater is the chance that this energy can pass into the bond that is to be broken and the greater, therefore, is the rate of decomposition.

After a lengthy statistical mechanical derivation which can be found in detail in Rice and Ramsperger's, and Kassel's papers, the expression for the high pressure, first-order rate constant becomes

$$k^{\infty} = k^{\neq} e^{-\varepsilon^{*}/k_BT} \tag{II-34}$$

with $k^{\neq}$ being the rate constant corresponding to the free passage of the reacting system over the potential-energy barrier. This equation can be compared with the usual Arrhenius expression for a rate constant, which is

$$k = A\, e^{-\varepsilon^{*}/k_BT} \tag{II-35}$$

with A equal to the frequency factor. The RRK theory does not predict the magnitude of $k^{\neq}$, but it is presumably of the order of the vibrational frequency. The equation from the activated complex theory would predict that frequency factors of first-order reactions should be of the order of k_BT/h, that is, of the order of 10^{13} at ambient temperatures. The RRK theories have general agreement with this value, but there are several exceptions, nitrous oxide being one of these.

An important aspect of the Kassel theory is the manner in which it predicts the variation of k^1 with the pressure of the reacting gas. Kassel has shown that the rate constant k^1 can be represented by the expression

$$k^1 = \frac{k^{\neq}\, e^{-\varepsilon^*/k_BT}}{(s-1)!} \int_0^{\infty} \frac{x^{s-1}\, e^{-x}\, dx}{1 + (k^{\neq}/k_2[A])\,(x/[b+x])^{s-1}} \qquad \text{(II-36)}$$

with $x = (\varepsilon - \varepsilon^*)/k_BT$ and $b = \varepsilon^*/k_BT$ (II-37)

The quantity x represents the energy imparted to the molecule in excess of that required for energization. With the use of the expression for the high pressure rate constant, Equation II-34, the ratio between the first-order rate constant at any pressure and the high pressure rate constant may be written as

$$\frac{k^1}{k^{\infty}} = \frac{1}{(s-1)!} \int_0^{\infty} \frac{x^{s-1}\, e^{-x}\, dx}{1 + (k^{\neq}/k_2[A])\,(x/[b+x])^{s-1}} \qquad \text{(II-38)}$$

The integral in Equation II-38, for a fixed value of s, corresponds to a particular variation with the concentration of A. In order to test the theory, the usual procedure is to see what value of s will predict the observed variation of k^1 with the pressure. The value of s that is generally required corresponds to about one-half the total number of normal modes in the molecule. The nitrous oxide decomposition reaction has been studied with reference to the Kassel theory and the results will be presented in a subsequent chapter.

In the treatments of Kassel and of Rice and Ramsperger, the only condition for energization is that the molecule must acquire the critical amount of energy ε^*; any molecule that has acquired this energy will, unless it is deenergized by subsequent collisions, pass through the activated state into products. This concept involves the assumption that the energy "flows" or exchanges freely between the normal modes of vibration. The frequency $k^{\neq}$ that appears in the above expressions is really the frequency of such energy redistributions.

Marcus (43) has developed what is essentially a quantum-mechanical formulation of the RRK theories. In the RRKM theory, zero-point energies, for example, are taken into account. The results of his treatment of the nitrous oxide data will be shown later.

An alternative explanation of the fall-off in reaction rate with a decrease in pressure has been developed by Slater (54). Slater's theory is purely a dynamical one, and takes explicit account of the vibrations of the reacting molecules. In the RRK and RRKM theories, it is assumed that energy flows freely between the normal modes during the course of vibration. Slater does not permit energy to flow between normal modes. He regards the reaction as occurring when a critical coordinate (a bond length) becomes extended to a specific extent. Such an extension occurs when different normal modes of vibration come into phase. Slater's theory involves a detailed treatment of molecular vibrations, and for it to be applied to the decomposition of an actual molecule, a complete vibrational analysis of the molecule must be made. In practice, Slater's assumption of no energy flow does not appear to be realistic, and a modification of the theory is required. However, Slater's picture of reaction occurring when a coordinate becomes critically extended does seem to be a very realistic concept.

A rather lengthy vibrational analysis gives Slater's expression for the high pressure first-order rate constant as

$$k^{\infty} = \bar{\nu}\, e^{-\varepsilon^{*}/k_B T} \tag{II-39}$$

$\bar{\nu}$, the average frequency, is defined by

$$\bar{\nu} = (\Sigma\, \mu_m^{\,2}\, \nu_m^{\,2})^{1/2} \tag{II-40}$$

where the ν_m are the frequencies of all the normal modes of vibration in the molecule and the μ_m are the normalized amplitude factors defined by the equation

$$\mu_1 = \frac{\alpha 1}{(\Sigma\, \alpha_m^{\,2})^{1/2}},\ \text{etc.} \tag{II-41}$$

The amplitude factors represent the contribution of a given amount of energy in a particular mode of vibration to the extension of the critical coordinate in question.

The physical significance of $\bar{\nu}$ is that it is the frequency of the molecule in which all the atoms have been removed except those related to the critical coordinate q. If q is a simple bond, then it is the frequency of the diatomic molecule.

Slater developed the general rate equation for the first-order rate constant, which is given by

$$k^1 = \frac{\bar{\nu}\, e^{-\varepsilon^*/k_B T}}{\Gamma\,(1/2\ n + 1/2)} \int_0^\infty \frac{x^{(n-1)/2}\, e^{-x}\, dx}{1 + x^{(n-1)/2}\, \theta^{-1}} \qquad \text{(II-42)}$$

where

$$x = \frac{(\varepsilon - \varepsilon^*)}{k_B T} \qquad \text{(II-43)}$$

θ is defined by

$$\theta = \frac{Z_1\,[A]}{\bar{\nu}} \left(\frac{\varepsilon^*}{k_B T}\, 4\pi\right)^{(n-1)/2} \Gamma\,(1/2\ n + 1/2)\ \mu_1\ \mu_2\ \cdots\ \mu_n \qquad \text{(II-44)}$$

It follows from Equations II-39 and II-42 that the ratio between the first-order and high pressure rate constants may be expressed as

$$\frac{k^1}{k^\infty} = \frac{1}{\Gamma(1/2\ n + 1/2)} \int_0^\infty \frac{x^{(n-1)/2}\, e^{-x}\, dx}{1 + x^{(n-1)/2}\, \theta^{-1}} \qquad \text{(II-45)}$$

The integral can be evaluated by numerical integration for various values of n.

Slater's treatment is of considerable interest because of his concept of a critical coordinate for reaction, but it appears that his initial assumption of no energy flow is unrealistic. Various attempts have been made to develop a treatment along similar lines to Slater's but without his no-energy flow assumption. Gill and Laidler (17) recently proposed a modified reaction mechanism for unimolecular reactions which makes a distinction between two types of energized molecules. The reaction scheme proposed by Gill and Laidler may be expressed as

$$A + A \underset{k_{-1}^{(H)}}{\overset{k_1^{(H)}}{\rightleftarrows}} A' + A \qquad \text{(II-46)}$$

$$A + A \underset{k_{-1}^{(S)}}{\overset{k_1^{(S)}}{\rightleftarrows}} A^* + A \qquad \text{(II-47)}$$

$$A' + A \underset{k_{-s}}{\overset{k_s}{\rightleftarrows}} A^* + A \qquad \text{(II-48)}$$

$$A^* + A \xrightarrow{k_2^{(S)}} A^{\neq} \qquad \text{(II-49)}$$

$$A^{\neq} \xrightarrow{k_3} P \text{ (products)} \qquad \text{(II-50)}$$

In this mechanism, a distinction is made between two types of energized molecules, represented by A' and A*. The A* molecules are those that are energized according to the Slater concept; they contain ε^* or more energy and have it distributed among the normal modes in such a manner that, when the vibrations become correctly in phase with each other, there can be a sufficient extension of the critical coordinate. The A' molecules are those that contain the critical energy ε^*, but do not have it distributed in such a way for reaction to occur without flow of energy. The energization rate constant $k_1^{(H)}$ is much larger than $k_1^{(S)}$, since Slater's condition is a more demanding one than the RRK condition.

If there is no flow of energy possible between the modes, the rate constants k_s and k_{-s} are equal to zero, and the reaction can only occur by direct energization to A*. This fact would mean that Slater's treatment is applicable. If, however, k_s is not negligible, as seems to be the true situation, A* can be formed from A' as well as directly. At very low pressures, most of the A* will probably be formed from A', since A' may be formed from A + A much more rapidly than A*. Also, practically every A' formed will eventually become an A*. At intermediate pressures, on the other hand, more of the A* may be produced directly from A + A, so Slater's treatment should be more correct. On the basis of Gill and Laidler's proposed mechanism, three regions of kinetic behavior may be expected.

1. A high pressure region where the kinetics will be first-order. Both A' and A* will be essentially at equilibrium, and the rate of reaction will be controlled by the breakdown of A*. In this region the RRK and Slater theories should be in agreement.
2. An intermediate pressure region where there is predominantly a direct energization to form A*. Slater's treatment may be applicable.
3. A low pressure region where A* will be formed predominantly from A', and the RRK treatment will be applicable.

In some cases, when k_s is sufficiently large, the intermediate pressure region noted above may effectively disappear. This disappearance has apparently been found to be the case with the H_2O_2, C_2H_6, and N_2O molecules.

If a steady-state analysis is applied to the reaction scheme of Gill and Laidler, the following expression for the rate of reaction results

$$r = \frac{k_2^{(S)}[A]^2 \left\{k_1^{(S)} k_{-1}^{(H)}[A] + k_s(k_1^{(S)} + k_1^{(H)})\right\}}{k_{-1}^{(H)}[A]\left(k_{-1}^{(S)}[A] + k_2^{(S)}\right) + \left(k_s k_{-1}^{(S)} + k_{-s}k_{-1}^{(H)}\right)[A] + k_s k_2^{(S)}} \qquad \text{(II-51)}$$

For nitrous oxide, the value of k_s can be assumed to be rather large. Also, the rate constant $k_1^{(S)}$ will generally be considerably smaller than $k_1^{(H)}$, since Slater's condition for energization is a more demanding one than the RRK condition. Taking these considerations into account, for very low pressures, Equation II-51 reduces to the form

$$r = \frac{k_s k_1^{(H)} k_2^{(S)} [A]^2}{k_s k_2^{(S)}} = k_1^{(H)} [A]^2 \qquad \text{(II-52)}$$

Thus, at low pressures, the reaction rate should be given by the RRK formula for energization. At very high pressures, Equation II-51 reduces to the form

$$r = \frac{k_2^{(S)} k_1^{(S)}}{k_{-1}^{(S)}} [A] \qquad \text{(II-53)}$$

Therefore, Slater's expression for the high pressure rate is shown to apply even if, in this case, k_s is very large.

From existing experimental data, it has been observed that there appears to be a more rapid energy flow between different normal modes in the N_2O, H_2O_2, and C_2H_6 molecules than in the N_2O_5 and C_2H_5Cl molecules. These results suggest that energy flow can occur more readily between a smaller number of normal modes than between a larger number. If a given amount of energy is distributed among a small number of normal modes, then the average amount in each mode may be sufficiently large that there is a significant amount of coupling occurring. Energy may then flow quite easily between the modes, and the RRK concept for energization should apply. However, if the number of modes is large, then each vibration will be occurring primarily in the harmonic region. There will be little coupling present, and reaction will only occur if the vibrations come correctly into phase. This mode of behavior was the concept advanced by Slater.

Effect of Temperature on the Rate Constant

The variation of the specific rate constant with temperature has been adequately described by the Arrhenius equation

$$k = A \exp (-E_o/RT) \qquad \text{(II-54)}$$

If this expression is differentiated with respect to temperature, one obtains

$$\frac{\partial k}{\partial T} = kE_o/RT^2 \qquad \text{(II-55)}$$

or

$$\frac{\partial \ln (k)}{\partial (1/T)} = -E_o/R \qquad \text{(II-56)}$$

The Arrhenius equation can be graphically represented by plotting ln (k) against the reciprocal of the absolute temperature. A straight line is obtianed with slope equal to $-E_o/R$. It should be mentioned here that the so-called "infinite pressure" rate constant, k^∞, can also be adequately represented by the Arrhenius equation.

Effect of Pressure on the Rate Constant

As shown earlier in this chapter, the effect of pressure on the specific rate constant can be determined by using the unimolecular theories attributable either to Rice, Ramsperger, and Kassel (RRK) or Slater (S). In both cases, a general decrease in the rate constant with a decrease in pressure is observed. While this behavior has been frequently verified at pressures near or below one atmosphere, some evidence exists that these theories are inadequate in determining the relationship between the rate constant and pressure at sufficiently high pressures.

In the theoretical development presented by Kassel, the pressure dependency was thought to result from the inability of the reaction system to maintain equilibrium between activated molecules and reactant molecules. This aspect of the theory has been adequately verified at low pressures by experimental observations covering a wide variety of unimolecular reactions. At high pressures, however, the reaction system would be expected to change from a system of ideal gases to a system of real, nonideal gases. The effects of nonideality have not been considered in the previous developments represented by the Kassel and Slater theories.

To account for high pressure rate constant deviations in their experimental studies with cyclopropane, Pipkin (49) and Johnson (31) developed a new expression based upon the absolute reaction rate theory, but with a new interpretation given to the transmission coefficient. The highlights of their development will be presented below. In the past, the transmission coefficient has generally been considered to be a probability factor which relates the number of activated species which become products to that number which are proceeding toward the product state. Using this interpretation, it is obvious that the transmission coefficient is not a function of pressure and, therefore, the absolute reaction rate theory cannot predict the experimentally observed decline in the rate constant with pressure at low pressures that is characteristic of unimolecular reactions. However, if the transmission coefficient is defined to be the ratio between the number of activated molecules at some pressure, p, and the equilibrium number of activated molecules present at some very high pressure, then the transmission coefficient can be considered to be pressure dependent. As indicated previously, the classical unimolecular theories of Kassel, et al., make an assumption of the rate constant ratio between a particular pressure and a so-called "infinite" pressure. Thus, Equation II-38 represents the transmission coefficient. The equation representing the absolute reaction rate theory then becomes

$$k = I(T,P) \frac{k_B T}{h} K^* \qquad \text{(II-57)}$$

with I(T,P) defined as the right-hand side of Equation II-38 and the other terms identical to those in Equation II-16.

Taking the logarithm of Equation II-57 and differentiating with respect to pressure at constant temperature produces

$$\left[\frac{\partial \ln k}{\partial P}\right]_T = \left[\frac{\partial \ln I(T,P)}{\partial P}\right]_T + \left[\frac{\partial \ln K^*}{\partial P}\right]_T \qquad \text{(II-58)}$$

Now, K^* can be expressed as

$$K^* = \frac{x^*}{x_A} \qquad \text{(II-59)}$$

and applying the Lewis and Randall fugacity rule to Equation II-59 gives

$$K_f^* = \frac{x^* f^*}{x_A f_A} \qquad \text{(II-60)}$$

with K_f^* being the pressure independent, equilibrium constant in terms of fugacities, f^* the fugacity of the activated species, and f_A the fugacity of the reactant. Thus

$$K_f^* = K^* \frac{f^*}{f_A} \qquad \text{(II-61)}$$

or

$$K^* = K_f^* \frac{fA}{f^*} \qquad \text{(II-62)}$$

The fugacity coefficient, f, at a given temperature is

$$RT\ d(\ln f) = \overline{V}\ dP \qquad \text{(II-63)}$$

with $\overline{V}$ being the molar volume. Substitution of Equations II-62 and II-63 into Equation II-58 together with some simplification produces

$$\left[\frac{\partial \ln k}{\partial P}\right]_T = \left[\frac{\partial \ln I(T,P)}{\partial P}\right]_T - \frac{\overline{V}^* - \overline{V}_A}{RT} \qquad \text{(II-64)}$$

with $\overline{V}^*$ the molar volume of the activated complex and $\overline{V}_A$ the molar volume of the reactant.

The classical unimolecular theories of Kassel, Rice and Ramsperger, and Slater assume that the effect of pressure on the rate constant is due to a displacement of the activated species from equilibrium, and that there is no difference in compressibility between the activated species and the reactant. In these theories the specific rate constant at any pressure was given by

$$k = k^{\infty}\ I(T,P) \qquad \text{(II-65)}$$

Taking the logarithm of both sides of Equation II-65 and differentiating with respect to pressure at constant temperature produces

$$\left[\frac{\partial \ln k}{\partial P}\right]_T = \left[\frac{\partial \ln I(T,P)}{\partial P}\right]_T \qquad \text{(II-66)}$$

Thus, the classical equation which relates the rate constant to pressure resembles Equation II-64 except for the omission of the second term. Since the development of the classical theories never included the possible effects of nonideal behavior, the additional term that is the difference between Equations II-64 and II-66 did not appear in the development of the expressions for either the RRK theory or the Slater theory.

The term $[\partial \ln I(T,P)/\partial P]_T$ can be determined by numerical differentiation of values obtained from Equation II-38. The numerical value of this term will decrease rapidly with increasing pressure, becoming very small at pressures above 30 atmospheres. The term $(\overline{V}^* - \overline{V}_A)/RT$ can usually only be roughly estimated since values of $\overline{V}^*$, the molar volume of the activated complex, are not known. However, it is reasonable to assume that since the activated complex is similar to the reactant, except for the stretching of a critical bond, its molar volume is slightly greater than that of the reactant. The value of this term should be a small positive number which increases slowly with increasing pressure.

At low pressures, the first term in Equation II-58 will be much larger than the second term and the rate constant will increase with increasing pressure. At sufficiently high pressures, the second term should predominate since the first term will be near zero, and the rate constant will decrease with increasing pressure. At some pressure, the rate constant will achieve a maximum value when the two terms in Equation II-58 cancel and the quantity $[\partial \ln k/\partial P]_T$ becomes zero. The application of Equation II-58 to the data from this investigation and the implications derived therefrom will be discussed in Chapter IX.

Effect of Pressure on the Activation Energy

The effect of pressure on the activation energy, E_o, can be determined by first considering the differentiated form of the Arrhenius equation.

$$\frac{d \ln(k)}{d\ (1/T)} = -\frac{E_o}{R} \qquad \text{(II-67)}$$

or

$$E_o = -\frac{R\ d \ln(k)}{d\ (1/t)} \qquad \text{(II-68)}$$

It was earlier established that

$$k^1 = k^\infty\ [I(T,P)] \qquad \text{(II-69)}$$

with [I(T,P)] representing the right-hand side of Equation II-38. Substituting Equation II-69 into Equation II-68 gives

$$E_o = -\frac{R\ d \ln(k^\infty)}{d\ (1/T)} - \frac{R\ d \ln[I(T,P)]}{d\ (1/T)} \qquad \text{(II-70)}$$

This equation then becomes

$$E_o = E^{\infty} - \frac{R\ d\ \ln[I(T,P)]}{d\ (1/T)} \qquad \text{(II-71)}$$

where E^{∞}, the so-called "infinite pressure" activation energy, is defined by

$$k^{\infty} = A^{\infty} \exp\ (-E^{\infty}/RT) \qquad \text{(II-72)}$$

CHAPTER III

REVIEW OF PREVIOUS WORK

Experimental Data Applied to Unimolecular Reaction Theories

The data on the decomposition of nitrous oxide available for application to the various unimolecular reaction theories are rather sparse. Most previous studies simply did not cover a wide enough range in pressure for the data to be useful in testing the various theories. The data from a few studies reporting pressures above one atmosphere are the ones being used in the subsequent discussion. A plot of the first-order rate constant, k^1, versus pressure for nitrous oxide is given in Figure 3. The experimental values were taken by Hunter (29) in 1934 and were subsequently corrected by Johnston (33) in 1951 to account for the heterogeneous reaction occurring on the glass vessel. The data represent a temperature of 888°K and a pressure range up to 38 atmospheres, and are the best "high pressure" data available to date. Other data were taken by Hunter at temperatures of 918° and 931°K at pressures up to 12 atmospheres, and by Nagasako and Volmer (45) at a temperature of 938°K and pressures to 11 atmospheres.

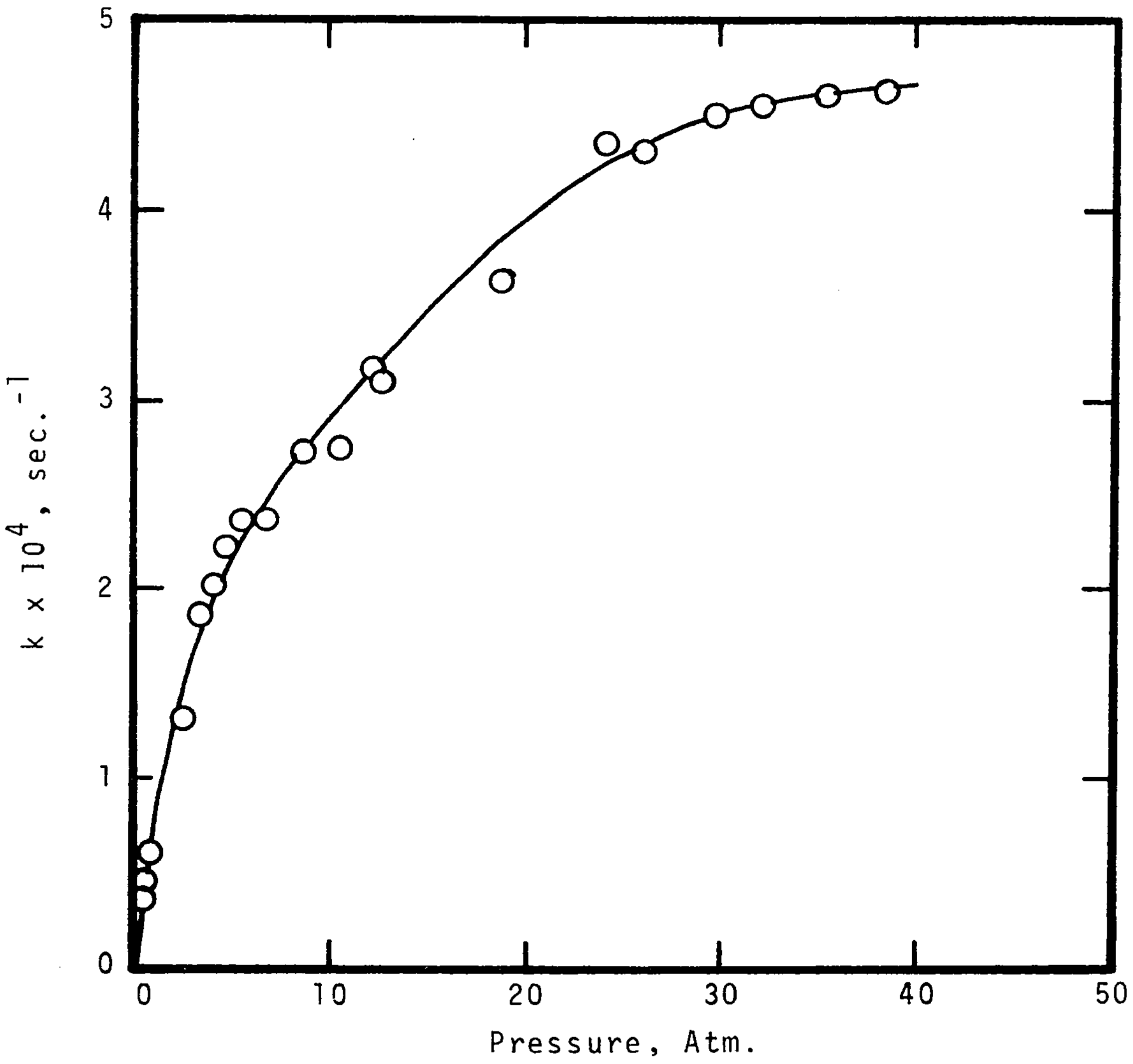

Figure 3. Hunter's Rate Constants at 888°K.

All existing "high pressure" data are shown in Tables 1, 2, and 3 along with the corrections proposed by Johnston. Since the pressure range of these last studies was only to about 12 atmospheres, they are not useful in testing the Lindemann theory or other unimolecular theories over the required large pressure range.

Johnston (33) made a correction in Hunter's data to account for heterogeneity due to the quartz glass reaction vessel which Hunter used in his investigation. This correction was based upon Johnston's observation of finite intercepts on plots of the rate constant against the concentration of nitrous oxide, which indicated a first-order heterogeneous reaction of low activation energy. Johnston's value of the high pressure activation energy of the reaction was taken to be close to 61 kcal. At a temperature of 888°K, the high pressure first-order rate constant was calculated to be $k^{\infty} = 7.47 \times 10^{-4}$ sec^{-1}. This value corresponds to a frequency factor of 8.13×10^{11} sec^{-1}. The calculated k^{∞} value appears to be too large when one observes the shape of the k^{1} versus pressure curve for Hunter's data in Figure 3. The curve appears to be leveling off at a lower value of k^{∞} than 7.47×10^{-4} sec^{-1}.

According to the Lindemann theory, a plot of $1/k^{1}$ against the reciprocal of the concentration should give a straight line. Deviations from linearity have been found,

TABLE 1

PREVIOUS EXPERIMENTAL PRESSURE DATA
HUNTER'S RESULTS AT 888°K

Pressure, Atm.	$k \times 10^4$, sec^{-1}	Johnston's correction $\times 10^4$	Corrected $k \times 10^4$
0.35	0.501	0.150	0.351
0.44	0.608	0.150	0.458
0.52	0.726	0.150	0.576
2.36	1.439	0.150	1.289
3.29	1.986	0.150	1.836
3.84	2.152	0.150	2.002
4.50	2.333	0.150	2.183
5.35	2.444	0.150	2.294
6.54	2.432	0.150	2.282
8.41	2.858	0.150	2.708
10.28	2.870	0.150	2.720
12.09	3.311	0.150	3.161
12.42	3.264	0.150	3.114
18.57	3.774	0.150	3.624
23.80	4.494	0.150	4.344
25.79	4.442	0.150	4.292
29.40	4.642	0.150	4.492
31.78	4.676	0.150	4.526
35.25	4.750	0.150	4.600
38.25	4.766	0.150	4.616

TABLE 2

PREVIOUS EXPERIMENTAL PRESSURE DATA HUNTER'S RESULTS AT 918°K AND 931°K

Pressure, Atm.	$k \times 10^4$, sec^{-1}	Johnston's correction $\times 10^4$	Corrected $k \times 10^4$
0.51 (918°K)	2.225	0.260	1.965
2.14	4.125	0.260	3.865
2.95	5.589	0.260	5.329
3.47	6.638	0.260	6.378
4.49	8.030	0.260	7.770
5.61	8.461	0.260	8.201
7.00	9.094	0.260	8.834
8.95	9.747	0.260	9.487
10.42	10.452	0.260	10.192
11.80	10.421	0.260	10.161
12.43	11.473	0.260	11.213
0.50 (931°K)	3.157	0.320	2.837
2.13	7.241	0.320	6.921
2.87	9.035	0.320	8.715
3.85	10.532	0.320	10.212
4.96	11.846	0.320	11.526
6.19	12.978	0.320	12.658
7.73	14.651	0.320	14.331
8.92	16.156	0.320	15.836
10.89	17.412	0.320	17.092
12.31	19.911	0.320	19.591

TABLE 3

PREVIOUS EXPERIMENTAL PRESSURE DATA, NAGASAKO AND VOLMER'S RESULTS AT 938°K

Pressure, Atm	k x 10^4, sec^{-1}	Johnston's correction x 10^4	Corrected k x 10^4
1.31	7.2	0.3	6.9
2.63	10.3	0.3	10.0
3.95	12.3	0.3	12.0
5.26	12.7	0.3	12.4
6.58	14.5	0.3	14.2
7.90	15.7	0.3	15.4
9.21	14.7	0.3	14.4
10.55	16.0	0.3	15.7

however, and Figure 4 shows such a deviation for nitrous oxide. The data are the corrected data of Hunter at 888°K.

Very early studies (5, 6, 30) of the decomposition of nitrous oxide indicated that the reaction was second-order at pressures near or slightly above atmospheric. However, later studies disputed this observation and indicated a first-order reaction. An analysis of Hunter's "high pressure" data shows that the reaction is indeed first-order. Figure 5 is a plot of the first-order behavior of the decomposition at three temperatures used in Hunter's experiments--585°C, 602°C, and 615°C. These temperatures correspond to initial operating pressures of 36.2, 17.8, and 23.7 atmospheres, respectively.

A survey of the literature revealed three sets of high pressure activation energy and frequency factor values. These values are

Source	E^{∞} (kcal/mole)	A^{∞} (sec^{-1})
Hunter (1934)	61.0	$10^{11.7}$
Powell (1959)	62.0	$10^{12.28}$
Gardiner (1969)	60.0	$10^{11.2}$

Since none of these sets of values is based directly upon high pressure experimental data but upon data extrapolated to high pressures, Hunter's values are possibly the most reliable since he covered the widest range of pressure together with temperature of any investigation that has been made prior to the present study.

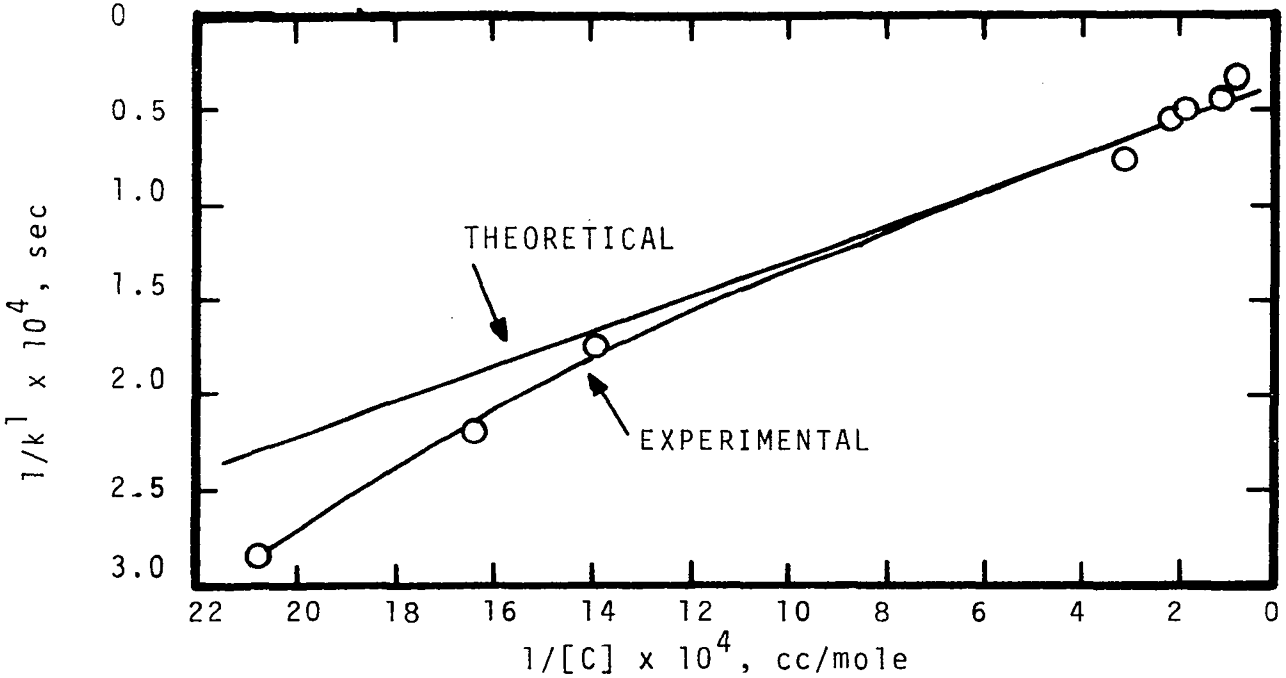

Figure 4. Lindemann Theory Applied to Nitrous Oxide Data--Hunter's Corrected Data at 888°K.

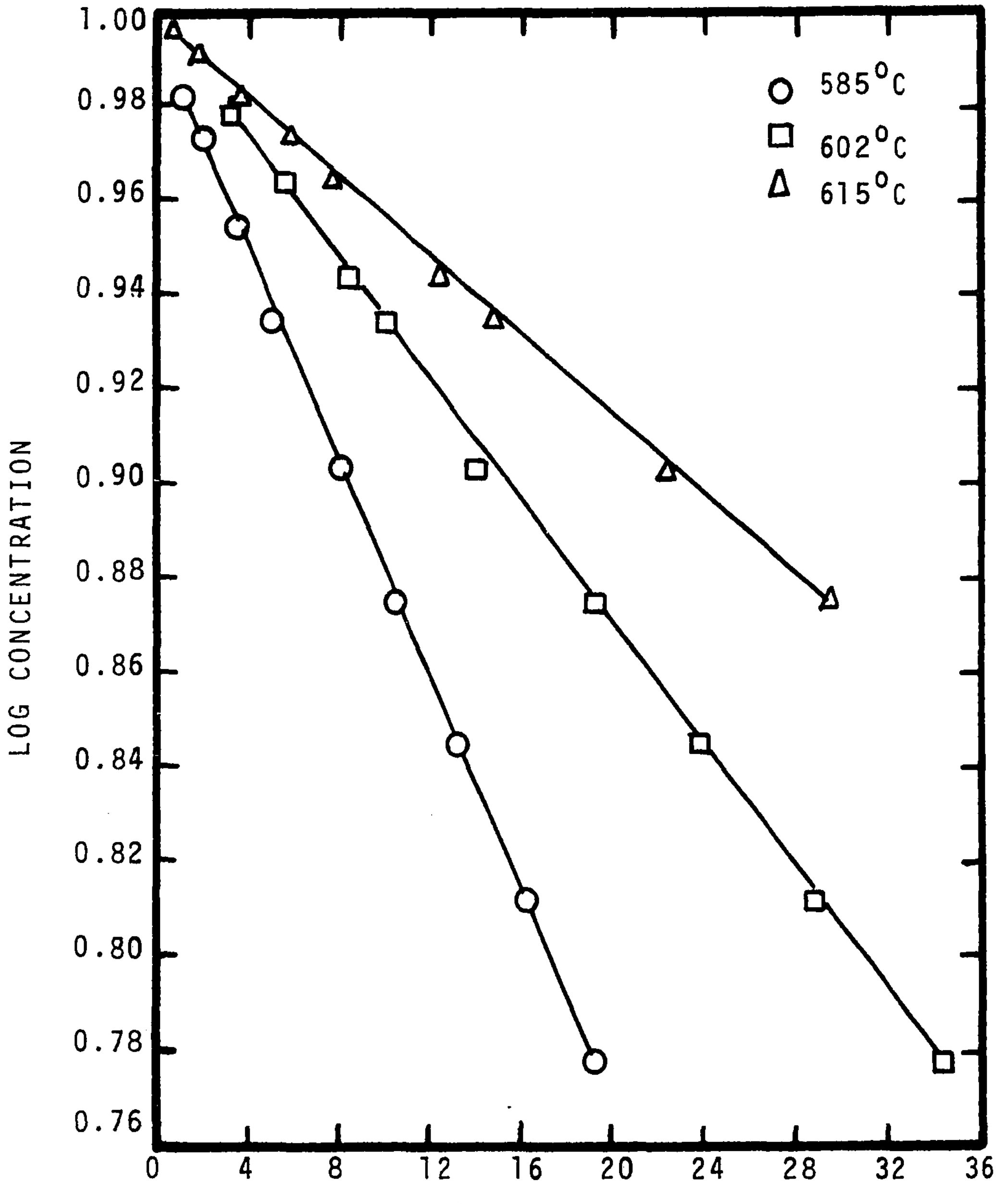

Figure 5. First Order Behavior of Nitrous Oxide Decomposition--Hunter's Corrected Data.

Using Hunter's parameters, values of k^{∞} were calculated for the temperatures at which high pressure data exist for the nitrous oxide decomposition. These values for k^{∞} are as follows:

$k^{\infty} = 4.86 \times 10^{-4}$ sec^{-1} at 888°K

$k^{\infty} = 15.0 \times 10^{-4}$ sec^{-1} at 918°K

$k^{\infty} = 24.1 \times 10^{-4}$ sec^{-1} at 931°K

$k^{\infty} = 30.6 \times 10^{-4}$ sec^{-1} at 938°K

The value for k^{∞} at 888°K appears to fall more closely in line with the curve in Figure 3 than did earlier values of k^{∞}, although k^{∞} still appears to be larger than the maximum value of the rate constant observed on Figure 3. It should be noted here that the values of k^{∞} given above are not based directly upon experimental data taken at very high pressures. Such data must be taken to get a reliable experimental value for k^{∞} which can be used in an analysis of the fall-off in reaction rate with decreasing pressure.

The experimental frequency factor at high pressures, 5.01×10^{11} sec^{-1}, is significantly below what might be expected on the basis of the discussion which follows. The value of k_BT/h at 888°K is equal to 1.85×10^{13} sec^{-1}. Slater's average vibrational frequency, $\bar{\nu}$, calculated by using values attributable to Gill and Laidler (18) is 4.50×10^{13} sec^{-1}. It can readily be seen that the experimental value is smaller by between one and two powers of 10.

The vibrational analysis of the nitrous oxide molecule according to Slater's theory is summarized below as outlined by Laidler (38). The normal vibrations of nitrous oxide--ν_1, ν_2, and ν_3--may be diagramed as

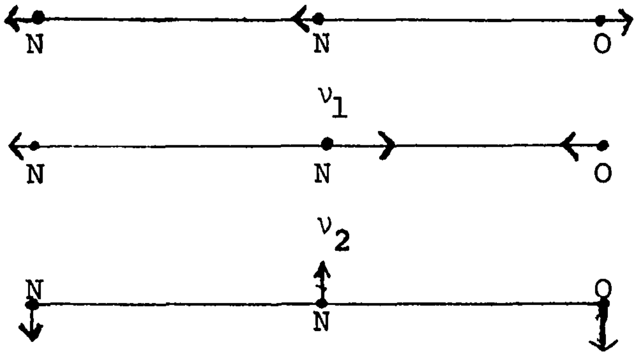

ν_3 (doubly degenerate)

The basic equations upon which calculations may be based are

$$\bar{\nu} = (\mu_1^2 \, \nu_1^2 + \mu_2^2 \, \nu_2^2)^{1/2} \qquad \text{(III-1)}$$

$$\mu_1 = \frac{\alpha_1}{(\alpha_1^2 + \alpha_2^2)^{1/2}} \qquad \text{(III-2)}$$

$$\mu_2 = \frac{\alpha_2}{(\alpha_1^2 + \alpha_2^2)^{1/2}} \qquad \text{(III-3)}$$

$$\mu_1^2 + \mu_2^2 = 1 \qquad \text{(III-4)}$$

In these equations $\bar{\nu}$ is the mean vibrational frequency, μ_1 and μ_2 are normalized amplitude factors, and α_1 and α_2 are amplitude factors which represent the contribution of a given amount of energy to the extension of the critical bond in the nitrous oxide molecule.

A number of assumed values of μ_1 and μ_2 together with the calculated values given by Gill and Laidler (18) are tabulated below. The resulting calculated values of $\bar{\nu}$ are also given for each set. Values of μ_1 smaller than 0.8 would have resulted in even larger values of $\bar{\nu}$ than are presented, so these were ignored.

μ_1	μ_2	$\bar{\nu}$	
0.80	0.60	5.02×10^{13}	
0.90	0.436	4.48×10^{13}	
0.9066	0.4218	4.46×10^{13}	(Gill and Laidler)
0.95	0.312	4.17×10^{13}	

For $\bar{\nu} = 4.46 \times 10^{13}$, k^{∞} at 888°K was calculated to be 219×10^{-4} sec^{-1}. For $\bar{\nu} = 4.17 \times 10^{13}$, k^{∞} at 888°K was 204 $\times 10^{-4}$ sec^{-1}. Both of these k^{∞} values are much too large when considered in respect to the shape of the curve in Figure 3, and when compared to the k^{∞} value of 4.9×10^{-4} sec^{-1} calculated from the RRK theories. Thus, even if there were considerable error in the measurement of the frequencies of the normal vibrational modes, the value of k^{∞} calculated from the Slater theory would still be much too large.

The falling off of the high pressure rate constant can be predicted from the RRK theory, the RRKM theory, or the Slater theory. Figure 6 compares the experimental first-order rate constants as a function of pressure at 888°K with the various unimolecular theories. The two curves indicated by

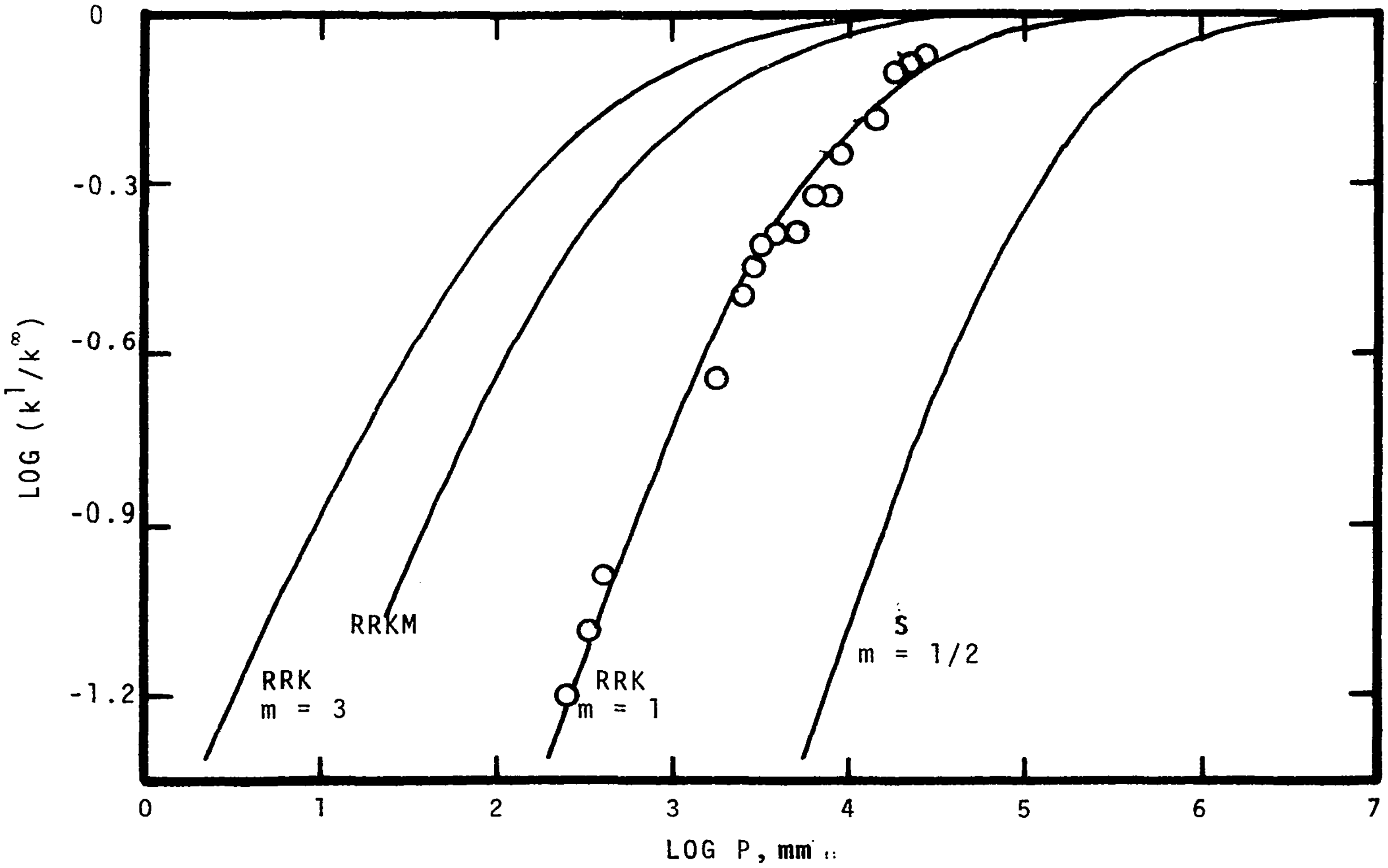

Figure 6. Hunter's Data at 888°K Applied to Unimolecular Theories.

by RRK show the theoretical behavior based upon the RRK theory with the parameter s equal to 2 and to 4. These curves were constructed by numerical integration of Kassel's general rate equation (Equation II-38) using graphs of numerical values for the integral based upon various values of s. In these graphs, m was the parameter considered with

$$m = (s - 1) \qquad \text{(III-5)}$$

Each of the numerical graphs was a plot of the integral value $I_m(\theta)$ as a function of log (θ). The graphs for $m = 1$ and $m = 3$ are presented in Appendix A in Figures 44 and 45, respectively.

The theoretical curve representing $s = 4$ $(m = 3)$ leads to reaction rates that are much greater than the experimental values at a given pressure. For $s = 2$ $(m = 1)$, however, the theoretical curve falls very close to the experimental values. The pressure for $s = 2$ at which k^1 reaches one-half the limiting rate is about 1.2×10^4 millimeters Hg, which is close to the experimental value. The relationship $[A]_{1/2} = k^{\infty}/k_1$ for the half pressure based upon Figure 3 indicates a value of about 7.6×10^3 millimeters Hg.

In Slater's development of unimolecular theory, the parameter m is related to his parameter n by the expression

$$m = 1/2(n - 1) \qquad \text{(III-6)}$$

The numerical graph of $I_m(\theta)$ as a function of log (θ) for $m = 1/2$ is given in Appendix A in Figure 43. Slater's theoretical curve in Figure 6 with $n = 2$ ($m = 1/2$) is of the same general shape as the RRK curves, but it is displaced to the right toward higher pressures. The curve indicated by RRKM in Figure 6 is based upon the RRKM theory and is taken from papers by Marcus (43) in 1951 and by Wieder and Marcus (60) in 1962. Marcus' curve for nitrous oxide is based upon as assumed value for the transmission coefficient, η, of 0.018 to get agreement with A^{∞}. However, the value of A^{∞} that he used was obtained from Johnston's paper (33) in 1951 and is not the same as Hunter's (29) value of A^{∞} resulting from his experimental observations. A correction in η for a change in A^{∞} should bring the RRKM curve slightly closer to the experimental data.

The RRK curve with $s = 2$ was plotted together with existing data at temperatures of 918°, 931°, and 938°K in Figures 7, 8, and 9, respectively. Here again, quite good agreement between the theoretical curves and the experimental data can be observed.

Review of Previous Studies

The first investigation into the kinetics of the nitrous oxide decomposition was reported in 1905 by M. Hunter (30). He studied the reaction in a flow system by passing the gas through a porcelain bulb in a furnace, all the runs

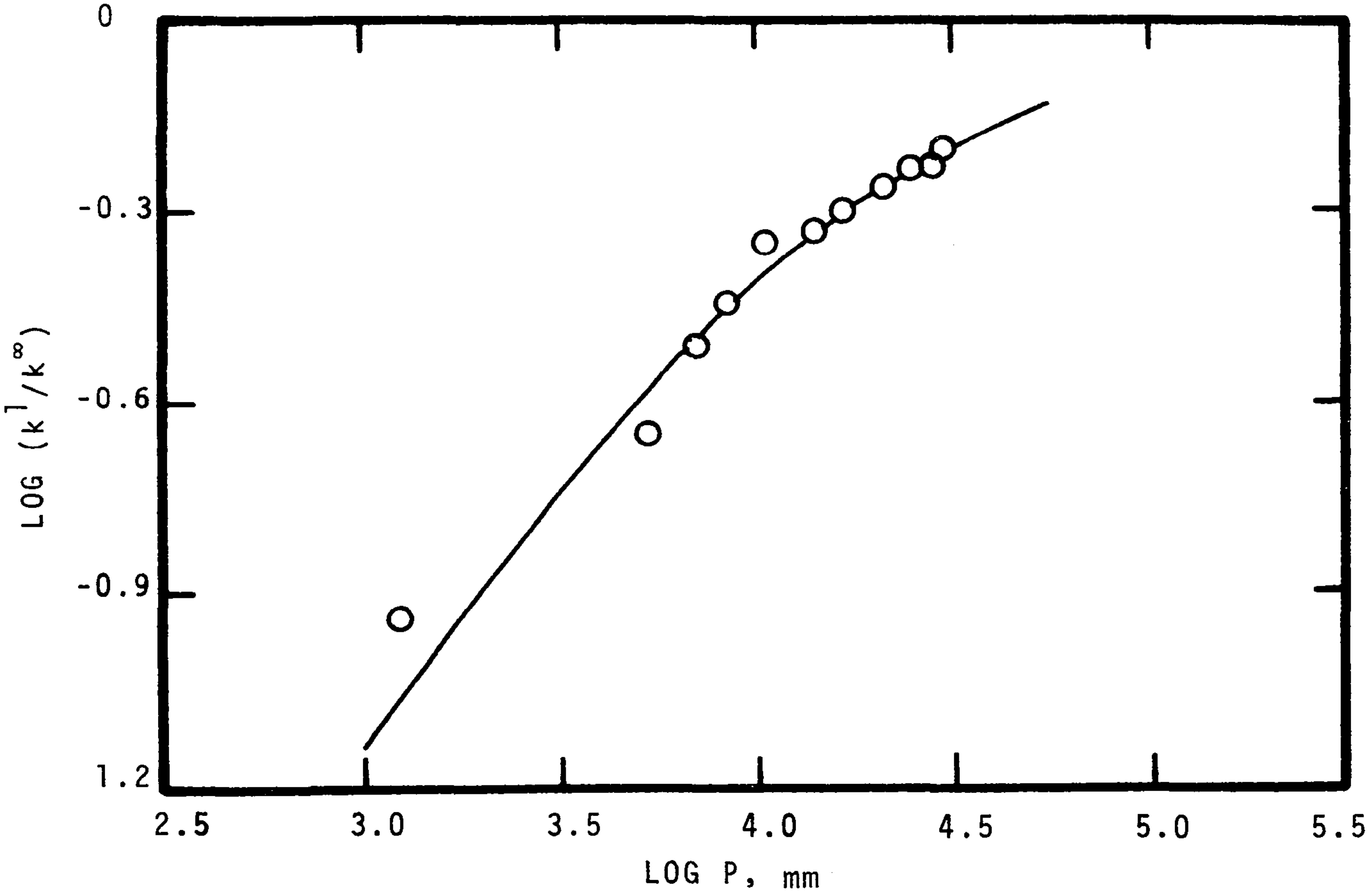

Figure 7. Hunter's Data at 918°K Applied to Kassel's Theory.

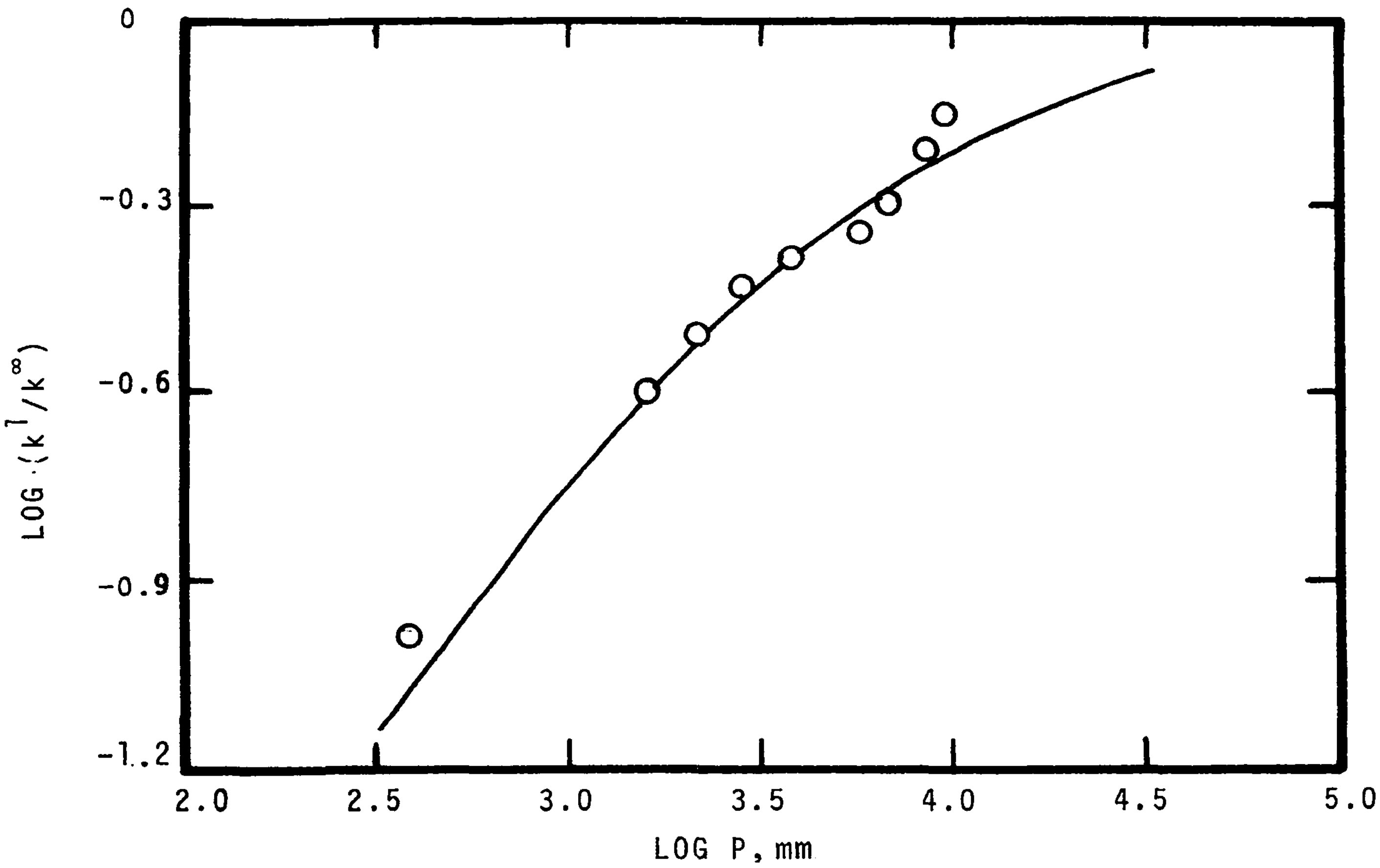

Figure 8. Hunter's Data at 931°K Applied to Kassel's Theory.

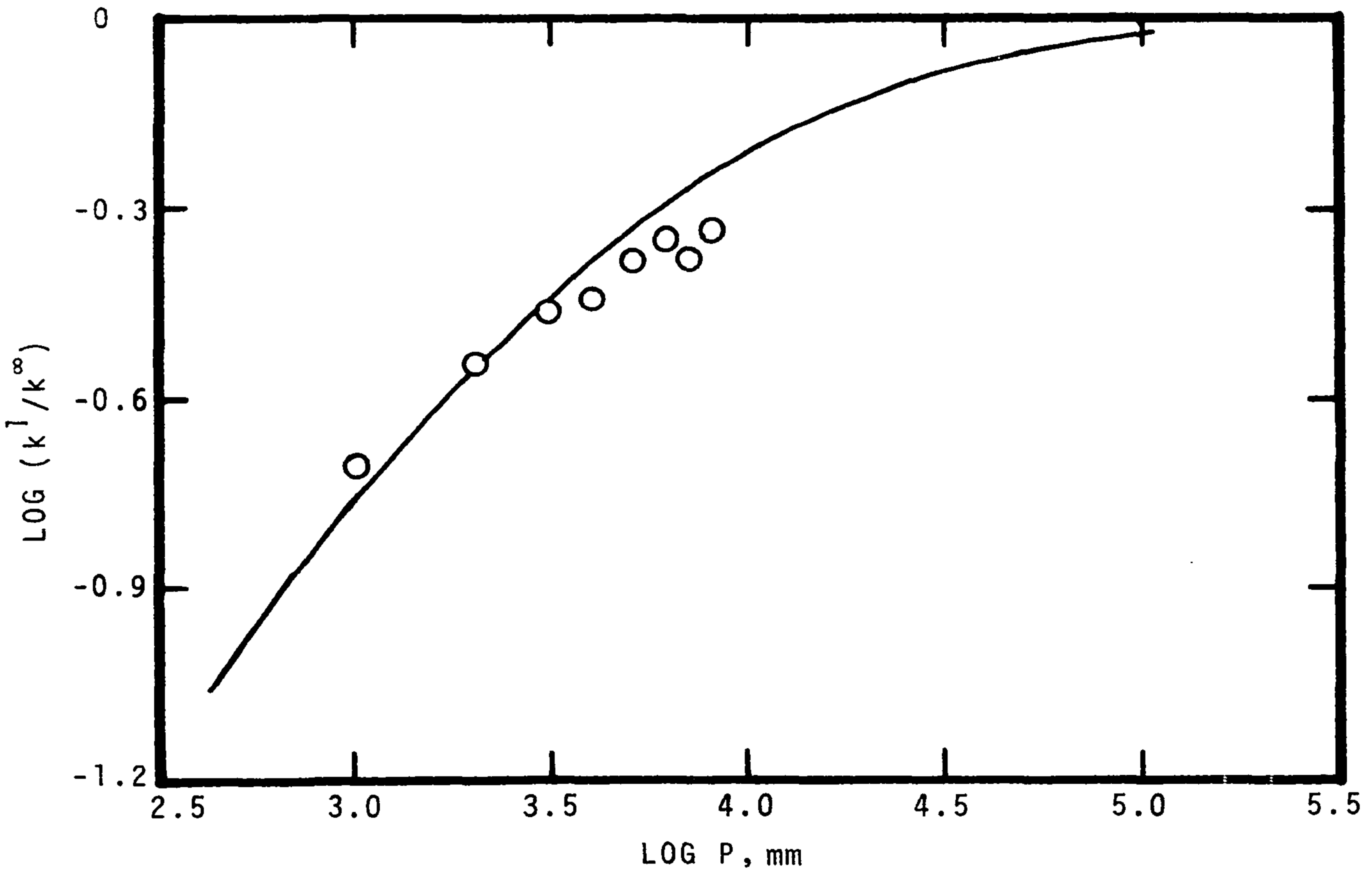

Figure 9. Hunter's Data at 938°K Applied to Kassel's Theory.

being made at about one atmosphere pressure. By varying the time of heating, he observed a second-order dependence upon the concentration of nitrous oxide. However, he did not correct for volume changes during the reaction, and no attempt was made to determine whether the reaction was homogeneous or heterogeneous.

A much more thorough examination of the reaction was made by Hinshelwood and Burk (6) in 1924, when they measured the rate of reaction by following the pressure increase at constant volume in a silica bulb. They used temperatures from 1125°K down to 838°K, although there were relatively few experiments made below 1030°K. Initial pressures were varied from 450 mm to 50 mm Hg. They confirmed that the reaction was second-order and observed no increase in reaction rate even with the reaction vessel filled two-thirds with coarse silica powder. They concluded, then, that the data were consistent with bimolecular collision theory. They noted, however, that the second-order constants rose as the reaction proceeded, indicating that the true order was lower, or that there was catalysis by the products, or both.

From Hinshelwood and Burk's investigation, it was noted previously that the second-order constants calculated for individual runs show a very pronounced drift. Satisfactory results are obtained upon recalculation considering a first-order reaction. The good first-order constants obtained suggested that the reaction was in reality unimolecular, which was a view strongly supported by the work of Volmer and Kummerow (59). Volmer and Kummerow made rate measurements at 665°C between 25 and 300 mm Hg pressure. They came to the conclusion that the rate of reaction was that which was to be expected from the low pressure part of a quasi-unimolecular reaction which, according to the Lindemann theory, may show a half-life independent of pressure over a wide pressure range and yet exhibit a falling-off in rate at some sufficiently low pressure. They expected that the decomposition reaction would give true unimolecular constants at some sufficiently high pressure. In a study by Volmer and Nagasako (45), data at pressures up to 8000 mm Hg were taken, and the results indicated agreement with the theory of a quasi-unimolecular reaction. First-order rate constants were obtained which were shown to be practically independent of pressure above a pressure of about 6-1/2 atmospheres. The value of k^{∞} was found to be 19.2×10^{-4} sec^{-1} and the activation energy was 53,000 cal/gm-mole.

Some measurements of the rate constant were made by Musgrave and Hinshelwood (44) during a study of the reaction at low pressures. Their data plotted with respect to rate constant as a function of pressure yielded two distinct regions. The first region was a straight line near the origin, but it passed through an area of great curvature at about 50 mm Hg and then straightened out into a second region which was a line of much smaller slope than the slope near the origin. On the basis of Volmer's theory of a simple quasi-unimolecular reaction, the data should give a curve rising smoothly from the origin and gradually becoming horizontal, and without the marked change in curvature observed by Musgrave and Hinshelwood. Musgrave and Hinshelwood concluded that the reaction that they observed was the sum of a unimolecular reaction and a bimolecular reaction. However, Volmer took their data and plotted the reciprocal of the rate constant against the reciprocal of the pressure, which resulted in a condition where the points corresponding to low pressures were spread out in an indefinite sweep which hid the composite appearance of the curve. If Volmer's theory were correct, the half-life of the reaction should be almost independent of pressure at pressures greater than 6 atmospheres. On the other hand, Musgrave and Hinshelwood's theory suggested that the half-life might still be pressure dependent even above 6 atmospheres. Therefore, at this point in time, data taken above 6 atmospheres pressure were essential to a correct understanding of the decomposition reaction.

The only existing high pressure data to date were obtained in 1933 by E. Hunter (29). He reported measurements of the decomposition reaction rate at pressures as high as 38 atmospheres. The reaction was studied at temperatures between 840° and 999°K and at pressures between 0.10 atm and 38 atms by measuring the rate of pressure increase in a batch system at constant temperature and volume in a silica bulb. The results obtained at pressures between 200 mm and 2000 mm Hg were in agreement with the earlier observations of Hinshelwood and Burk, and Musgrave and Hinshelwood, since straight lines could be drawn for the reciprocal half-life time against the pressure as far as 2000 mm Hg. These lines were expected to bend sharply toward the origin at a pressure in the vicinity of 60 mm Hg. At 2000 mm Hg, the pressure at which Volmer found the rate constants approaching true unimolecular constants, there was no evidence that the curve representing $1/t_{1/2}$ against p was tending to become horizontal. Hunter felt that the shape of this curve was not due to a combination of a unimolecular reaction and a bimolecular reaction, but to the contributions of three separate quasi-unimolecular reactions which each had a different mode of activation. Each of the reactions was thought to have its own activation energy. The low pressure reaction was associated with an activation energy of about 50,500 cal/gm-mol and the high pressure activation energy was about 65,000 cal/gm-mol. The value of the medium pressure reaction was between 50,500 and 62,000 cal/gm-mol. Hunter's extrapolated value of the high pressure rate constant was

$$k^{\infty} = 10^{11.7} \exp(-61{,}000/RT) \qquad \text{(III-7)}$$

Subsequent experiments by several investigators showed that the reaction scheme was not as simple as originally formulated. These results, summarized by Johnston (33) and Lindars and Hinshelwood (41), indicated that the governing rate expression was

$$-\frac{d[N_2O]}{dt} = \frac{k_1[N_2O]^2}{1 + k_2[N_2O]} \qquad \text{(III-8)}$$

The data compiled by Johnston showed that the reaction was a single unimolecular reaction, giving the low concentration limit and approaching the high concentration limit. These data were plotted by Johnston as log k against log $[N_2O]$, giving a smooth continuous curve characteristic of a straightforward unimolecular reaction, and without the prior evidence of discontinuous bends in the curve.

The only previous investigations of the effect of gold on the decomposition of nitrous oxide were made in 1925 by Hinshelwood and Prichard (27), in 1968 by Yagodovski and Fontes (62), and in 1971 by Halladay (22). Hinshelwood and Prichard used a gold wire which was located in a fused quartz tube. The tube was filled with nitrous oxide, sealed, and placed in an ice bath. The gold wire was then heated electrically, and the resulting reaction was monitored by observing the increase in the pressure of the system. They concluded that the bulk temperature of the gas was approximately 60°C, while the temperature of the wire varied from 834° to 990°C. The initial pressures varied from 200 mm to 400 mm Hg. Hinshelwood and Prichard did not account for possible diffusionlimitation effects and could not experimentally verify their assumption that the homogeneous reaction was negligible. They concluded that the reaction was heterogeneous and first-order with respect to nitrous oxide. A similar experimental procedure was used by Hinshelwood and Prichard (26) to study the catalytic effect of platinum upon the reaction. Platinum was also found to catalyze the reaction, but was found to be poisoned by the product oxygen (51, 55, 56).

Yagodovski and Fontes (62) studied the decomposition at 300° to 410°C in a cylindrical glass cell, the walls of which were covered with a granular gold film. The reaction was followed by observing the increase in the pressure of the system. They found that the catalytic decomposition on gold was first-order. The interaction of the nitrous oxide molecules with the negatively-charged adsorbed oxygen atoms was considered to be the rate determining step of the reaction.

Halladay (22) used a continuous-flow, stirred reactor made of fused quartz for his investigation. He varied the amount of gold catalyst in the reactor by using various lengths of gold ribbon which were wrapped on a catalyst rack. His experiments were carried out between 700° and 800°C and at atmospheric pressure. Halladay was able to resolve the total reaction rate for the decomposition into its homogeneous contribution and its heterogeneous contribution. Both contributions were found to be first-order with respect to nitrous oxide. The total reaction rate may be expressed as

$$R_T = R_H + R_S \qquad \text{(III-9)}$$

where R_T = total reaction rate in moles/time

R_H = homogeneous reaction rate

R_S = surface (heterogeneous) reaction rate

Ranges of Pressure and Temperature

Most of the previous studies relating to the thermal decomposition of nitrous oxide have been made at pressures either below atmospheric pressure (down to less than 1 mm Hg) or just slightly above atmospheric pressure. There have been just two studies made at pressures significantly above atmospheric. Nagasako and Volmer's study (45) covered up to 10 atmospheres pressure and Hunter's study (29) extended the pressure range to 38 atmospheres at selected temperatures. The other studies have provided data relating to the low pressure unimolecular theory, but data providing indications of high pressure behavior are extremely scarce.

Data for the decomposition of nitrous oxide have been taken in the temperature range from 550°C to 1350°C. Table 4 summarizes the nitrous oxide thermal decomposition studies to date. Figures 10 and 11 indicate graphically the ranges of pressures and temperatures covered by the various investigations.

Types of Apparatus

Most of the previous nitrous oxide thermal decomposition studies have been made using batch-type apparatus

TABLE 4

PRESSURE AND TEMPERATURE RANGES OF NITROUS OXIDE DECOMPOSITION STUDIES

Number	Reference	Year	Pressure mm	Temperature °C
1	M. Hunter (30)	1905	N.R.	713-895
2	Hinshelwood and Burk (6)	1924	50-500	565-852
3	Hinshelwood and Prichard (27)	1925	200-400	834-900
4	Briner (5)	1926	N.R.	700-1350
5	Hibben (23)	1928	0.03-0.07	550-625
6	Nagasako and Kummerow (35)	1930	80-970	627-667
7	Nagasako and Volmer (45)	1930	760-7600	557-667
8	Volmer and Kummerow (59)	1930	25-300	560-650
9	Musgrave and Hinshelwood (44)	1931	50-800	719-779
10	Volmer and Froehlich (58)	1932	2-300	625-680
11	Volmer and Froehlich (58)	1932	2-350	625-670
12	E. Hunter (29)	1934	76-28,900	567-726
13	Volmer and Briske (57)	1934	15-130	700-750
14	Lewis and Hinshelwood (40)	1938	0-600	650-750
15	Friedman and Bigeleisen (15)	1953	80	750
16	Lindars and Hinshelwood (41)	1955	50-500	720
17	Bell, Robinson and Trenwith (2)	1956	50-100	650-750
18	Graven (20)	1959	N.R.	800-1000
19	Halladay (22)	1971	751-767	700-800
20	This investigation	1973	1500-53,200	445-605

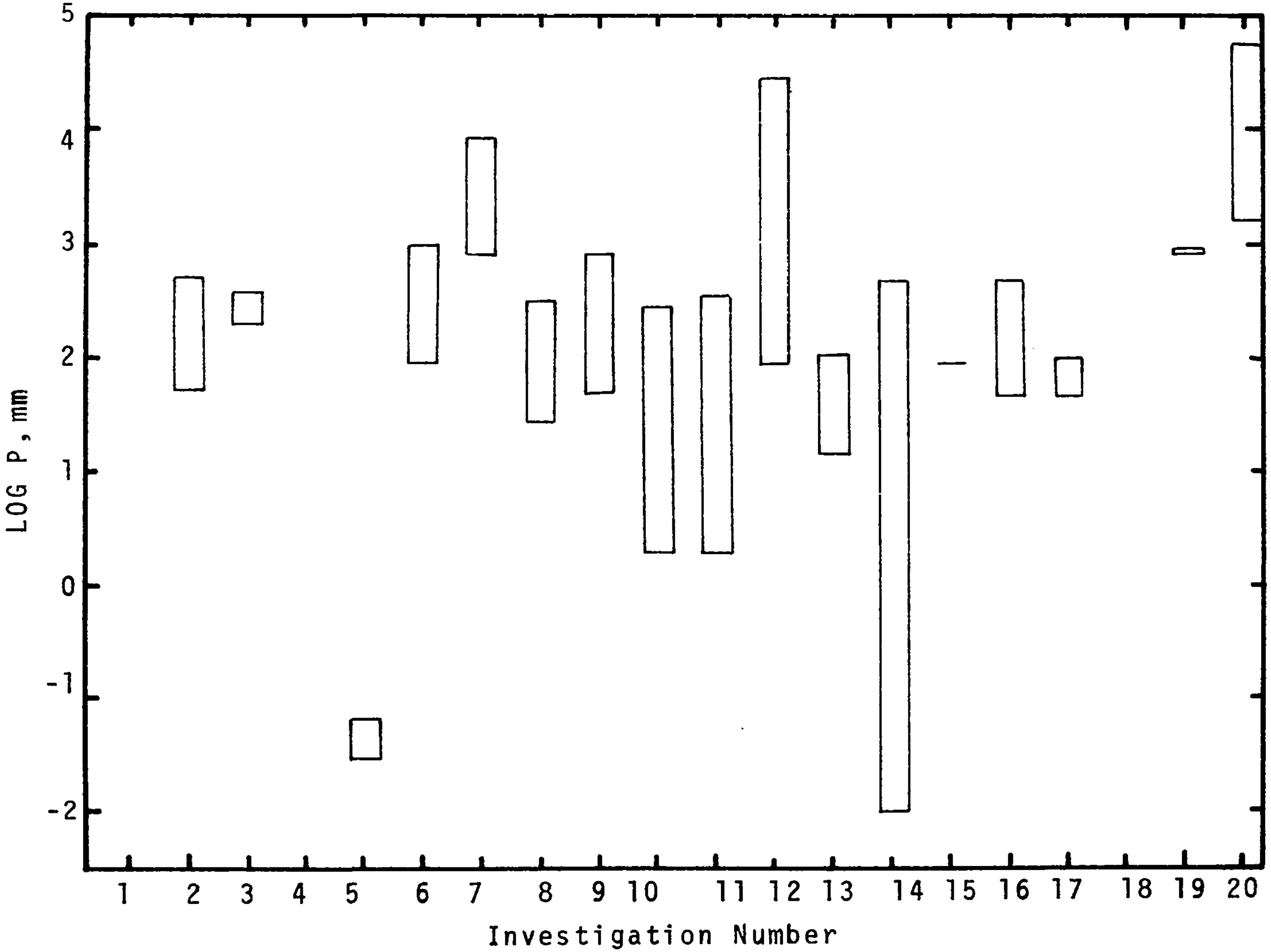

Figure 10. Pressure Ranges of Decomposition Studies.

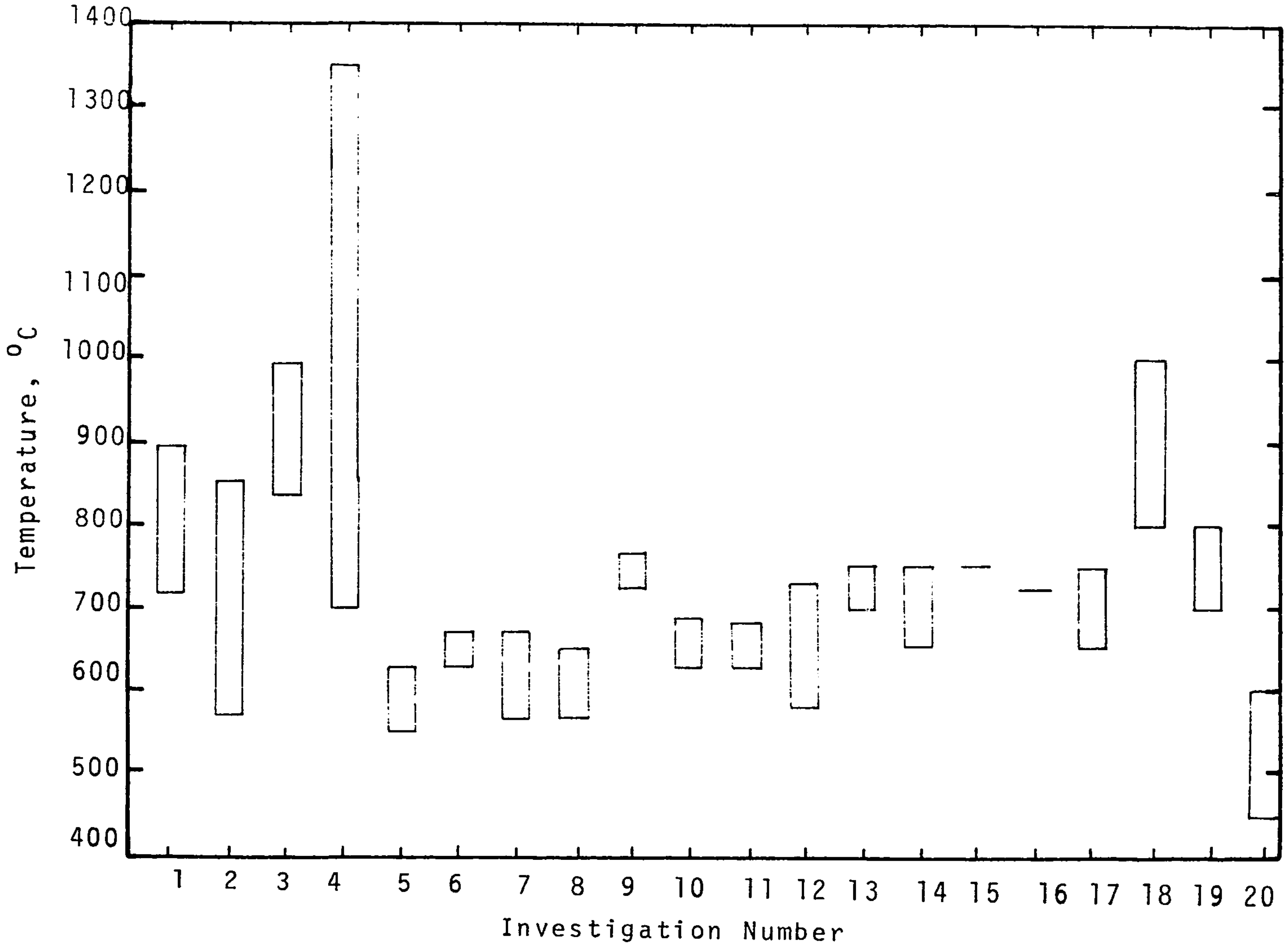

Figure 11. Temperature Ranges of Decomposition Studies.

constructed either of silica glass or fused quartz. Flow reactors have been used only in a couple of instances. In the earliest work by M. Hunter (30), a flow system was used. More recently, Halladay (22) used a flow system with a backmix reactor for his investigation. As mentioned previously, the work of M. Hunter was questionable because he did not correct for the volume increase occurring during the reaction.

All the batch thermal decomposition studies have been performed in glass vessels of some type. The role played by the glass in the mechanism of the reaction has not yet been adequately determined. Hinshelwood and Burk (6) tested the effect of silica by adding coarse silica powder to their reactor, and no measurable increase in reaction rate was observed. However, Hibben (24) found that at 600°K and a few hundredths of a mm pressure, the observed reaction rate was about 1000 times faster than that predicted by Hinshelwood and Burk, and he attributed this increase to catalysis by the quartz in his reaction vessel. He determined the reaction to be entirely heterogeneous and first-order in quartz at the conditions he employed. Johnston (33), in his article on the interpretation of previous decomposition data, showed by extrapolating the rate constants of various studies to zero nitrous oxide composition that there apparently was a surface reaction on quartz present. The intercepts on the concentration versus rate constant curves were less for studies using large reaction vessels than for studies using smaller reaction vessels.

Johnston felt that the intercepts represented a heterogeneous first-order reaction, and he corrected the existing data by subtracting the value of each intercept from each observed first-order constant for a particular temperature. Lindars and Hinshelwood (41) showed in their experiments that fresh quartz surfaces in the reactors could catalyze the decomposition reaction, but that aged surfaces did not catalyze the reaction. The aging process in the reaction vessels was thought to involve the adsorption of oxygen atoms on the quartz surface.

CHAPTER IV

DESCRIPTION OF EXPERIMENTAL APPARATUS

The apparatus used in this investigation was unique in the study of the thermal decomposition of nitrous oxide. Almost all previous studies were made in batch reaction systems, and all used either silica glass or quartz for the reactor. The present reactor system in general form had been used earlier by Pipkin (49) and Johnson (31) to study the thermal isomerization of cyclopropane. Their studies demonstrated the facility of using a flow system to study the kinetics of a reaction at elevated pressures.

In this investigation, the thermal decomposition of nitrous oxide was undertaken using a system which is illustrated in the overall flow diagram in Figure 12. The process involved flowing nitrous oxide from its gas cylinder to a tubular stainless steel preheater, and then to a gold-lined tubular reactor. Both the preheater and reactor were situated in a constant temperature bath of fluidized sand. The decomposition product gases were regulated through a pressure control valve into a product cooler, followed by a gas sampling system, and gas measuring system. For a more detailed

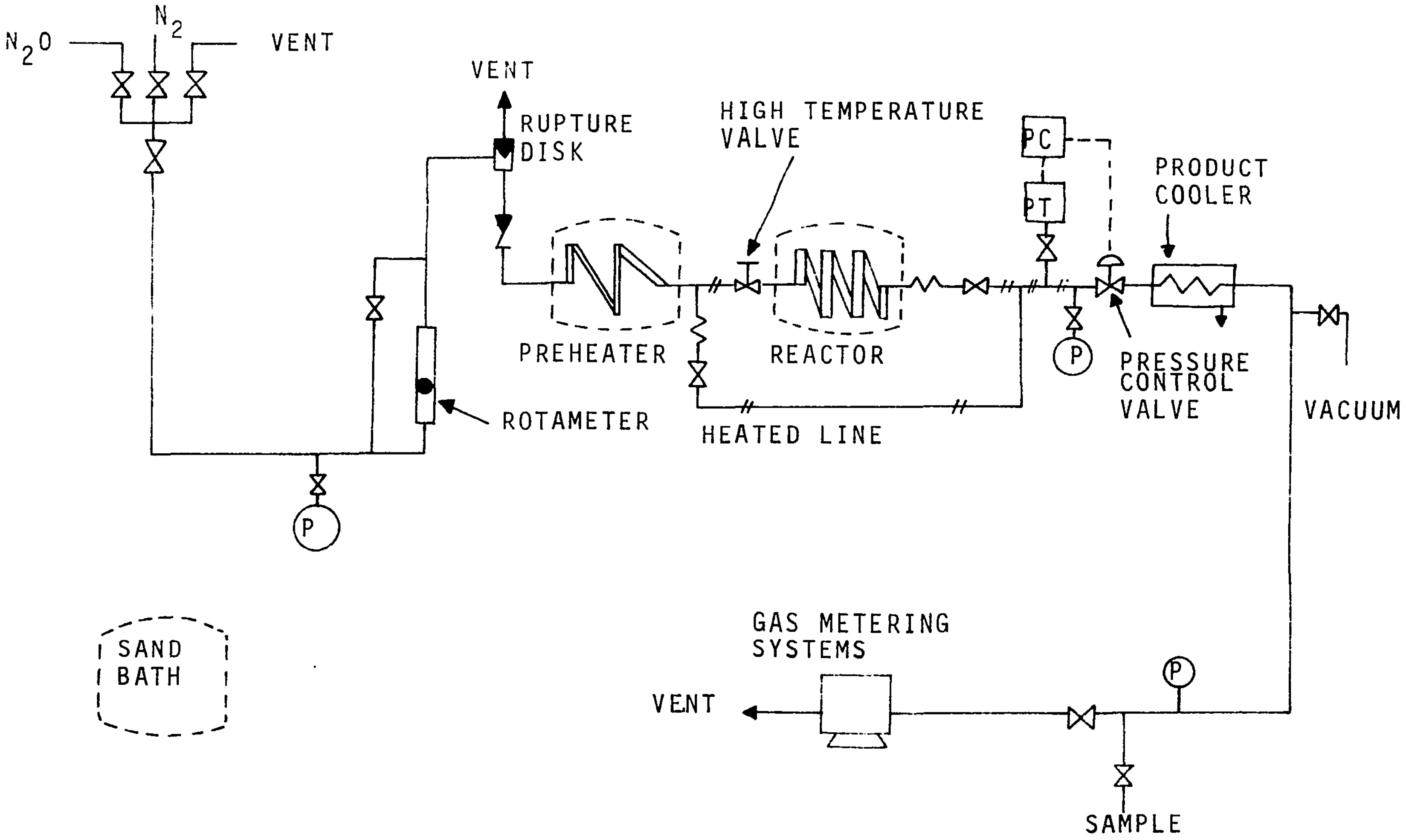

Figure 12. Overall Flow Diagram.

discussion, the total system may be divided into four sections: (1) feed section, (2) reactor section, (3) product section, and (4) auxiliaries.

Feed Section

The main components of the feed system were the nitrous oxide cylinder, nitrogen pressuring and purge system, flow rotameter, and flow metering valve. Figure 13 shows the feed section in complete detail.

Nitrous oxide flowed under its own vapor pressure from the cylinder through a Matheson Model 2-1320 high pressure regulator and an Accessory Products Co. Model 1B pressure regulator valve, a check valve, flow rotameter or flow metering valve to the reactor section. The nitrous oxide was from Matheson Co. and was 99.85 percent N_2O with the remainder being small amounts of nitrogen, oxygen, and nitrogen dioxide. The check valve was a Nupro Model 4C with a 10 lb spring. The flow rotameter, a Fischer and Porter Model 10A1700 with tube size 02, was used to measure the gas flow into the reactor during a run. The rotameter had a safe working pressure of 28.9 atmospheres (410 psig). For runs above 29 atmospheres, the rotameter was bypassed and the gas flow was fed through a Whitey Model 22RS4 Micro-Metering valve.

The vapor pressure of nitrous oxide at 72°F is only 795 psia, but at 95°F, the pressure is 1035 psia. To obtain vapor pressures from the nitrous oxide cylinder in excess of

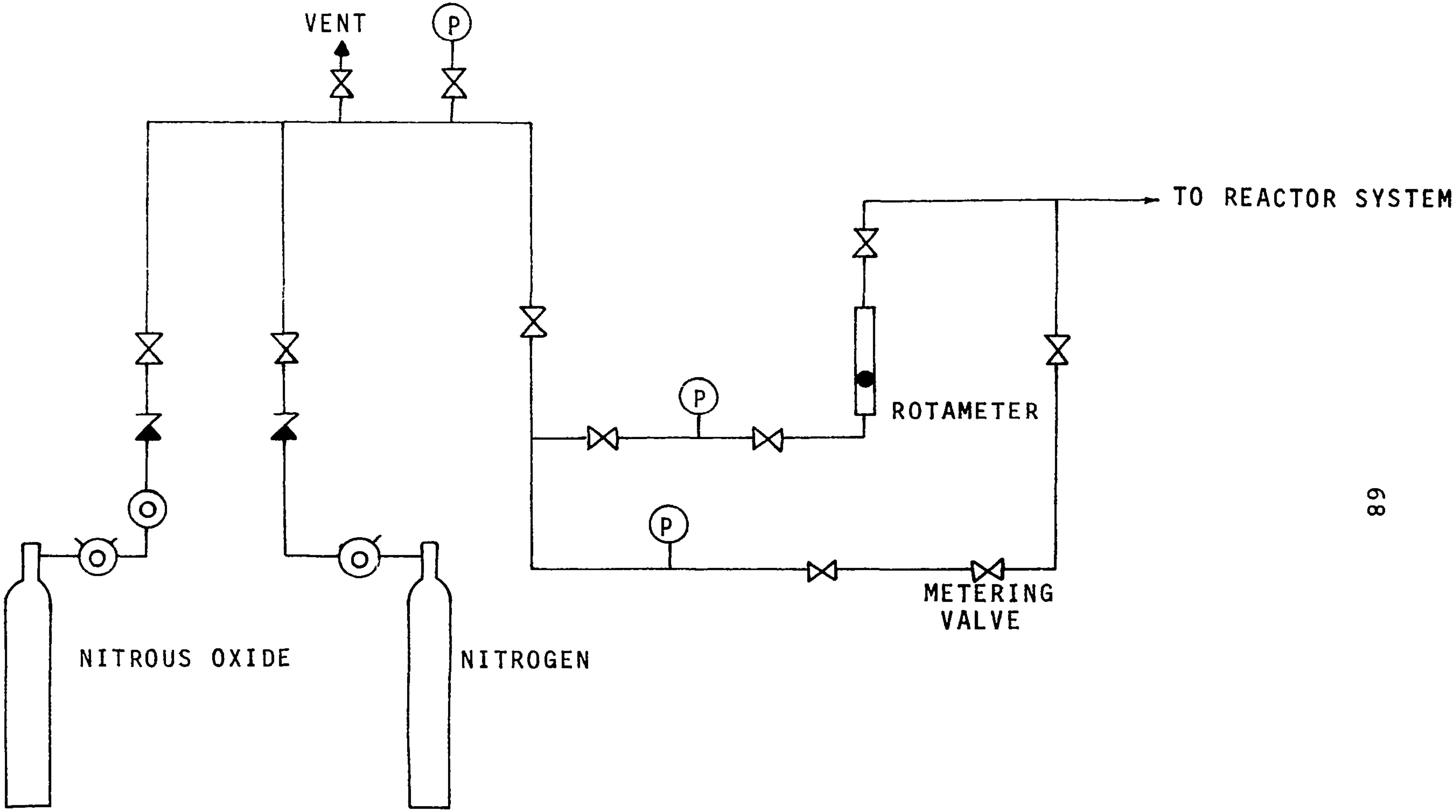

Figure 13. Feed Diagram.

1000 psig, the cylinder was immersed to about 2/3 of its length into a constant temperature bath of water maintained at 96°F. The water in the bath was stirred by a Lightnin Model F mixer and was heated by a 500-watt immersion heater wired to a Fenwall No. 18001-0 Thermoswitch.

All connecting lines used in the feed section were either 6.35 mm OD by 3.18 mm ID or 3.18 mm OD by 1.59 mm ID, Type 304 stainless steel tubing. Tubing connections were made either with Ermetto fittings or Swagelok fittings.

Reactor Section

Nitrous oxide from the feed section passed through a Nupro Model 4C check valve and a 3000 lb/sq in pressure relief disc assembly before entering the preheater. A detailed diagram of the reactor section is given in Figure 14.

The preheater, located in the fluidized sand bath, was constructed from a 3.18 mm OD by 1.59 mm ID by 457 mm length of Type 316 stainless steel tubing. After passing through the preheater, the nitrous oxide could either pass into the reactor or bypass the reactor whenever the preheater conversion levels were desired. The tubing connecting the preheater to the reactor and lying outside of the constant temperature bath was kept very near the reaction temperature by the use of Nichrome heating wires located beneath the tubing insulation. The outer wall tubing temperature could be continuously recorded from a chromel-alumel thermocouple imbedded between the tubing and insulation.

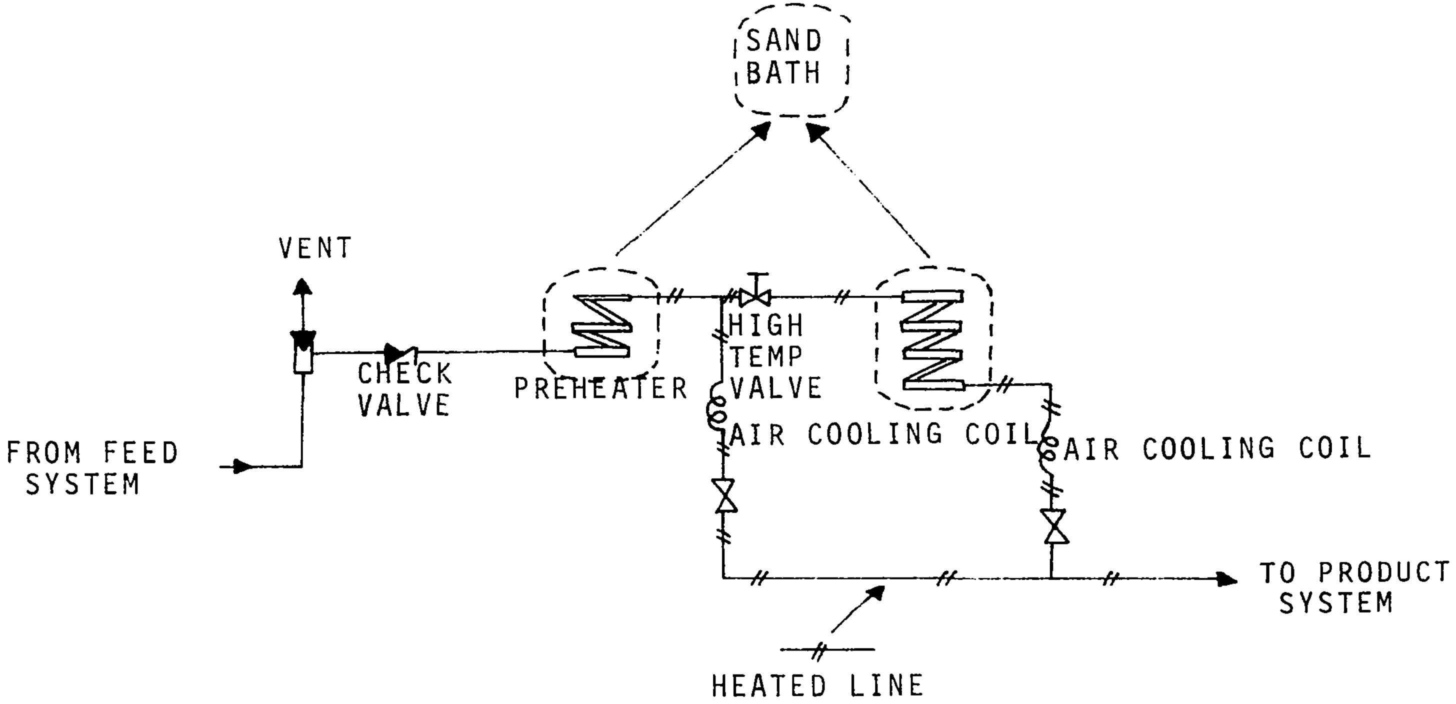

Figure 14. Reactor System Diagram.

The reactor itself was constructed from a 1.43 cm OD by 0.95 cm ID by 487.7 cm length of Type 316L stainless steel tubing. The tubing was lined with a 0.76 mm thickness of gold by Englehard Industries, Inc. The lining was achieved by first inserting a cold gold sleeve into a straight length of the tubing and then pulling a "torpedo" through the gold to press it firmly against the tubing. The reactor tubing was then coiled with a resulting coil diameter of 19.1 cm. The volume of the reactor was determined to be 239.9 ± 0.1 ml.

The constant temperature bath for the preheater and reactor was a fluidized sand bath previously used by Pipkin (49) and Johnson (31). Since the sand bath's operation has been explained in detail by these two authors, just a brief discussion will be presented here. The fluidized sand bath consisted of a burner section, the fluidized sand section, and a sand disengaging section. A regulated volume of air was heated by an enclosed propane burner located at the base of the sand bath. The heated air then passed through a grid-plate and fluidized the sand in which the gold-lined reactor coil was located. The air leaving the fluidized bed then passed through a disengaging section which removed all but the very smallest entrained particles of sand. Details of the fluidized sand heating system are shown in Appendix F.

The air for fluidization of the sand was regulated at 2 atmospheres by a Fisher No. 95L pressure regulator. The flow of air was regulated by hand adjustment of a standard brass globe valve. Indication of the air flow was made by a Barton Model 200 pressure differential indicator with a range of 50.8 cm of water. A 12.9 mm sharp-edged orifice served as the pressure differential generator for the Barton indicator.

Coupling of the reactor to the connecting tubing was made using a modified 6M44C8 coupling from Autoclave Engineers, Inc. All of the remaining couplings in the reactor section were made using Ermetto fittings or Swagelok fittings of the appropriate size.

All lines leading from the reactor or preheater to the pressure control valve were insulated and heated to 95°C by Nichrome wire wrapped under the insulation. The transfer line temperature, product gas temperature before the control valve, and product gas temperature after the water cooler were monitored on a Leeds and Northrup Micromax 8-point recorder fitted with chromel-alumel thermocouples.

The basic heat load for the sand bath was supplied by a propane burner designed by John Zink Company. A sectional view of the burner is shown in Appendix F. The burner was designed for a heat output of 7,560 kcal/hr. Commercial grade propane, regulated to 1.6 atmospheres by a Matheson No. 70A pressure regulator, was used as the fuel for the burner. Propane flow was regulated by adjustment of a stainless steel needle valve and indicated by a Matheson No. 662 PBV rotameter with a No. 604 tube. As a safety feature, a BASO device, activated by a shielded thermocouple in the burner flame, was used to shut off the propane flow to the burner in case the flame was inadvertently extinguished. The burner was ignited using a spark ignitor located inside the burner, which is illustrated in Appendix F.

Additional heat was supplied to the sand bath by three 500-watt Chromalox strip heaters mounted vertically on the exterior throat of the bath body and wired in series. These heaters were wired to a 115 V power supply which was kept on continuously during each run. Final control of the temperature of the bath was accomplished using a Bayley Model 96, Precision Temperature Controller modified for use to 650°C. Under operating conditions, the controller was capable of sensing temperature deviations of 0.2°C. Trim heat current from the controller was supplied to a 675-watt Chromalox cartridge heater located in a horizontal copper well directly above the air distribution plate.

A Rosemount Engineering Company, Model 104MA, platinum resistance thermometer was the primary temperature indicator for the sand bath. Resistance of the thermometer was measured using a Leeds and Northrup Model 8067 Mueller Bridge and Hewlett-Packard Model 419A electronic null detector. Two chromel-alumel thermocouples together with a Leeds and Northrup 8686 millivolt potentiometer and a Hewlett-Packard Model 413A null detector were used as alternative temperature sensors of the sand bath's temperature. These thermocouples were Leeds and Northrup Compacted Thermocouples equipped with Conax Safetywell Assemblies. One was located near the top of the bath and the other just above the air distribution grid plate. Both thermocouples extended approximately 13 cm into the bath. An additional chromel-alumel thermocouple was located in a retractable well above the fluidizing section. From this position, it could be adjusted to cover the entire sand-filled portion of the bath. This thermocouple was connected to two points on the 8-point Leeds and Northrup Micromax Recorder so that the bath temperature could be recorded continuously.

Product Section

A detailed diagram of the product section is given in Figure 15. The reactor pressure was indicated on either a 100, 500, 1000, or 3000 psig Heise pressure gage. Scale divisions on these gages were 0.1, 1.0, 2.0, or 4.0 psi, respectively. All of the gages used were dead weight tested for accuracy before being installed on the unit.

Reactor pressure was controlled by regulating the flow of product gases with a Research Controls, 1/4-inch, 304 stainless steel, air-operated control valve with either a P2 or P4 trim as required. The control air supply for the valve was provided by a Bristol, Series 650, Metagraphic pressure transmitter and Foxboro M-58 Consotrol pressure controller.

From the pressure control valve, the product gases passed through a product cooler where cooling was supplied by

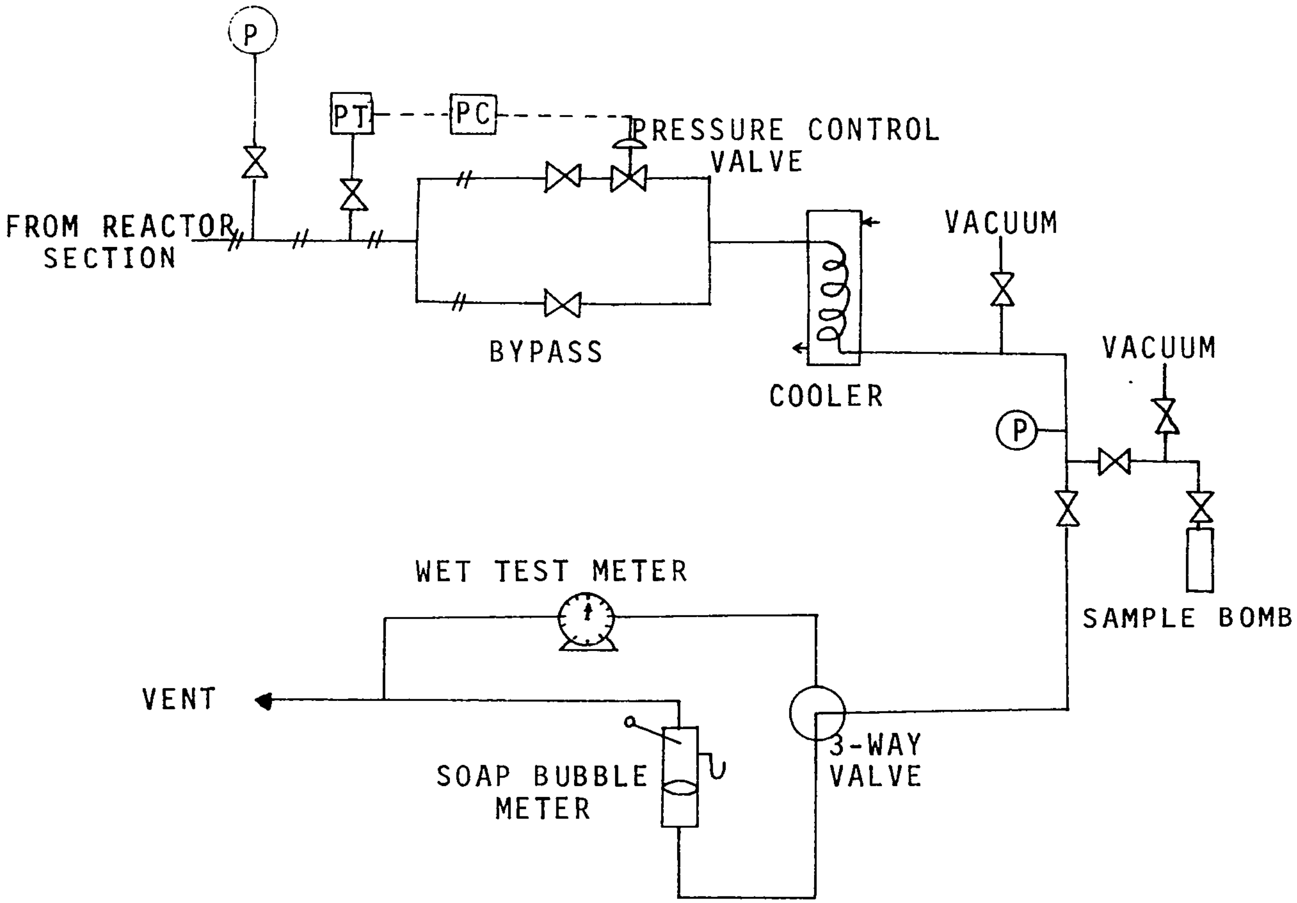

Figure 15. Product System Diagram.

countercurrent flow of refrigerated water. The cooling coil was constructed from 3.35 meters of 6.35 mm OD stainless steel tubing. Gases from the cooler passed through a sintered metal filter before proceeding to the product sampling system. The product sampling system consisted of a pressure gage and a tap for collecting samples in evacuated bottles for later analysis. Final measurement of the product gas flow rates was made using either a Precision Scientific, Model 3110-12, wet test meter or a soap bubble meter designed by Johnson (31). Switching between the two meters could be accomplished by means of a 3-way valve. After passing through the flow meters, the product gases were vented to the exterior of the building.

Auxiliaries

A Cenco-Pressovac 4 vacuum pump served as the means of evacuating the reactor system and the sample containers. The vacuum in the system was measured either by means of a mercury manometer or by a U.S. Gage vacuum gage. High pressure nitrogen for purging and pressurizing the unit was provided by 1A sized cylinders of Matheson high-purity nitrogen connected to the system by way of a Victor Model LR17BSS pressure regulator with a range of 10-1000 psig.

The refrigerated water system used to provide cooling for the product gas cooler consisted of a Copeland Model E75C refrigeration unit, a small Teel centrifugal circulating pump, and a 30 liter refrigerated water reservoir. The chilled water reservoir was painted inside with waterproof paint to minimize corrosion. Water was circulated by the Teel pump through Tygon tubing to and from the product cooler.

The reactor sand bath and most of the connecting pressure tubing were located in a high pressure cell constructed from a wooden framework covered with sheets of 6.35 mm thick cold-rolled steel. A heavy woven rope blast mat covered the wooden top of the high pressure cell. Additional safety features of the cell included a water spray nozzle located over the sand bath and an explosion-proof exhaust fan on the exterior wall of the cell. The spray nozzle was connected through a solenoid valve to the main water line. The solenoid valve could be activated by means of a switch located on the front panel of the cell. The switch for the exhaust fan was also located on this front panel.

CHAPTER V

EXPERIMENTAL PROCEDURE

Introduction

Before any runs using nitrous oxide were made, two preliminary runs were made to determine workable startup, on-stream, and shut-down procedures. These runs were made with nitrogen at flow conditions similar to those to be expected during the actual runs with nitrous oxide. Approximate control settings for the various temperature and pressure controllers were obtained during these two "dry runs." These runs also provided information as to the length of heating time to be expected in reaching a specified bath temperature.

Startup Procedure

The most time consuming procedure during startup was the heating of the sand in the fluidized sand bath. After experiencing very slow warm-up periods during the dry runs, the exterior metal of the lower portion of the bath was covered with asbestos and fiberglass wrap, which reduced the warm-up period by about two hours. Nevertheless, approximately 3 to 6 hours were required to bring the sand bath to a stable temperature, the length of heating time varying with the temperature desired over the range used in this investigation. Thus, the first item in the startup procedure was always the ignition of the burner and the heating of the sand bath.

Before the burner was to be ignited, the flow of air was started through the sand bath. The air flow rate was regulated at 283 std. liters/min (60°F, 1 atm) and the propane flow rate set at a reading of 5.5 on the rotameter glass float (5.5 gm/min propane). The burner was then ignited using the enclosed electrical ignition system shown in Appendix F. A BASO device shut off the propane flow in case the flame went out. After ignition of the burner, the propane and air rates were maintained at their ignition levels for about 10 minutes. The air flow rate was then increased to 400 std. liters/min, and the propane rate was increased to the maximum value of 11 on the rotameter (11.5 gm/min propane). Propane feed was continued at this rate until the sand bath temperature came within 10°C of the desired run temperature. The propane rate was then gradually decreased to its estimated base load rate. The base load rate was achieved near the time when the bath reached the desired run temperature. The base load propane rate was designed to allow the Bayley temperature controller to hold the run temperature. After attaining initial control at the desired run temperature, the temperature was then monitored from 15 to 30 minutes to make sure that it was not drifting.

During the warmup period of the sand bath, the refrigeration unit and water circulation pump for the cooling water system were started. When the sand bath temperature had reached 300°C, all product line and transfer line heaters were turned on. The Variacs were adjusted to give a transfer line temperature within approximately ± 6°C of the bath temperature and a product line temperature of about 100°C. When the bath temperature came within 10°C of the desired run temperature, a flow of nitrous oxide maintained at the first pressure level to be used during the run was begun through the preheater and reactor. This flow enabled the pressure control valve and controller to be placed in operation and the flow rate adjusted for the initial phase of the run.

Run Procedure

When the temperature in the sand bath was under control, the flow rate of nitrous oxide adjusted to its proper value, and all the auxiliaries were in operation, the run procedure was initiated. At each pressure level attained during the run, from 20 to 90 minutes were allowed for the system to reach equilibrium. The length of time allowed depended on the system flow rate, since a target value of six turnovers through the reactor before reaching equilibrium was assumed for the system. At each pressure level, flow rate data were recorded at 2.5-minute intervals during the last half of the run period. Data from each run period were recorded on a prepared run sheet, a sample of which is given in Appendix D. When equilibrium had been reached in the reactor at a particular pressure level, a gas sample was taken into an evacuated sample bomb. The gas samples were analyzed on the gas chromatograph at a later time.

In order to calculate the rate constant at a particular temperature and pressure, both the reactor inlet and outlet gas compositions are required. The reactor inlet (preheater outlet) gas composition was obtained in the following manner. When the reactor gas sample had been taken at a particular pressure level, the reactor inlet and outlet block valves were closed. The preheater outlet valve was opened, and all variables were maintained as they were during the run period. After a 15-minute equilibration period during which flow rates were recorded, a gas sample was taken into an evacuated sample bomb. The inlet and outlet valves were then returned to their original configuration, and the next pressure level was applied to the reactor system.

Because of the large heat capacity of the sand bath, a significant amount of time was required to change from one temperature to another, especially if this change were greater than 10°C. Therefore, the system was brought to just one temperature for each run, and several pressure levels were run at that particular temperature. If no difficulties were encountered during the run, four to six pressure levels could be obtained at that temperature level. While the system was in operation, the cell was entered only to perform the necessary valving operations.

Shutdown Procedure

The first step in the shutdown of the unit was to stop the propane flow to the sand bath burner. Once the burner had been shut off, the fluidizing air supply was then turned off. The valve on the nitrous oxide feed cylinder was closed and the pressure relieved on the pressure regulators. Then the pressure control bypass valve was opened slightly and the system was slowly bled down to zero gage pressure. A small flow of nitrogen was passed through the system as a purge. The transfer line and product line heaters were shut off and these lines were permitted to cool. No attempt was made to cool the sand bath itself following a run. In fact, the electric trim heater, which kept the sand bath at 150°C whenever the system was not being run, was left on constantly in order to establish a base heat load. The weight of propane consumed during the run was recorded, and the valves on the propane cylinder were closed. The oil traps on both the instrument air supply and the air supply to the sand bath were drained of the oil-water emulsion which was collected during the run. The final two steps in the shutdown procedure were to shut off the refrigeration unit and water circulation pump, and to turn off all the electrical instrumentation.

Calibrations

The temperature of the fluidized sand bath in which the preheater and reactor were immersed was measured during each run with a calibrated platinum resistance thermometer. The thermometer, model number 104MA, was obtained from Rosemount Engineering Company. The thermometer, calibrated by Rosemount according to their schedule GF (0° to 1200°F), was guaranteed to represent the international temperature scale to ± 0.3°C (± 0.5°F) within this range. The resistance-temperature relationship of the thermometer was fitted to a quadratic polynomial over the temperature range from 850° to 1200°F using the ORNOR program developed by Hall and Canfield (21). The following relationship was found

$$T\ (°F) = -338.5656738 + 18.0166168\ R + 0.0769561\ R^2 \qquad (V-1)$$

with R = resistance in ohms.

The resistances of the thermometer were measured using a model 8067, Leeds and Northrup Mueller Bridge. The bridge was calibrated with Leeds and Northrup instructions using a calibrated 10-ohm standard resistance (L + N Model 4025-B) and a calibrated 1-ohm standard resistance (L + N Model 4020-C). The calibration is shown in Table 5.

Null points for the resistance thermometer were indicated on a Hewlett-Packard Model 419A null voltmeter. With this equipment, a 0.001-ohm change in the thermometer's

TABLE 5

CALIBRATION FOR MUELLER BRIDGE AT 25°C

Measured Resistance (ohms)	Actual Resistance (ohms)
1.0000	1.0005
5.0000	5.0012
10.0000	10.0023
20.0000	20.0045
30.0000	30.0073
40.0000	40.0097
50.0000	50.0122
60.0000	60.0144
70.0000	70.0168

resistance could be detected using the 1-millivolt range of the null voltmeter. At the highest temperature level of this investigation, 605°C, a 0.001-ohm change in resistance corresponded to a 0.015°C change in temperature. Therefore, the sensitivity of the temperature measurement was much greater than the actual calibration of the thermometer. The maximum error expected in the bath temperature when the temperature was measured by the resistance thermometer was no more than ± 0.3°C.

The voltages generated by the chromel-alumel thermocouples in the sand bath were measured on a Leeds and Northrup Model 8686 millivolt potentiometer. A Hewlett-Packard 413A null voltmeter served as a galvanometer for the potentiometer. Reference junction temperature was kept at 0°C by immersing the reference junction thermocouple in an ice bath. With this system, the thermocouple temperature measurements were felt to be accurate to within ± 0.5°C.

Pressure fluctuations about the controller set point were 0.5 psi or less. Reactor pressure was measured from a tap 1.2 meters downstream of the reactor exit, but at the low flow rates used for all the runs, the pressure drop corrections were negligible. Generally, pressure drops through the entire system were about 2 psi.

The wide range in flow rates anticipated in this investigation made it necessary to have two different flow metering systems available. Flows in the range from 0.5 cc/sec. to 9 cc/sec were measured with a calibrated soap bubble meter. The soap bubble meter was a glass tube of uniform diameter which had connections for gas inlet and outlet, a thermowell for temperature measurement, a tap for pressure measurement, and a rubber bulb for soap bubble formation. During operation, the time required for a soap bubble to pass between two graduation markings was measured, and, knowing the volume contained between the two markings, the volumetric flow rate was determined. Figure 16 is an illustration of the soap bubble meter. Flow rates in the range from 9 cc/sec to 15 cc/sec could be measured with a Precision Scientific Model 3110 wet test meter. Reported accuracy of this type meter was 0.5 percent.

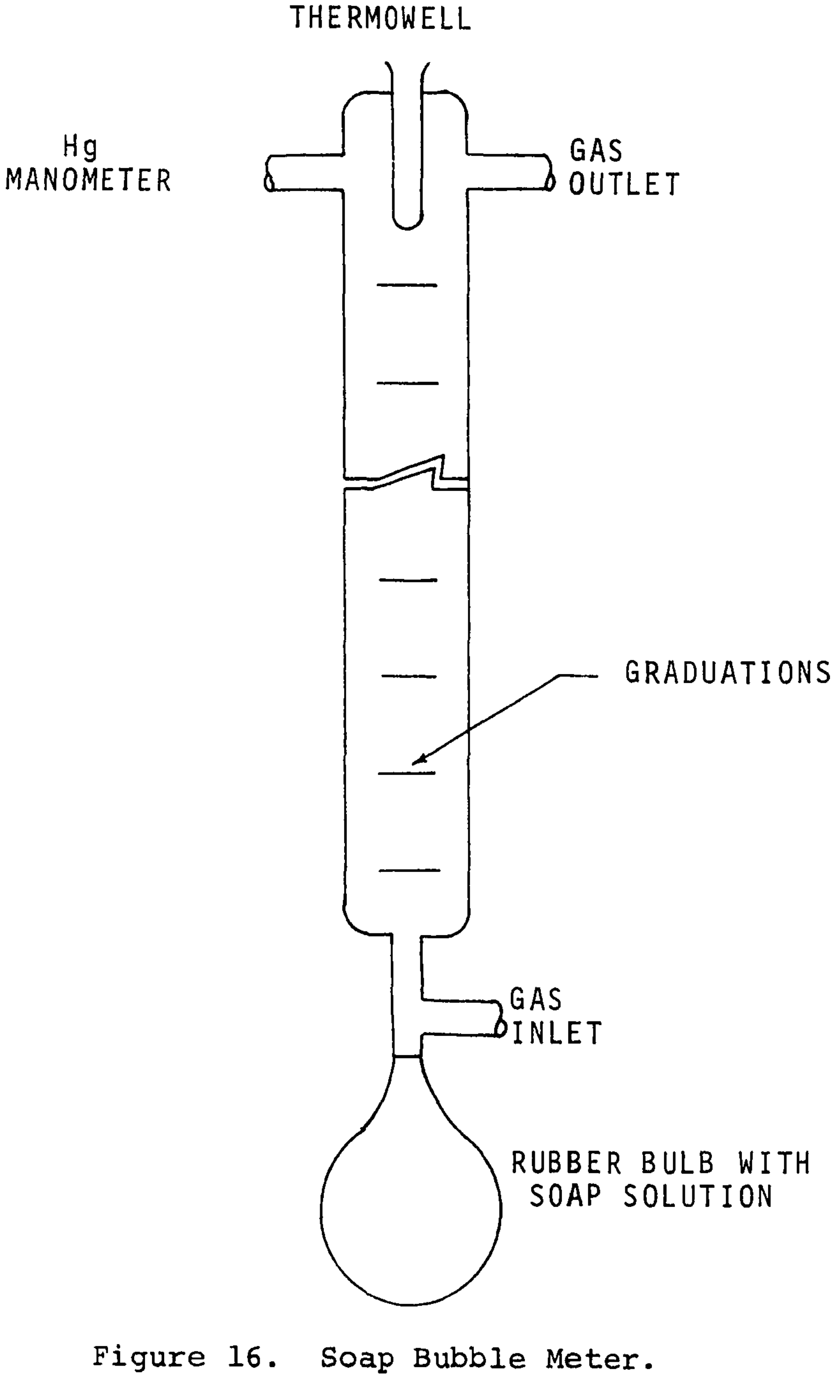

Figure 16. Soap Bubble Meter.

CHAPTER VI

ANALYTICAL PROCEDURE

Chromatograph and Columns

The determination of conversion in a tubular reactor such as the one used in this investigation requires some form of chemical analysis of the reactant and product gases. Gas chromatographic separation of N_2, O_2, N_2O, and NO_2 was found to be a convenient method of analysis for this study. However, the separation of N_2 and O_2, and the separation of the nitrogen oxides are rather difficult to achieve. Graven (19) recommended using type 5A molecular sieves as a packing for the required analysis, but Wilhite and Hollis (61) recommended Porapak Q from Waters Associates. Both packings are capable of separating nitrogen and oxygen, but Porapak Q is more effective for the separation of the nitrogen oxides. Billeb (4) recommended the use of Chromosorb 102 from Perkin-Elmer, claiming that it performed exactly the same as Porapak Q for the analysis required in this study.

While 5A molecular sieves, Porapak Q, and Chromosorb 102 will all separate N_2 and O_2, 5A molecular sieves will achieve the separation at ambient temperatures or above. The other two packings require a dry ice - acetone bath temperature (-80°C) in order to effectively separate nitrogen and oxygen. In order to avoid the use of subambient temperatures, the 5A molecular sieve packing was selected as the primary packing to be used in this investigation. As a backup analysis for nitrogen oxides, Chromosorb 102 was selected as an alternative packing.

This study used gas chromatographic analysis with helium as the carrier gas. One column, 6.4 mm (1/4-inch) in diameter by 183 cm in length, was packed with type 5A molecular sieves. The other column, 3.2 mm (1/8-inch) in diameter by 366 cm in length, was packed with Chromosorb 102. By suitably choosing the operating conditions, the molecular sieve columns could separate N_2, O_2, and N_2O. The Chromosorb 102 columns could separate N_2 and O_2 as air, NO_2, and N_2O. A complete analysis could be obtained for a particular sample by passing the sample through both sets of columns.

A Hewlett-Packard, F and M Model 700, gas chromatograph equipped with dual thermal conductivity detectors, an automatic attenuator, and a linear temperature programmer was used as the analytical instrument in this investigation. The chromatograph peaks were recorded on a Hewlett-Packard Model 17503A 1-millivolt recorder, which was equipped with a Disc integrator of 0.1 percent accuracy.

Operating conditions for the chromatograph were determined primarily by trial-and-error since no references existed in the literature for the size columns that were being used. The best operating conditions were found to be:

Injection port temperature	200°C
Detector temperature	300°C
Carrier gas supply pressure	40 psig
Carrier gas flow rate	25 ml/min
Detector current	150 ma
Attenuation	as necessary

For the molecular sieve columns, the columns were run isothermally at 100°C until the N_2 and O_2 were eluted. The temperature was then programmed upward at 30°C/min until a limit of 250°C was reached. The temperature programming decreased the elution time necessary for N_2O. Using these conditions, a sample could be analyzed in approximately 18 minutes. For the Chromosorb 102 columns, the columns were run isothermally at 24°C until all peaks had eluted. In this manner, a sample could be analyzed in approximately 7 minutes.

Calibrations

Eight nitrogen-oxygen-nitrous oxide standard samples were prepared in the following manner:

1. A sample cylinder was evacuated and attached to the inlet side of an evacuated 60-inch mercury manometer.
2. The required amount of nitrous oxide was admitted to the sample cylinder.
3. The manometer was evacuated and the required amount of nitrogen was admitted to the sample cylinder.
4. The manometer was again evacuated and the required amount of oxygen was admitted to the sample cylinder.

Since the gases used in the preparation of these standard samples were all at the same temperature at the time they were introduced to the sample cylinders, the composition of each sample could be expressed in terms of mole percentages. The mole percentages could then be related directly to area percentages from the chromatographic charts.

The calibration curves determined for nitrous oxide using the eight standard samples are shown in Figures 17 and 18. Figure 17 represents the calibration on molecular sieves and Figure 18 the calibration on Chromosorb 102. Each data point on the curves is the average of several chromatographic analyses taken over a six month period. Calibration curves for nitrogen and oxygen on molecular sieves are given in Figures 19 and 20. Area percentages were used in these calibrations in preference to peak heights since area percentages are more insensitive to variations in flow rate and temperature and area values were available due to the recorder being equipped with a Disc integrator. Typical chromatograms on molecular sieves and Chromosorb 102 are given in Figures 21 and 22. Using this method of analysis, errors in the reactant and product gas analyses were felt to be about 0.5 percent.

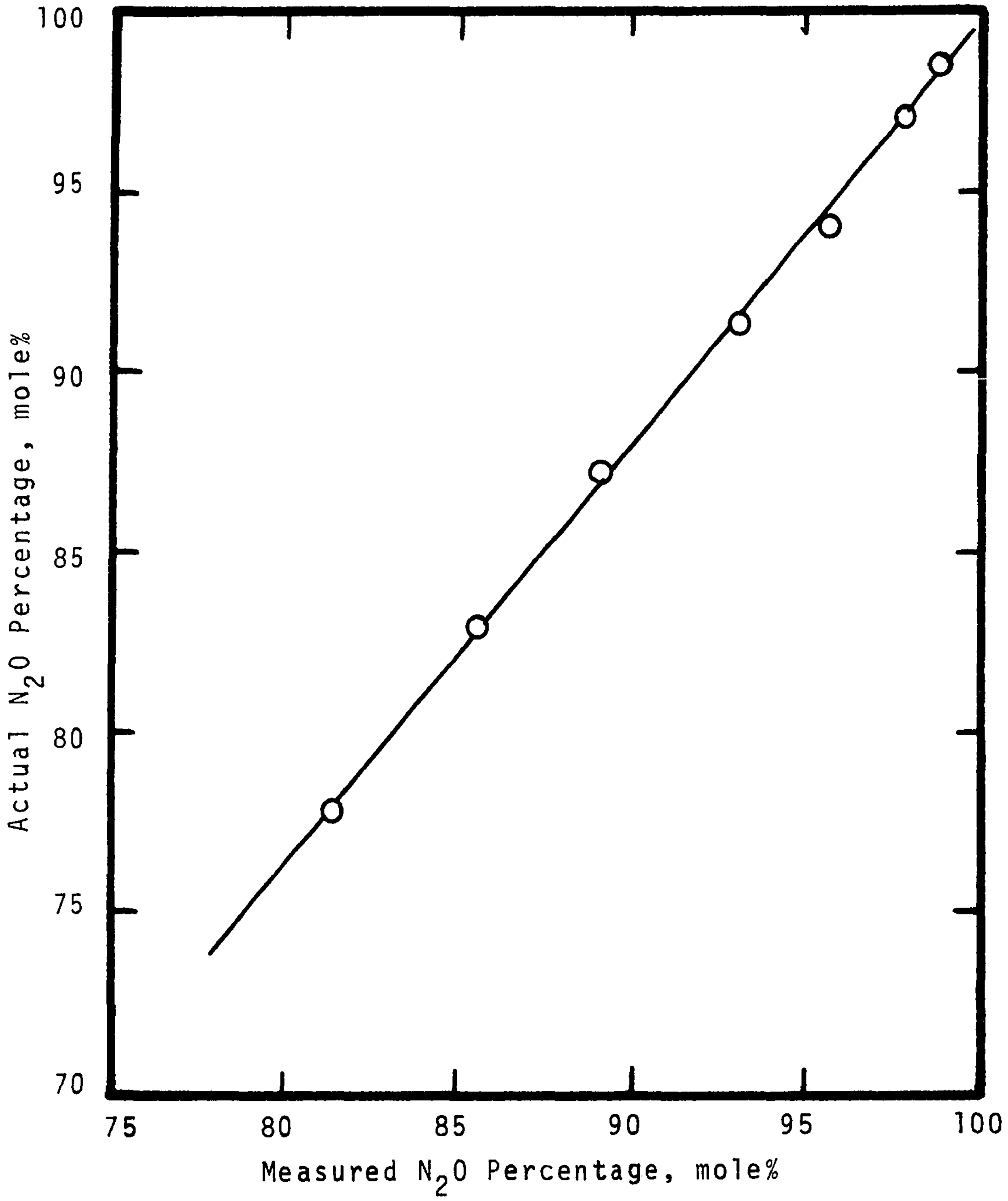

Figure 17. Nitrous Oxide Calibration on Molecular Sieves.

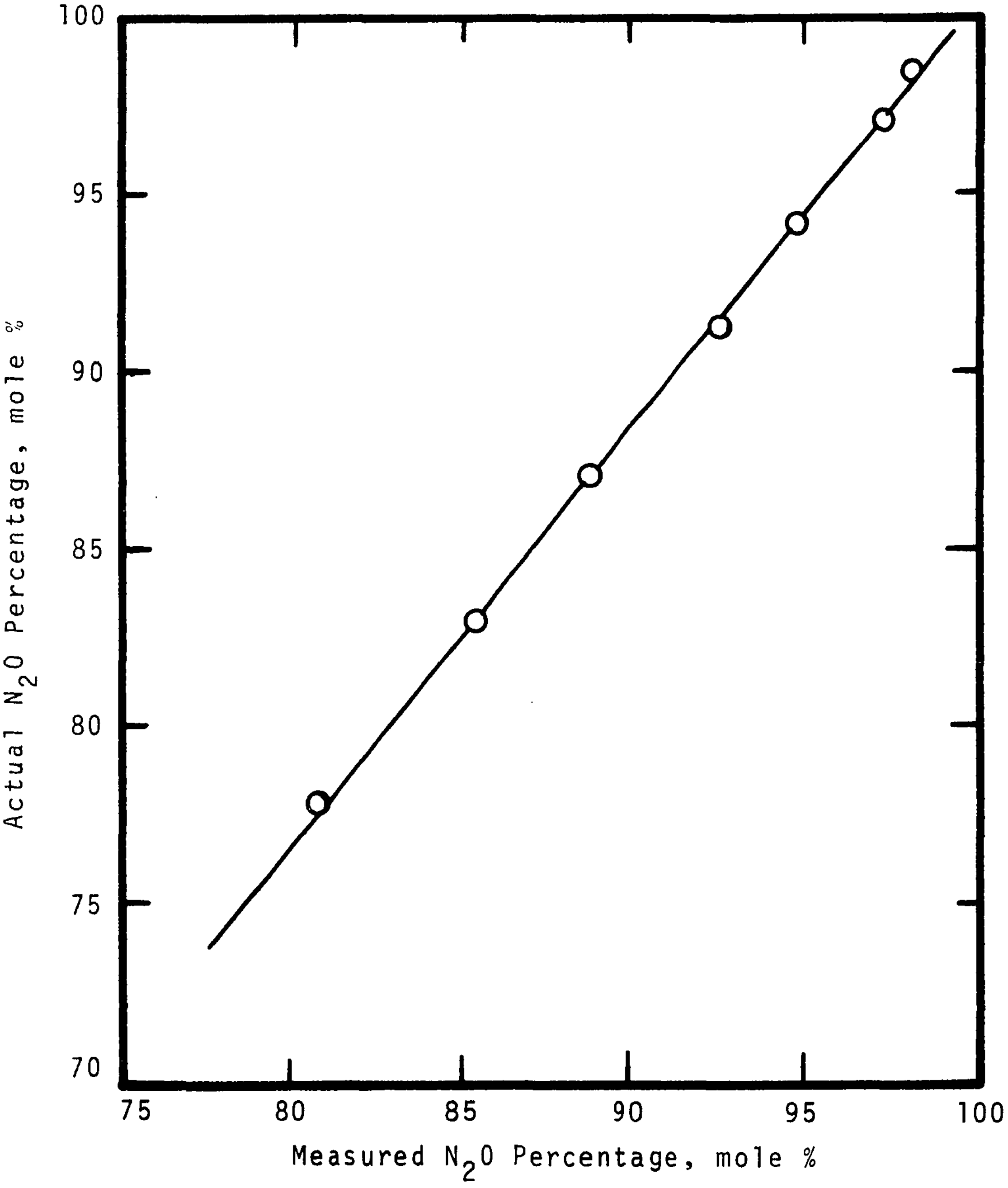

Figure 18. Nitrous Oxide Calibration on Chromosorb 102.

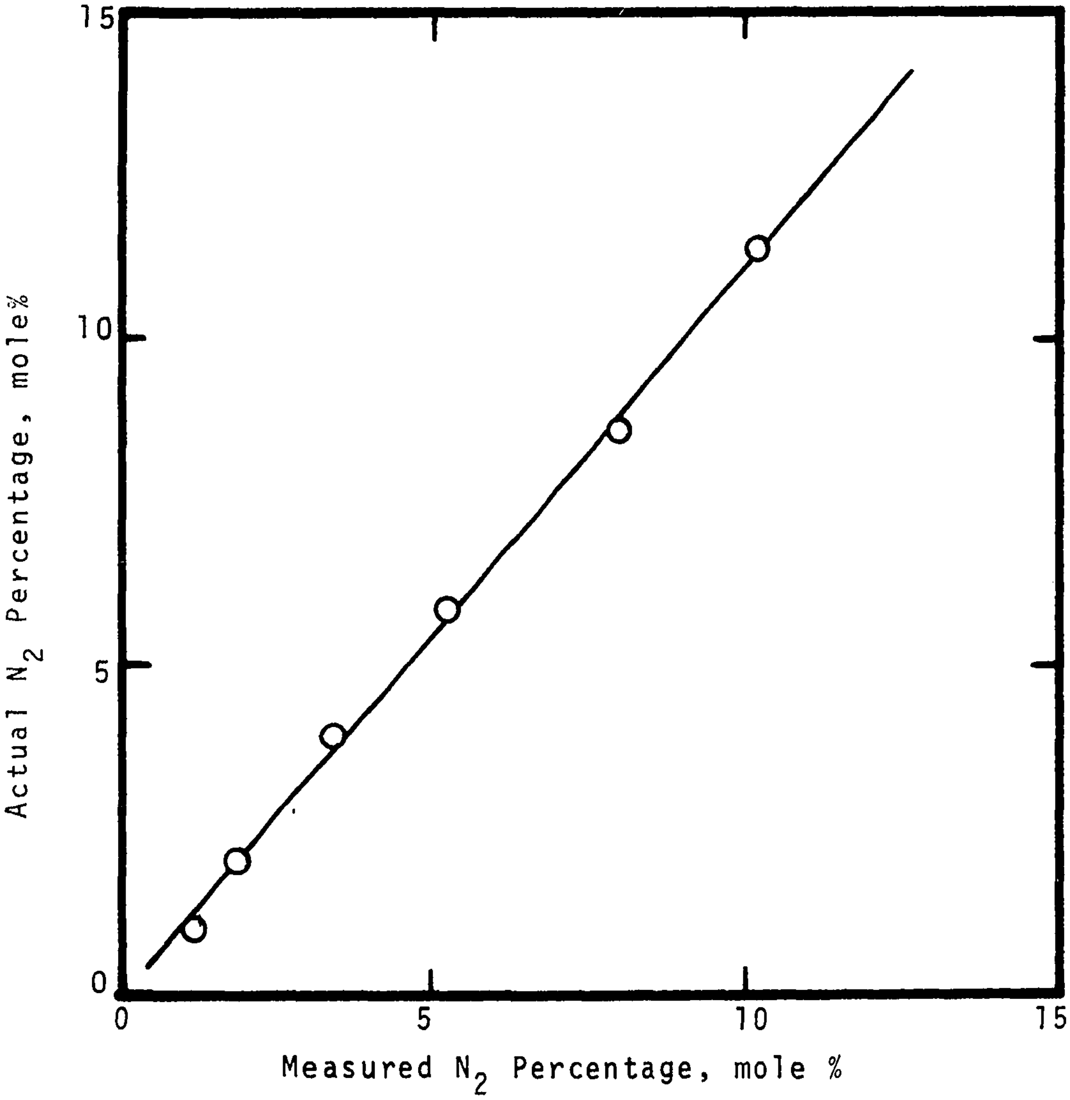

Figure 19. Nitrogen Calibration on Molecular Sieves.

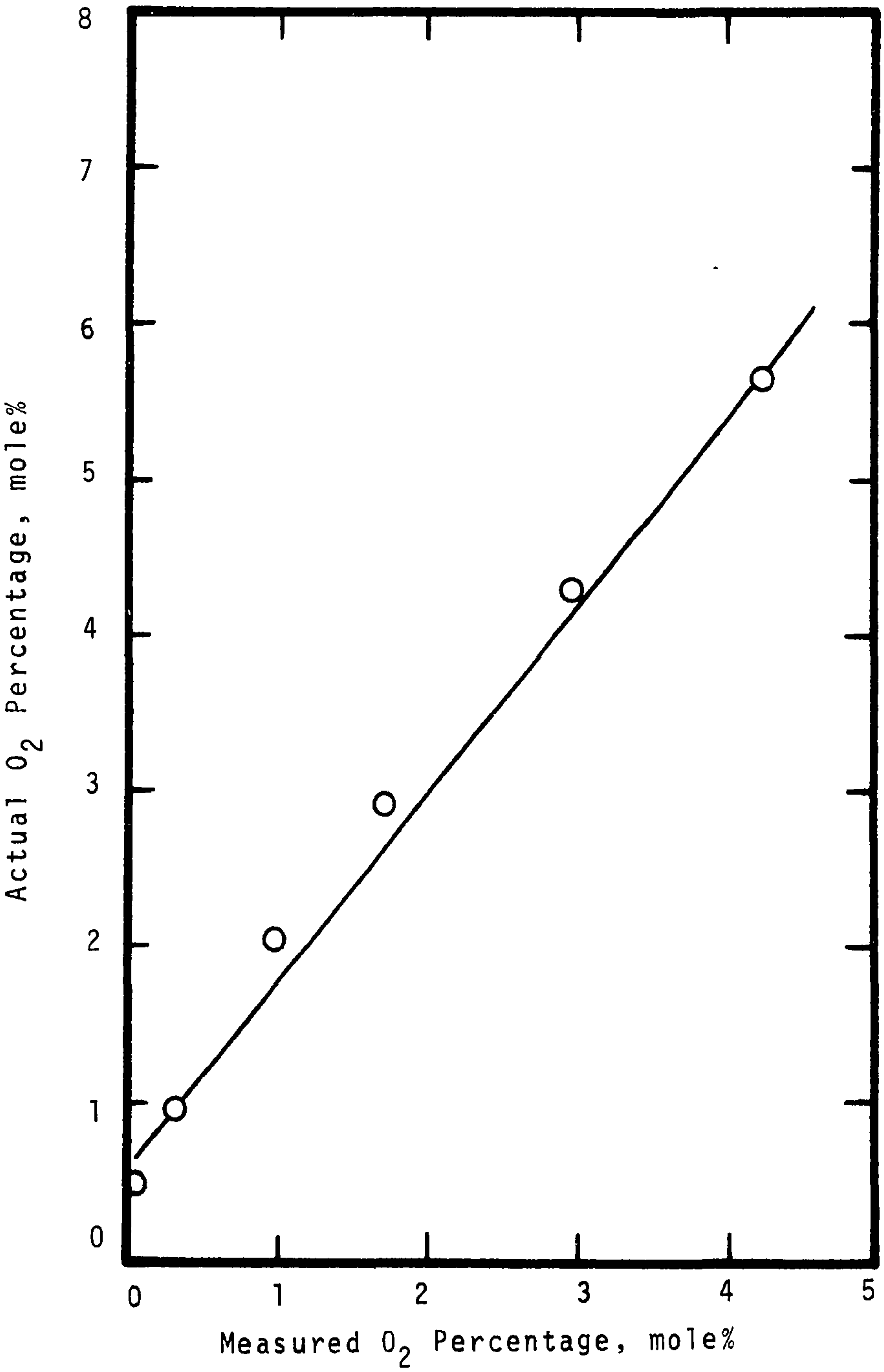

Figure 20. Oxygen Calibration on Molecular Sieves.

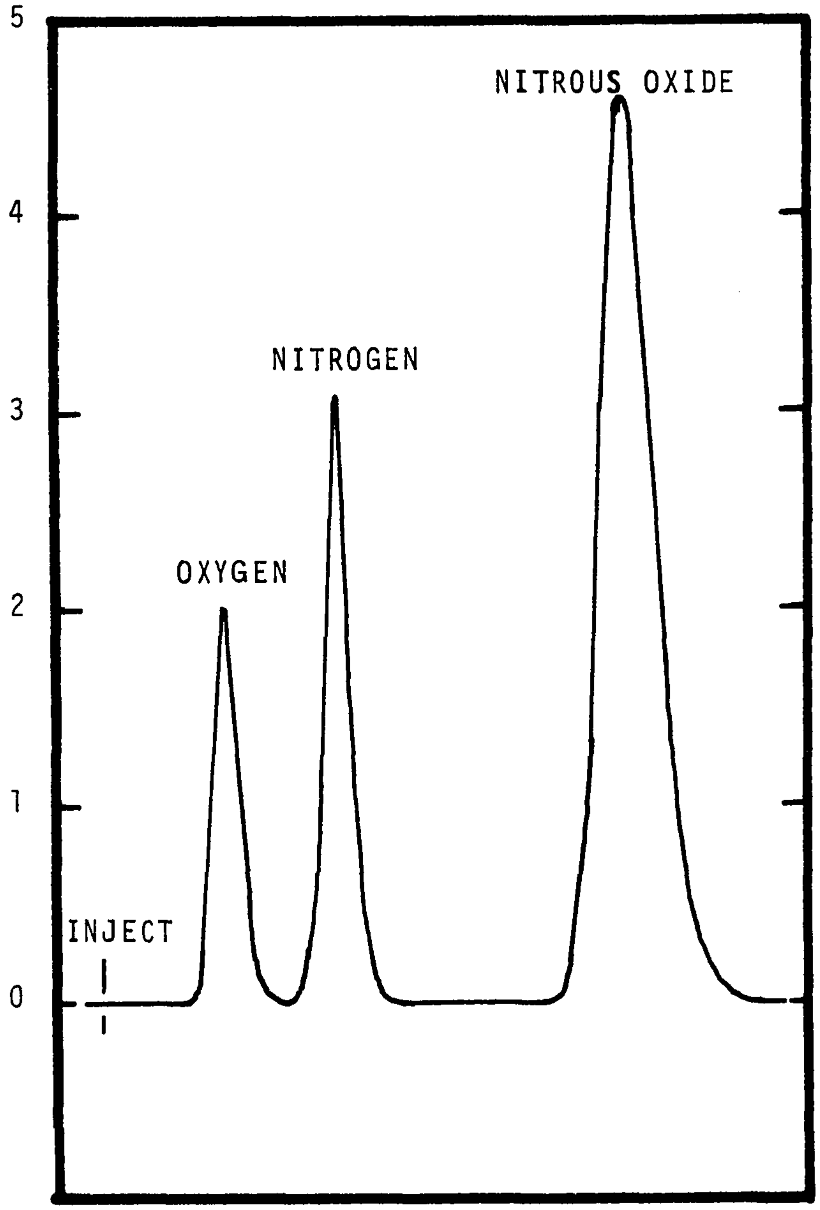

Figure 21. Typical Chromatogram on Mole-
Cular Sieves.

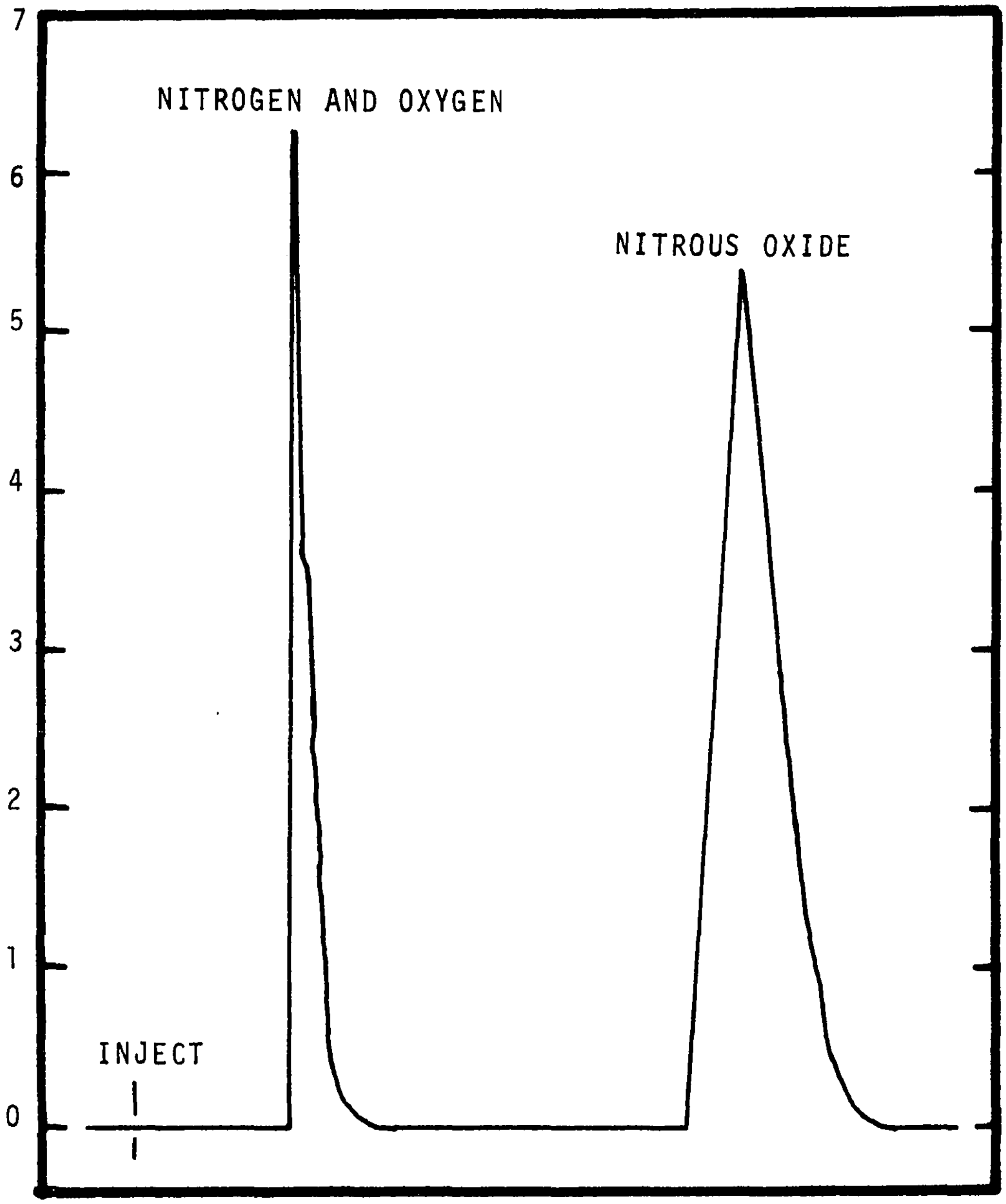

Figure 22. Typical Chromatogram on Chromosorb 102.

CHAPTER VII

PROBLEMS ENCOUNTERED

Inherent in the execution of each run was the extended period of time required to heat the body of sand in the bath to the required run temperature. While this was an annoying procedure, it was by no means a major problem. The majority of the runs in this investigation proceeded smoothly with few problems. Occasionally, the pressure transmitter and controller would become contaminated with a small amount of oil which had bypassed the trap in the instrument air line. The result would be very ragged pressure control with fluctuations of several pounds pressure, making it impossible to get accurate flow measurement of the product gas stream. After the air lines were cleaned, this problem would correct itself and the subsequent runs would then proceed smoothly with excellent pressure control.

During Run 26, the Research pressure control valve became "frozen" in the closed position and the run had to be halted. Subsequent disassembly of the valve revealed that localized stress corrosion caused by the hot gases and the constant movement of the valve stem in the seat had resulted in a corrosive fusion between the stem and seat, making the valve inoperative. The corroded portions of the valve were replaced and no further problems were encountered with the valve. The corrosion occurred with a type 316 stainless steel valve stem, so a type 316L or 317 stainless steel would probably be required to prevent a similar stem failure.

The only major problem faced during the investigation was a detonation in the feed gas system during the course of Run 24. The detonation occurred in the check valve immediately preceeding the reactor, resulting in the complete destruction of the check valve and in the rupture of a 3000 psia pressure relief disc located immediately upstream from the check valve. It is estimated that the operating conditions of the check valve at the time of the detonation were about 105°F and 855 psia pressure. Since the maximum operating pressure of the relief disc and check valve was reported to be 3000 psia at 72°F, the detonation created a pressure surge at least 3.55 times the operating pressure at that time.

Subsequent inspection of the exploded check valve revealed that the connecting threads on each end unexpectedly indicated the presence of graphite thread lubricant. It is proposed that the detonation was caused by direct contact between a portion of this lubricant and nitrous oxide under pressure. Nitrous oxide behaves very similarly to oxygen when under pressure. Therefore, as for oxygen, all equipment to be used for nitrous oxide service should be thoroughly cleaned with a degreasing solvent before use.

Following the detonation, all portions of the system were again thoroughly cleaned with trichloroethylene, an approved degreasing solvent for oxygen service. No further problems were encountered with detonations, and the experimental program was completed.

Although nitrous oxide is non-toxic and non-flammable, it is still potentially a hazardous material to handle when heated under pressure. Nitrous oxide is an oxidizing agent which will detonate upon contact with grease, oil, or carbonaceous material under pressure. Furthermore, since it decomposes on a self-sustaining basis if sufficient heat is added initially, nitrous oxide itself will explode when the appropriate pressure and temperature conditions prevail. However, the theoretical analysis of the explosion mechanism of nitrous oxide is not developed sufficiently at present to be able to predict accurately the conditions at which explosions will occur.

Hunter (29) reported that when pressures in the range of 60-70 atmospheres were attempted in his investigation, several explosions resulted, destroying the apparatus in each case. He felt that the explosions were the result of contamination of the nitrous oxide with grease forced from the valve packings by the heating. In 1962, studies of the detonability of pure nitrous oxide and several mixtures with nitrogen and air were made at elevated temperatures and pressures by Krisjansons, Bollinger, and Edse (36). Using exploding wire and glow wire ignitors, they found that explosions could be created in the temperature range of 500° to 600°C for pure nitrous oxide if the operating pressure was above 5 atmospheres. Explosions could not be produced in the nitrous oxide - air mixture, but slow reactions were observed between 593° and 887°K. No reactions could be initiated in any of the mixtures containing nitrogen.

Laughrey, Bollinger, and Edse (39) studied the detonability of pure nitrous oxide at initial temperatures from 23° to 210°C and initial pressures from 21 to 207 atmospheres in a high-pressure detonation tube. The maximum impact pressure obtained was 3.66 times the initial pressure which is lower than the value expected for a detonation wave. Also, the time interval between ignition of the gas and occurrence of maximum pressure was a relatively long one-to-four seconds. However, during some of the experiments at initial pressures of 78 atmospheres and above, and at initial temperatures near 210°C, a more rapid reaction occurred as the pressure rise neared its maximum value. The investigators felt that this observation was characteristic of a moderate explosion of the remaining nitrous oxide in the tube.

Thus, in the present investigation, an explosion occurring at 855 psia could have easily resulted in the creation of an impact pressure capable of destroying the check valve and pressure relief disc. Of course, the presence of carbon contamination in the check valve created a condition all the more favorable for an explosion.

CHAPTER VIII

METHOD OF ANALYSIS

Homogeneous Reaction

The stoichiometric equation for the decomposition of nitrous oxide may be expressed as

$$2\ N_2O \longrightarrow 2\ N_2 + O_2 \qquad \text{(VIII-1)}$$

The actual decomposition, however, occurs in a manner much more complicated that Equation VIII-1 would indicate. The first step in the decomposition mechanism is assumed to be a collision between nitrous oxide molecules. A collision of this sort may produce two results, either a decomposition to NO or the production of the activated species N_2O^*. This behavior may be represented by

$$N_2O + N_2O \xrightarrow{k_2} 2\ NO + N_2 \qquad \text{(VIII-2)}$$

$$N_2O + N_2O \underset{k_{-1}}{\overset{k_1}{\rightleftarrows}} N_2O^* + N_2O \qquad \text{(VIII-3)}$$

The activated species can then either deactivate by collision, as shown in Equation VIII-3, or decompose in a unimolecular step.

$$N_2O^* \xrightarrow{k_3} N_2 + O \qquad \text{(VIII-4)}$$

$$O + O \xrightarrow{k_4} O_2 \qquad \text{(VIII-5)}$$

Pease (47) proposed that the unimolecular step could also produce NO through the expression

$$N_2O^* \xrightarrow{k_3} NO + N \qquad \text{(VIII-6)}$$

He considered Equation VIII-6 as the primary reaction and proposed a chain mechanism involving N to describe the decomposition behavior. Using this chain mechanism, Pease developed a rate expression which indicated that the reaction would be of intermediate order. However, in his development of the rate expression, Pease (47) treated both N and NO as transient intermediates. In the same paper Kassel indicated that this procedure is not correct for NO, which accumulates as a reaction product. When only N is taken as a transient, the resulting rate expression shows that the initial rate follows a first-order law, and the half-life, no simple law. The derived rate expression from Kassel's assumptions is

$$-\frac{d(N_2O)}{dt} = 2\,\frac{k_1k_2[N_2O]^2 + k_2k_3[N_2O]^2\,[NO]}{k_2[N_2O] + k_4[NO]} \qquad \text{(VIII-7)}$$

If it is accepted as true that NO must accumulate, then the fact follows that $k_2[N_2O] > k_4[NO]$, and this condition makes it difficult for the apparent reaction order to be much greater than unity under any conditions. On this basis, the Pease mechanism would appear to be invalid.

Equation VIII-4, then, is the correct unimolecular step in the nitrous oxide decomposition. It is assumed in Equation VIII-5 that the recombination of atoms is a fast step. If the steady-state approximation is applied to the activated nitrous oxide molecules, then the following expression is obtained for the concentration of the activated species

$$[N_2O^*] = \frac{k_1[N_2O]^2}{k_3 + k_{-1}[N_2O]} \qquad \text{(VIII-8)}$$

The assumption is made that k_4 is very large, so the rate expression for the primary reaction is

$$-r_1 = \frac{k_3k_1[N_2O]^2}{k_3 + k_{-1}[N_2O]} \qquad \text{(VIII-9)}$$

This expression can be converted to the form

$$-r_1 = \frac{k_1[N_2O]^2}{1 + k_5[N_2O]} \qquad \text{(VIII-10)}$$

with $k_5 = k_{-1}/k_3$. Equation VIII-10 indicates a reaction that is first-order at high pressures and becomes second-order at very low pressures. The mechanism of the secondary reaction producing NO results in the following second-order rate expression at all pressures.

$$-r_2 = k_2[N_2O]^2 \qquad \text{(VIII-11)}$$

Heterogeneous Reaction

The heterogeneous reaction is thought to initiate with the adsorption of a molecule of nitrous oxide in an active site, S, on the gold surface. This behavior may be expressed by

$$N_2O + S \underset{k_{-1}^S}{\overset{k_1^S}{\rightleftarrows}} N_2O \cdot S \qquad \text{(VIII-12)}$$

The decomposition of the adsorbed species then occurs, followed by a recombination of the oxygen atoms and desorption of the products from the gold surface.

$$N_2O \cdot S \xrightarrow{k_3^S} N_2 + O \cdot S \qquad \text{(VIII-13)}$$

$$2\ O \cdot S \xrightarrow{k_4^S} O_2 + 2\ S \qquad \text{(VIII-14)}$$

The rate of decomposition is thus proportional to the number of adsorbed nitrous oxide molecules. If S^o is the total number of active sites available and a fraction, θ, of them are occupied by the adsorbed nitrous oxide, the rate of the surface reaction may be expressed by the product $S^o\theta$. The Langmuir adsorption isotherm (1) relates θ and the concentration of nitrous oxide in the gas phase as

$$\theta = \frac{b[N_2O]}{1 + b[N_2O]} \qquad \text{(VIII-15)}$$

with $b = k_1^S/k_{-1}^S$. The rate of decomposition can then be expressed as

$$-r_S = k_3^S \theta S^o \tag{VIII-16}$$

or

$$-r_S = \frac{k_3^S S^o b[N_2O]}{1 + b[N_2O]} \tag{VIII-17}$$

With weak adsorption, the surface is sparsely covered and $b[N_2O] << 1$. Thus, Equation VIII-17 becomes

$$-r_S = k_S[N_2O] \tag{VIII-18}$$

with $k_S = k_3^S S^o b$. The reaction is seen to be first-order.

Conversely, assuming strong adsorption and high surface coverages, $b[N_2O] >> 1$ and Equation VIII-17 becomes

$$-r_S = k_S' \tag{VIII-19}$$

with $k_S' = k_3^S S^o$. The reaction is now seen to be zero-order. For the conditions employed in this investigation of the nitrous oxide decomposition, the surface reaction on gold may possibly be either zero-order or first-order. An analysis of the data with respect to the two possibilities of reaction order was made, and this discussion appears in a subsequent chapter.

Stoichiometric Analysis

At elevated temperatures, nitrous oxide decomposes primarily to nitrogen and oxygen and secondarily to nitric oxide. This behavior can be represented by the equations

$$\text{(Primary reaction)} \quad N_2O \longrightarrow N_2 + \frac{1}{2} O_2 \qquad \text{(VIII-20)}$$

$$\text{(Secondary reaction)} \quad N_2O \longrightarrow NO + \frac{1}{2} N_2 \qquad \text{(VIII-21)}$$

The nitric oxide formed in the secondary reaction can be oxidized to nitrogen dioxide. This oxidation is thermodynamically favored by lower temperatures. The oxidation of nitric oxide to nitrogen dioxide can occur only to a very small extent at reactor temperatures, 500°-600°C, but it proceeds to completion at the temperature of the water cooler, 5°C (22). This reaction is

$$NO + \frac{1}{2} O_2 \longrightarrow NO_2 \rightleftarrows \frac{1}{2} N_2O_4 \qquad \text{(VIII-22)}$$

Thus, the product gases coming from the water cooler have undergone slightly different reactions than the product gases coming directly from the reactor. These reactions are

$$N_2O \longrightarrow N_2 + \frac{1}{2} O_2 \qquad \text{(VIII-23)}$$

$$N_2O + \frac{1}{2} O_2 \longrightarrow NO_2 + \frac{1}{2} N_2 \qquad \text{(VIII-24)}$$

Due to the difference in the reactions involved, the composition of the product stream leaving the product cooler is slightly different from the composition of the gas leaving the reactor. The product gas samples taken for chromatographic analysis reflect the gas composition following the product cooler. Thus, any NO formed in the decomposition will be chromatographically represented by NO_2. With the knowledge that the product gas changes composition as it passes through the water cooler, the chromatographic analyses can be properly related to the gas composition and conversion in the reactor. A discussion of the formation of NO during the runs of this investigation is presented in Chapter IX.

Development of the Rate Equation

In a tubular flow reactor such as the one used in this investigation, the composition of the flowing fluid varies from position to position along the length of the reactor. Thus, any material balance for a reaction component must be made over a differential element of volume dV in the reactor. The general material balance for a reaction component contained in the differential element of volume at steady-state is

$$\text{Input} = \text{Output} + \text{Conversion by Reaction} \qquad \text{(VIII-31)}$$

Assuming that A is the reacting specie, in a reactor volume dV, the following terms can be defined:

$$\text{Input of A (moles/time)} = F_A$$

$$\text{Output of A (moles/time)} = F_A + dF_A$$

$$\text{Conversion of A by reaction (moles/time)} = (-r_A)\ dV$$

Introducing these terms into Equation VIII-31 gives

$$F_A = (F_A + dF_A) + (-r_A)\ dV \qquad \text{(VIII-32)}$$

Now

$$dF_A = d[F_{A_o}(1 - X_A)] = -F_{A_o}\ dX_A \qquad \text{(VIII-33)}$$

where F_{A_o} = input of A to the reactor (moles/time)

X_A = fraction of reactant A converted into product

Then, substituting Equation VIII-33 into Equation VIII-32 gives

$$F_{A_o}\ dX_A = (-r_A)\ dV \qquad \text{(VIII-34)}$$

which is the basic equation accounting for reactant A in the differential section of the reactor having volume dV. To obtain the expression for the entire reactor, Equation VIII-34 must be integrated. The feed rate to the reactor, F_{A_o}, is constant, but r_A is dependent on the concentration of reactant or conversion, and consequently varies throughout the reactor. Rearranging and integrating Equation VIII-34 gives

$$\int_o^V \frac{dV}{F_{A_o}} = \int_0^{X_{Af}} \frac{dX_A}{-r_A} \qquad \text{(VIII-35)}$$

Thus,

$$\frac{V}{F_{A_o}} = \int_0^{X_{Af}} \frac{dX_A}{-r_A} \qquad \text{(VIII-36)}$$

In any system involving the decomposition of nitrous oxide, a greater number of moles per unit of time exit the reactor than enter, so there is a corresponding volume increase through the reactor. Assume, then, that the volume of the reacting fluid varies linearly with conversion or

$$V = V_o \ (1 + \varepsilon_A X_A) \tag{VIII-37}$$

with V_o being the initial volume and ε_A being the fractional change in the volume of the system between no conversion and complete conversion.

Equation VIII-36 can be considered to be the basic equation for developing the expression for the specific rate constant, k_c, from experimental data. The rate term, $-r_A$, for a first-order reaction is

$$-r_A = k_c \ C_A \tag{VIII-38}$$

Since the total rate of nitrous oxide decomposition was shown by Equation III-9 to be the sum of a homogeneous reaction rate and a surface reaction rate, some accounting must be made in the tubular reactor equation for such behavior. If the assumption is made that both reactions are first-order, then the overall equation for the rate of decomposition is

$$-r_A = k_h \ C_A + k_s \ C_A \tag{VIII-39}$$

where k_h = homogeneous specific rate constant

k_s = surface specific rate constant

The concentration of reactant A can be expressed as

$$C_A = N_A/V \tag{VIII-40}$$

With volume expansion proportional to conversion, we have for Equation VIII-40

$$C_A = \frac{N_{A_o}}{V_o} \frac{(1 - X_A)}{(1 + \varepsilon_A X_A)} = C_{A_o} \frac{1 - X_A}{1 + \varepsilon_A X_A} \qquad \text{(VIII-41)}$$

Substituting Equation VIII-41 into Equation VIII-39 gives

$$-r_A = k_h \, C_{A_o} \frac{1 + X_A}{1 + \varepsilon_A X_A} + k_s \, C_{A_o} \frac{1 + X_A}{1 + \varepsilon_A X_A} \qquad \text{(VIII-42)}$$

Therefore

$$\frac{V}{F_{A_o}} = \int_0^{X_{Af}} \frac{dX_A}{(k_h C_{A_o} + k_s C_{A_o})(1 - X_A)/(1 + \varepsilon_A X_A)} \qquad \text{(VIII-43)}$$

Rearranging Equation VIII-43 gives

$$\frac{C_{A_o} V}{F_{A_o}} = \frac{1}{k_h + k_s} \int_0^{X_{Af}} \frac{(1 + \varepsilon_A X_A)\, dX_A}{1 - X_A} \qquad \text{(VIII-44)}$$

Since τ, the space time, can be defined as

$$\tau = C_{A_o} V/F_{A_o} \qquad \text{(VIII-45)}$$

then Equation VIII-44 becomes

$$\tau = \frac{1}{k_h + k_s} \int_0^{X_{Af}} \frac{dX_A}{1 - X_A} + \frac{1}{k_h + k_s} \int_0^{X_{Af}} \frac{\varepsilon_A X_A \, dX_A}{1 - X_A} \qquad \text{(VIII-46)}$$

Integration and rearrangement gives

$$(k_h + k_s)\tau = -(1 + \varepsilon_A) \ln(1 - X_A) - \varepsilon_A X_A \qquad \text{(VIII-47)}$$

or

$$(k_h + k_s)\tau = (1 + \varepsilon_A) \ln[1/(1 - X_A)] - \varepsilon_A X_A \qquad \text{(VIII-48)}$$

From the defining expression for τ given in Equation VIII-45 and the fact that

$$C_{A_o} = p_{A_o}/RT \qquad \text{(VIII-49)}$$

an equation relating τ to inlet conditions can be given by

$$\tau = p_{A_o}V/RTF_{A_o} \qquad \text{(VIII-50)}$$

For the nitrous oxide decomposition, the value of ε_A is calculated to be 0.5. Thus, substituting Equation VIII-50 and the calculated value of ε_A into Equation VIII-48 gives

$$k_h + k_s = \frac{1.5\ RTF_{A_o}}{p_{A_o}V}\,[\ln(1/(1-X_A))] - \frac{0.5\ RTF_{A_o}}{p_{A_o}V}\,X_A \qquad \text{(VIII-51)}$$

Equation VIII-51 is the basic equation which can be used to evaluate the rate constants k_h and k_s under the assumption that both the homogeneous and surface reactions are first-order.

If the alternative assumption is made that the homogeneous reaction is first-order and the surface reaction is zero-order, then the overall equation for the rate of decomposition is

$$-r_A = k_hC_A + k_s{}^o \qquad \text{(VIII-52)}$$

where k_h = homogeneous specific rate constant

$k_s{}^o$ = surface specific rate constant

Since volume expansion is proportional to conversion, we have

$$-r_A = k_h C_{A_o} \frac{1 - X_A}{1 + \varepsilon_A X_A} + k_s^o \qquad \text{(VIII-53)}$$

Substitution of Equation VIII-53 into Equation VIII-36 produces

$$\frac{V}{F_{A_o}} = \int_0^{X_{Af}} \frac{(1 + \varepsilon_A X_A)\, dX_A}{k_h C_{A_o} (1 - X_A) + k_s^o (1 + \varepsilon_A X_A)} \qquad \text{(VIII-54)}$$

A lengthy but straightforward integration of Equation VIII-54 results in the following

$$\frac{V}{F_{A_o}} = \frac{-1.5\ k_h C_{A_o}}{(\varepsilon_A k_s^o - k_h C_{A_o})^2} \ln \left[1 + \frac{\varepsilon_A k_s^o - k_h C_{A_o}}{k_h C_{A_o} - k_s^o} X_A\right] \qquad \text{(VIII-55)}$$

$$+ \frac{\varepsilon_A X_A}{\varepsilon_A k_s^o - k_h C_{A_o}} \qquad \text{(VIII-55)}$$

The substitution of Equation VIII-45 representing τ and the calculated value of ε_A into Equation VIII-55 gives

$$\tau = \frac{-1.5\ k_h C_{A_o}^2}{(0.5\ k_s^o - k_h C_{A_o})^2} \ln \left[1 + \frac{0.5\ k_s^o - k_h C_{A_o}}{k_h C_{A_o} + k_s^o} X_A\right]$$

$$+ \frac{0.5\ X_A C_{A_o}}{0.5\ k_s^o - k_h C_{A_o}} \qquad \text{(VIII-56)}$$

Equation VIII-56 is the basic equation which can be used to evaluate the rate constants k_h and k_s^o.

Residence Time Calculation

When the density of the fluid flowing in a reactor is the same at all points within the reactor, the following expression is true

$$t = \tau \qquad \text{(VIII-57)}$$

Equation VIII-57 indicates that the mean residence time, t, for fluid in the reactor and the space time, τ, can be used interchangeably. When constant density cannot be assumed, the mean residence time is not related in a simple manner to the other variables and must be determined for each specific situation.

In the tubular reactor used in this investigation, the composition of the fluid changes from point to point within the reactor, so constant density cannot be assumed. As a result, the velocity of flow varies as the fluid passes through the reactor. Therefore, to find the flow rate of fluid, one must determine the residence time dt in a volume element dV and then integrate along the length of the reactor. At conversion X_A for an element of volume dV, we have

$$dt = \frac{dV}{F_A/C_A} = \frac{N_{A_O}\ dV}{F_{A_O} V} \qquad \text{(VIII-58)}$$

From Equation VIII-34 for any differential section of the reactor

$$dV = (F_{A_O}/-r_A)\ dX_A \qquad \text{(VIII-59)}$$

Substituting Equation VIII-59 into Equation VIII-58 and integrating along the length of the reactor gives

$$t = N_{A_o} \int_0^{X_{Af}} \frac{dX_A}{(-r_A)V} \qquad \text{(VIII-60)}$$

With the assumption that both reactions are first-order and the fact that the fluid density change is proportional to conversion, we have

$$t = \frac{1}{k_h + k_s} \int_0^{X_{Af}} \frac{dX_A}{1 - X_A} \qquad \text{(VIII-61)}$$

Upon integration

$$t = - \frac{1}{k_h + k_s} \ln(1 - X_A) \qquad \text{(VIII-62)}$$

If the alternative assumption is made that one reaction is first-order and the other reaction zero-order, the residence time expression is

$$t = \frac{C_{A_o}}{C_{A_o} k_h + \varepsilon_A k_s^o} \ln \left(1 + \frac{C_{A_o} k_h + \varepsilon_A k_s^o}{C_{A_o} k_h + k_s^o} X_A \right) \qquad \text{(VIII-63)}$$

Thus, a survey of Equation VIII-46, Equation VIII-62 and Equation VIII-63 reveals that space time and residence time are not related in a simple manner for the decomposition of nitrous oxide in a tubular reactor.

Estimation of the Experimental Error

An estimate of the error involved when calculating the total specific rate constant by Equation VIII-51 is desired. Error estimates are also desirable for the surface rate constant, k_s, and the homogeneous rate constant, k_h. Since the results are only an estimate, it may be assumed that all the errors in the measured variables contribute independently to the total error. To estimate the error of a function such as $y = \phi(a, b, c, \ldots, z)$, the following expression is used

$$dy = \frac{d\phi}{da}\,\Delta a + \frac{d\phi}{db}\,\Delta b + \ldots + \frac{d\phi}{dz}\,\Delta z \qquad \text{(VIII-64)}$$

where a through z are known to within Δa to Δz for each variable. For the existing reaction system, we have the rate expression

$$k_h + k_s = \frac{1.5\ RT\ F_{A_o}}{p_{A_o}\ V} \ln\left(\frac{1}{1 - X_A}\right) - \frac{0.5\ RT\ F_{A_o}}{p_{A_o}\ V} X_A$$

The estimated deviations of the measured variables are:

Temperature	± 0.3°C
Flow rate	± 0.5 percent
Pressure	± 0.03 atm
Concentration	± 0.5 percent
Reactor volume	± 0.1 ml

These values produced the following expected variations in the parameters in Equation VIII-51

$F_{A_o} = \pm$ 1 percent

$T = \pm 0.3°K$

$V = \pm 0.1$ ml

$p_{A_o} = \pm 0.03$ atm

$X_A = \pm 0.5$ percent

The expected error in the total rate constant is then given by

$$\begin{aligned}
d(k_h + k_s) = {} & \left[\frac{1.5\ RT}{p_{A_o} V} \ln\left(\frac{1}{1-X_A}\right) - \frac{0.5\ RT}{p_{A_o} V} X_A\right] d\ F_{A_o} \\
& + \left[\frac{1.5\ RF_{A_o}}{p_{A_o} V} \ln\left(\frac{1}{1-X_A}\right) - \frac{0.5\ RF_{A_o}}{p_{A_o} V} X_A\right] dT \\
& + \left[-\frac{1.5\ RT\ F_{A_o}}{p_{A_o} V^2} \ln\left(\frac{1}{1-X_A}\right) + \frac{0.5\ RT\ F_{A_o}}{p_{A_o} V^2} X_A\right] dV \\
& + \left[-\frac{1.5\ RT\ F_{A_o}}{p_{A_o}^{\ 2}\ V} \ln\left(\frac{1}{1-X_A}\right) + \frac{0.5\ RT\ F_{A_o}}{p_{A_o}^{\ 2}\ V} X_A\right] dp_{A_o} \\
& + \frac{1.5\ RT\ F_{A_o}}{p_{A_o} V} \left(-\frac{dX_A}{1-X_A}\right) + \frac{0.5\ RT\ F_{A_o}}{p_{A_o} V} dX_A
\end{aligned} \tag{VIII-65}$$

Now, let each of the terms on the right side of Equation VIII-65 be represented by ΔF_{A_o}, ΔT, ΔV, Δp_{A_o}, and ΔX_A respectively. Then the error $\Lambda(k_h + k_s)$ is represented by

$$\Lambda(k_h + k_s) = \pm\sqrt{(\Delta F_{A_o})^2 + (\Delta T)^2 + (\Delta V)^2 + (\Delta p_{A_o})^2 + (\Delta X_A)^2} \tag{VIII-66}$$

Using the run variables of Run 20-315

$F_{A_o} = 0.0062151 \pm 0.0000621$ gm-moles/min

$T = 878.2 \pm 0.3°K$

$V = 239.9 \pm 0.1$ ml

$p_{A_o} = 21.43 \pm 0.03$ atm

$X_A = 0.2240 \pm 0.0011$

and substituting into Equation VIII-66 gives

$$\Delta(k_h + k_s) = \pm 0.00156$$

The computed rate constant at the above conditions was $(k_h + k_s) = 0.0234$ which results in an estimated error of ± 6.67 percent.

Since the value of k_h must be obtained by subtracting the appropriate value of k_s from $(k_h + k_s)$, a separate error analysis was made to determine the expected error in the determination of k_s. Using the run variables of Run 22-485°

$F_{A_o} = 0.0017917 \pm 0.0000179$ gm-moles/min

$T = 758.2 \pm 0.3°K$

$V = 239.9 \pm 0.1$ ml

$p_{A_o} = 7.76 \pm 0.03$ atm

$X_A = 0.0070 \pm 0.000035$

the calculated value of Δk_s was found to be $\pm 50 \times 10^{-7}$. The computed value of k_s was 42×10^{-5} which gives an estimated error of ± 1.18 percent.

While the above percentage values are the expected errors when determining the rate constants, a separate error analysis must be considered for the absolute temperature.

Using the Arrhenius equation, the temperature error in the rate constant can be found in the following manner. For a first-order homogeneous reaction

$$k_h = A_h \exp(-E_h/RT) \tag{VIII-67}$$

and

$$dk_h = \frac{k_h E_h}{RT^2}\, dT \tag{VIII-68}$$

Similarly, for a first-order surface reaction

$$k_s = A_s \exp(-E_s/RT) \tag{VIII-69}$$

and

$$dk_s = \frac{k_s E_s}{RT^2}\, dT \tag{VIII-70}$$

Substitution of numerical values from Runs 20-315 and 22-485° gives $dk_h = 0.000178$ or a ± 1.30 percent error, and $dk_s = 0.0000039$ or a ± 0.88 percent error.

Thus, the total expected error in the value of the surface rate constant, k_s, is ± 2.1 percent. The total expected error in the value of the homogeneous rate constant, k_h, is ± 10.0 percent.

CHAPTER IX

DISCUSSION OF RESULTS

The data obtained in this investigation were analyzed with respect to the unimolecular theories presented in Chapter II using the equations developed in Chapter VIII for the analysis. Rate data were taken for the following ranges of variables:

	Range
Pressure	2 - 69.9 atm 29.5 - 1027 psia
Temperature	445 - 605°C 833 - 1121°F
Feed Rate	40 - 475 std ml/min
Residence Time	2.6 - 17.4 min
Conversion	0.23- 25.80 percent

Table 9 of Appendix E summarizes the results of all the experimental runs. Of the 146 sets of data taken during this investigation, there were 131 data points which appeared to be free from any run abnormalities and could be used in the data analysis.

The runs in this investigation were made at conditions which favored the primary decomposition reaction to nitrogen and oxygen. The primary decomposition is favored by both high temperatures and pressures. In this investigation, the contribution of the secondary reaction producing nitric oxide was very slight, and the amount of NO formed decreased rapidly with pressure. At the lowest pressures studied, the amount of NO formed was not greater than 0.25 percent of the product gas composition. At the high pressures, the amount of NO present had dropped to approximately 0.05 percent of the product gas composition. These results compare quite favorably to those of Hunter (29) taken at 590°C. Hunter found that the mole percent of NO present in the product at the half-life varied from 0.11 percent to 0.07 percent at pressures from 11 atm to 32 atm, respectively. When considering pressures below one atmosphere, Musgrave and Hinshelwood (44) found that at an initial pressure of 200 mm Hg of nitrous oxide, about 3.5 percent of NO was formed during the reaction; at 500 mm Hg, this amount had fallen to less than 2 percent. Therefore, in consideration of operating pressures in excess of several atmospheres, the presence of the small amount of NO formed does not markedly affect the analysis of the primary decomposition reaction. Chromatographic analysis of all run samples revealed the presence of no materials other than N_2, O_2, NO_2, and unreacted N_2O.

As mentioned earlier in Chapter VIII, the total reaction rate observed in this investigation was the sum of a homogeneous reaction rate and a surface reaction rate on the gold. The homogeneous reaction had been shown from past data to be first-order at the conditions employed in this investigation. However, an uncertainty existed as to the reaction order of the surface reaction at these same conditions since kinetic data on a gold surface were not available at pressures above atmospheric. The reaction order of the surface reaction could possibly be either zero-order or first order according to the nature of the Langmuir adsorption isotherm. In order to resolve this question, the data had to be fitted to Equations VIII-51 and VIII-55 to determine which of these equations clearly gave more consistent results.

An examination of Equation VIII-51 reveals that the quantity to be calculated is $k_h + k_s$. A similar examination of Equation VIII-55 indicates that both k_h and k_s^o must be determined. In both cases, it is apparent that the equation alone will not produce explicit values of either k_h and k_s, or k_h and k_s^o. Some manner of isolating the effects of the surface reaction from those of the homogeneous reaction must be employed. Fortunately, data taken during this investigation in the temperature region from 445°C to 485°C at low operating pressures provided information on the surface reaction alone, since the homogeneous reaction was essentially nil under these conditions. An extrapolation of Hunter's rate data (29) to the 445°C to 485°C temperature range revealed that the rate constants obtained in this temperature region were far too small to produce any measurable decomposition of nitrous oxide with the residence times employed in this investigation. Low operating pressures further assured that the homogeneous reaction contribution was negligible in this temperature region.

The values of the surface rate constant obtained at these lower temperatures were then extrapolated to the higher temperature region of the investigation. In this manner, values for both the homogeneous and surface reaction rate constants were obtained over the entire temperature range of the study.

With the knowledge that the rate constants for the homogeneous and heterogeneous reactions could be separated and analyzed independently, the data were first analyzed on the basis of a zero-order surface reaction and first-order homogeneous reaction model using Equation VIII-55. Approximate values of the homogeneous rate constant based upon Kassel's integral from Equation II-38 were introduced to the equation for each point, and a solution by numerical iteration was made for the appropriate surface rate constants. The results indicated that consistent values for a zero-order surface rate constant could not be achieved at any of the temperature levels studied in this investigation. The values of the calculated zero-order rate constants showed a strong drift upward with pressure, resulting in approximately a hundredfold change in the value over the range of pressures considered. Alternatively, the data in the temperature range from 445°C to 485°C were used to calculate zero-order surface rate constants. These rate constants were subsequently used in an extrapolation to temperatures up to 605°C. The extrapolated values of k_s^o were substituted into Equation VIII-55 and a value of k_h was calculated for each data point. The resultant values of k_h were completely inconsistent with the Kassel theory curves developed from Equation II-38. All previous pressure studies have been shown to follow these curves quite closely over the ranges of pressure studied.

Since this inconsistency should not appear in the values of the homogeneous rate constant, the k_s^o values used in Equation VIII-55 must, of necessity, be incorrect. Therefore, the complete lack of agreement of the data with Equation VIII-55 indicated that the surface reaction could not be assumed to be zero-order but might instead be first-order.

If the mechanism of the surface reaction on gold presented in Chapter VIII is again analyzed, adding an extra step to the mechanism as proposed by Yagodovskii and Garsia-Fontes (62) from their decomposition studies on gold films, the resultant rate expression gives a reasonable qualitative explanation for considering the reaction to be first-order. Taking account of the fact that oxygen adsorbed on the surface was considered to be negatively charged, the following mechanism was proposed.

$$N_2O_{(g)} + O^-_{(ads)} \xrightarrow{k_1} N_{2(g)} + O_{2(g)} \qquad \text{(IX-1)}$$

$$S + N_2O_{(g)} \xrightarrow{k_2} N_{2(g)} + S{\cdot}O^-_{(ads)} \qquad (IX-2)$$

$$2\ S{\cdot}O^-_{(ads)} \underset{k_{-3}}{\overset{k_3}{\rightleftarrows}} 2\ S + O_2 \qquad (IX-3)$$

with S referring to an active site on the surface. The authors determined that the rate expression for the disappearance of N_2O could be written as

$$-r_{N_2O} = \frac{2\ k_1 k_2}{k_1 + k_2} C_{N_2O} \qquad (IX-4)$$

The limiting stage of the reaction was thought to be the interaction between the gaseous N_2O and the negatively charged oxygen on the surface. Therefore, it was assumed that $k_1 << k_2$ and the resultant rate expression became

$$-r_{N_2O} = 2\ k_1\ C_{N_2O} \qquad (IX-5)$$

indicating first-order behavior.

Failing to confirm zero-order behavior for the surface reaction as indicated by Equation VIII-55, the data were then analyzed using Equation VIII-51 to determine values of k_h and k_s. The data in the temperature range from 445°C to 505°C were used to calculate k_s at these temperatures, since the homogeneous reaction could be considered as being negligible. The resultant values of k_s were fitted to an Arrhenius plot, and the values from 445°C to 605°C are listed in Table 6. As Figure 23 indicates, the plot of ln k_s versus 1/T followed the expected straight line relationship. The

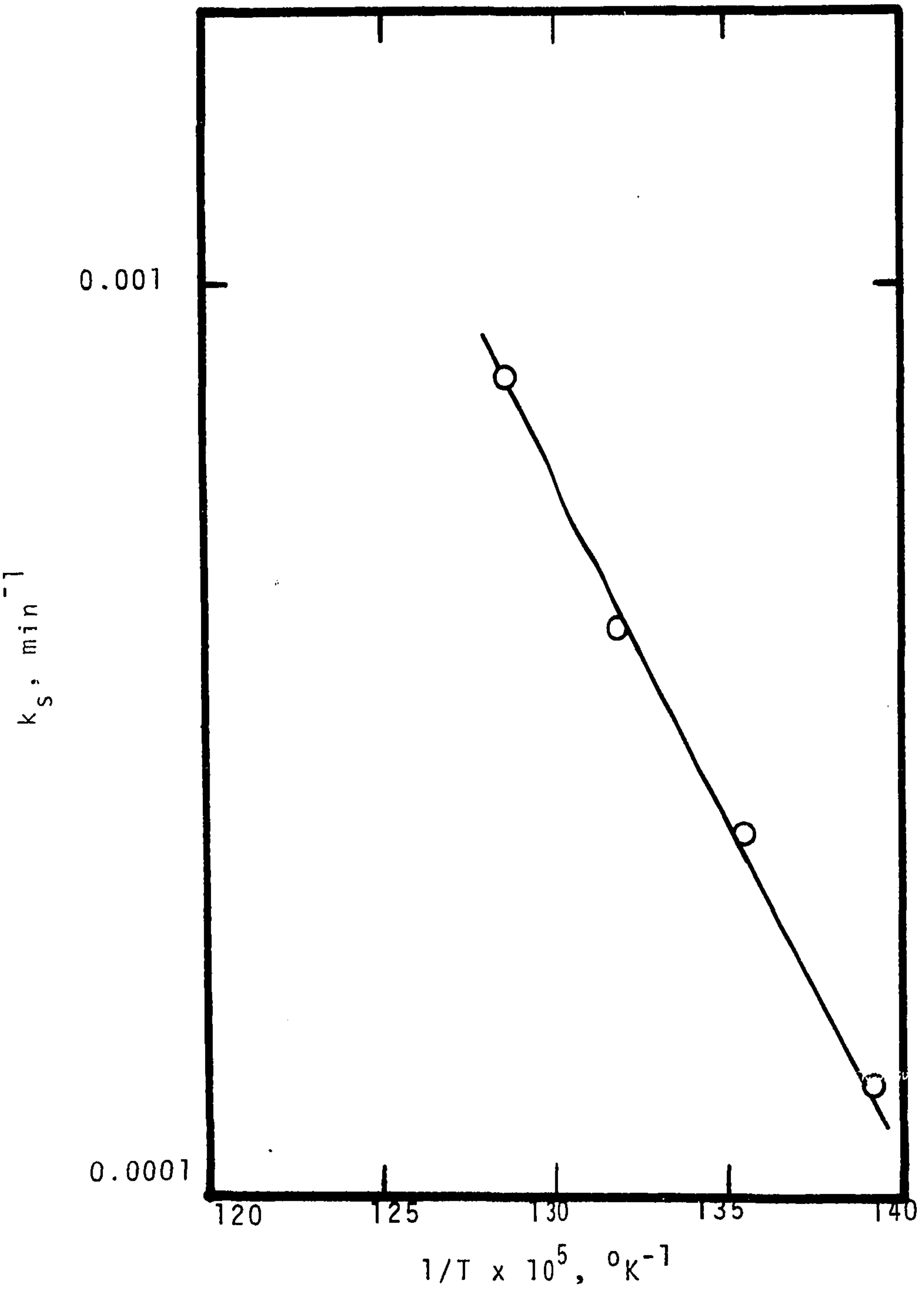

Figure 23. Arrhenius Plot of the Surface Rate Constant.

TABLE 6

SURFACE RATE CONSTANTS

Temperature, °C	k_s, min.$^{-1}$
445	0.00013
465	0.00024
485	0.00044
505	0.00079
525	0.00135
545	0.00235
565	0.00380
585	0.00615
595	0.00770
605	0.00970

activation energy determined from the slope of the curve was 33,900 cal/gm-mole. This value compares favorably with the values of 30,900 cal/gm-mole and 34,600 cal/gm-mole determined by Hinshelwood and Prichard (27) and by Halladay (22), respectively. The surface reaction rate constants obtained from this study are somewhat smaller than those obtained by extrapolating the Arrhenius plot of the Hinshelwood and Prichard constants to the temperatures used in this investigation. The magnitude of the difference is a factor of about five. The most probable explanation for the difference is that the two gold surfaces were different; the wire used by Hinshelwood and Prichard was evidently more active than the gold lining used in this investigation, although no details about the wire were available to compare it to the present gold surface.

Having values of the surface rate constant, k_s, available over the entire temperature range studied in this investigation, Equation VIII-51 again was used to determine the homogeneous rate constants, k_h. Appropriate data were used at six pressure levels to construct Arrhenius plots. As Figures 24 to 29 illustrate, the plots of ln k_h versus 1/T followed a straight line relationship. For each pressure level plotted, the data were fitted to an expression of the form

$$\ln k_h = \ln (A) - E/RT \qquad \text{(IX-6)}$$

using a least-squares technique. Results of these fittings

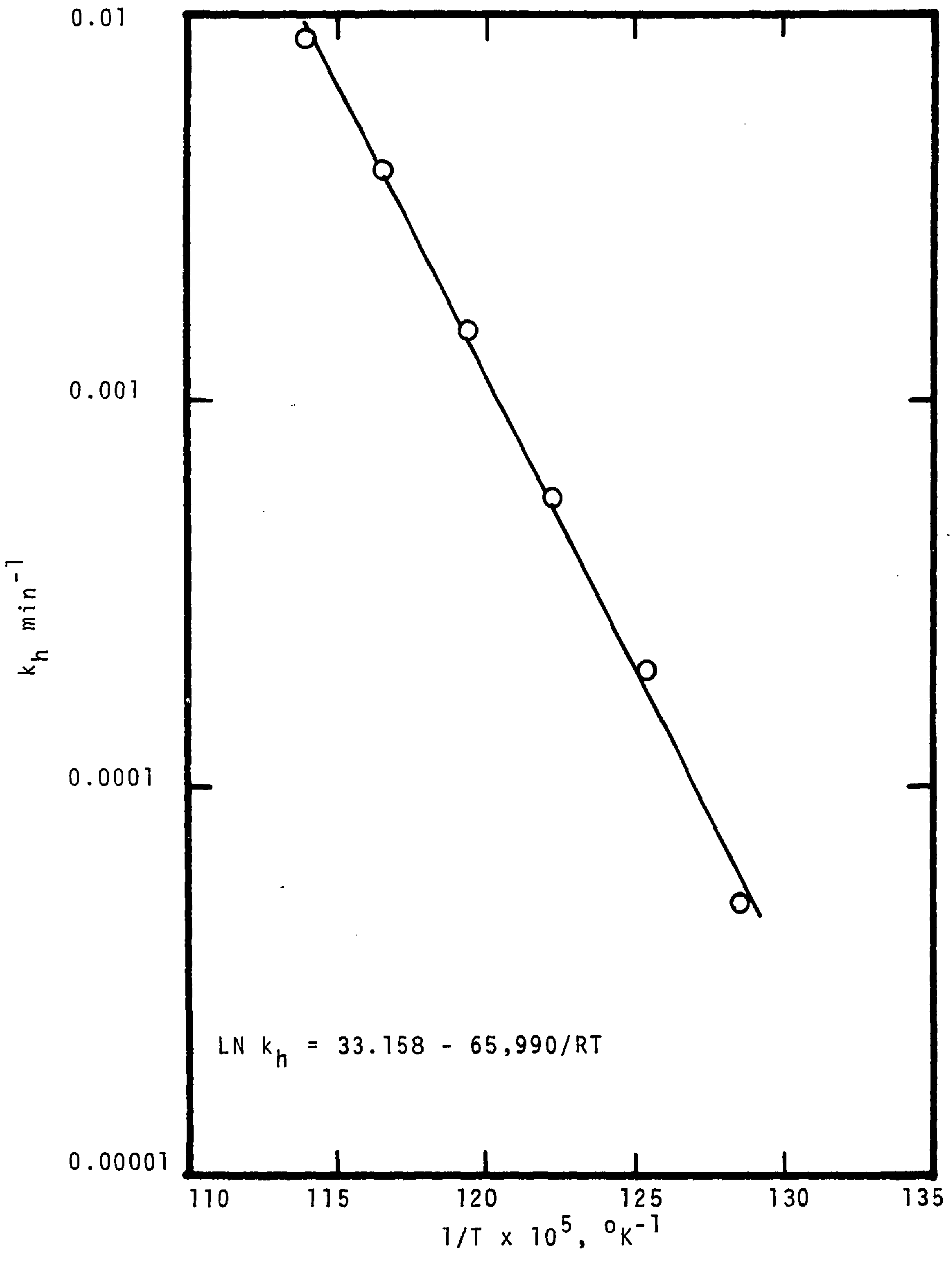

Figure 24. Arrhenius Plot of the Homogeneous Rate Constant at 6.5 Atmospheres.

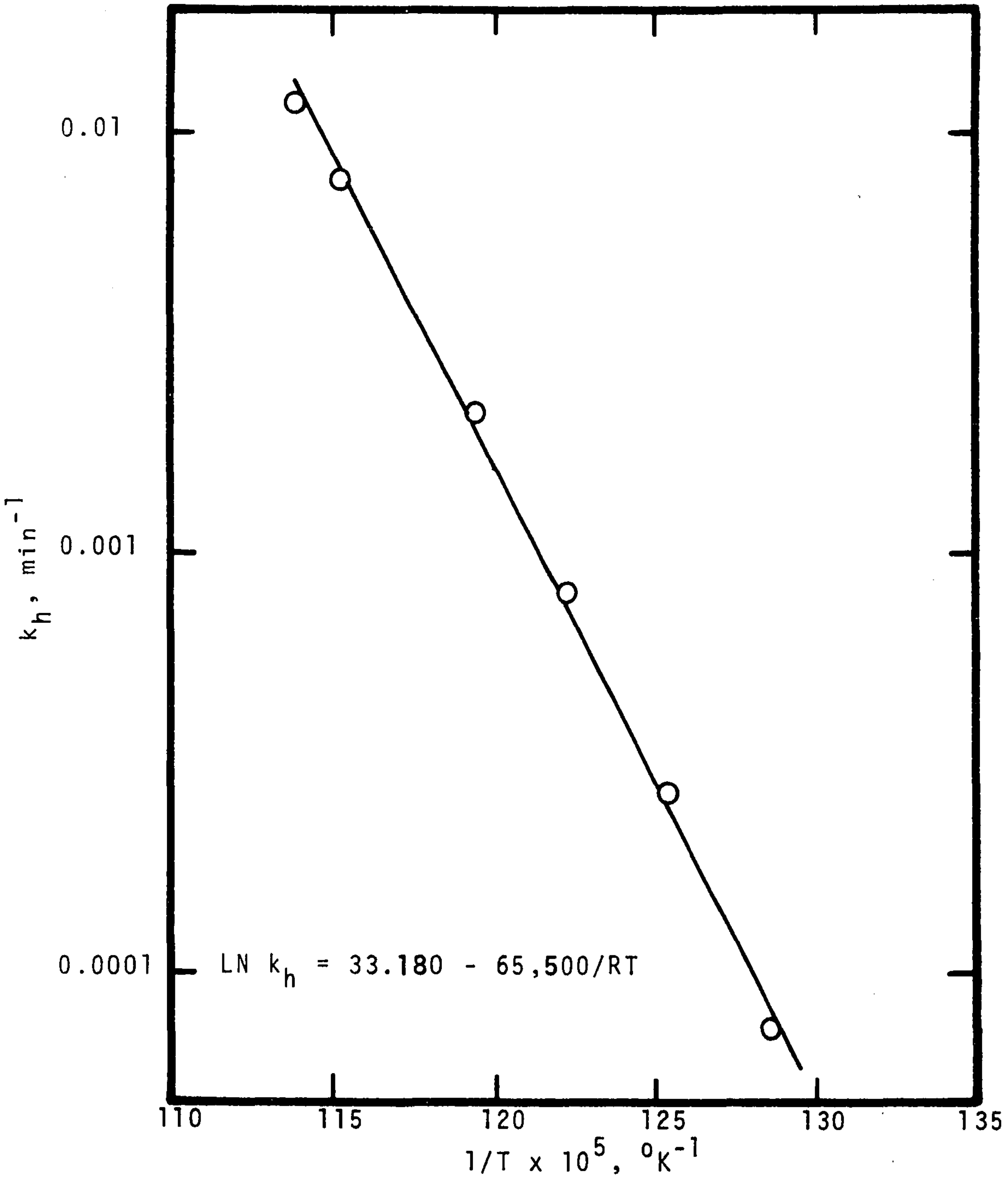

Figure 25. Arrhenius Plot of the Homogeneous Rate Constant at 15.3 Atmospheres.

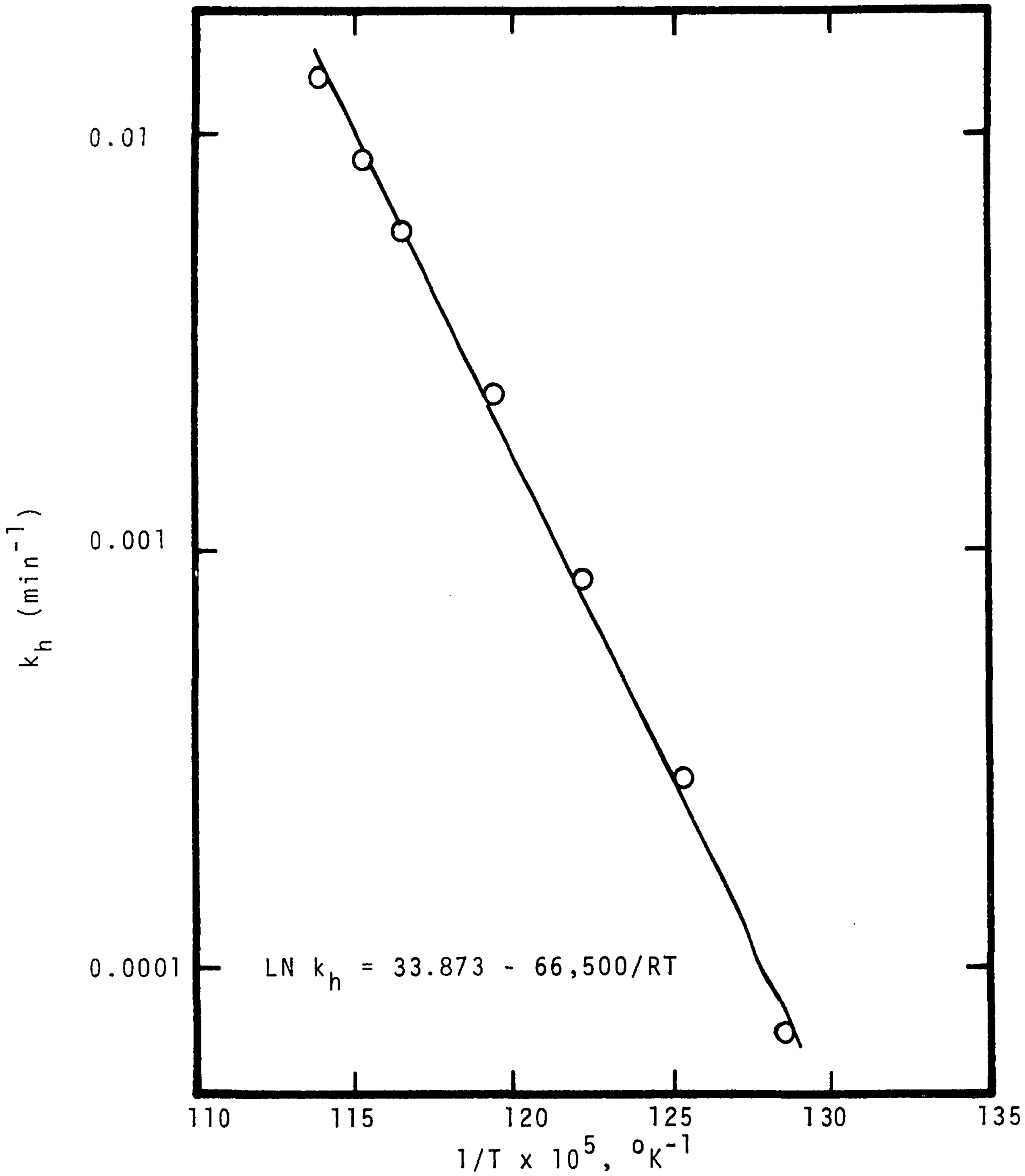

Figure 26. Arrhenius Plot of the Homogeneous Rate Constant at 21.4 Atmospheres.

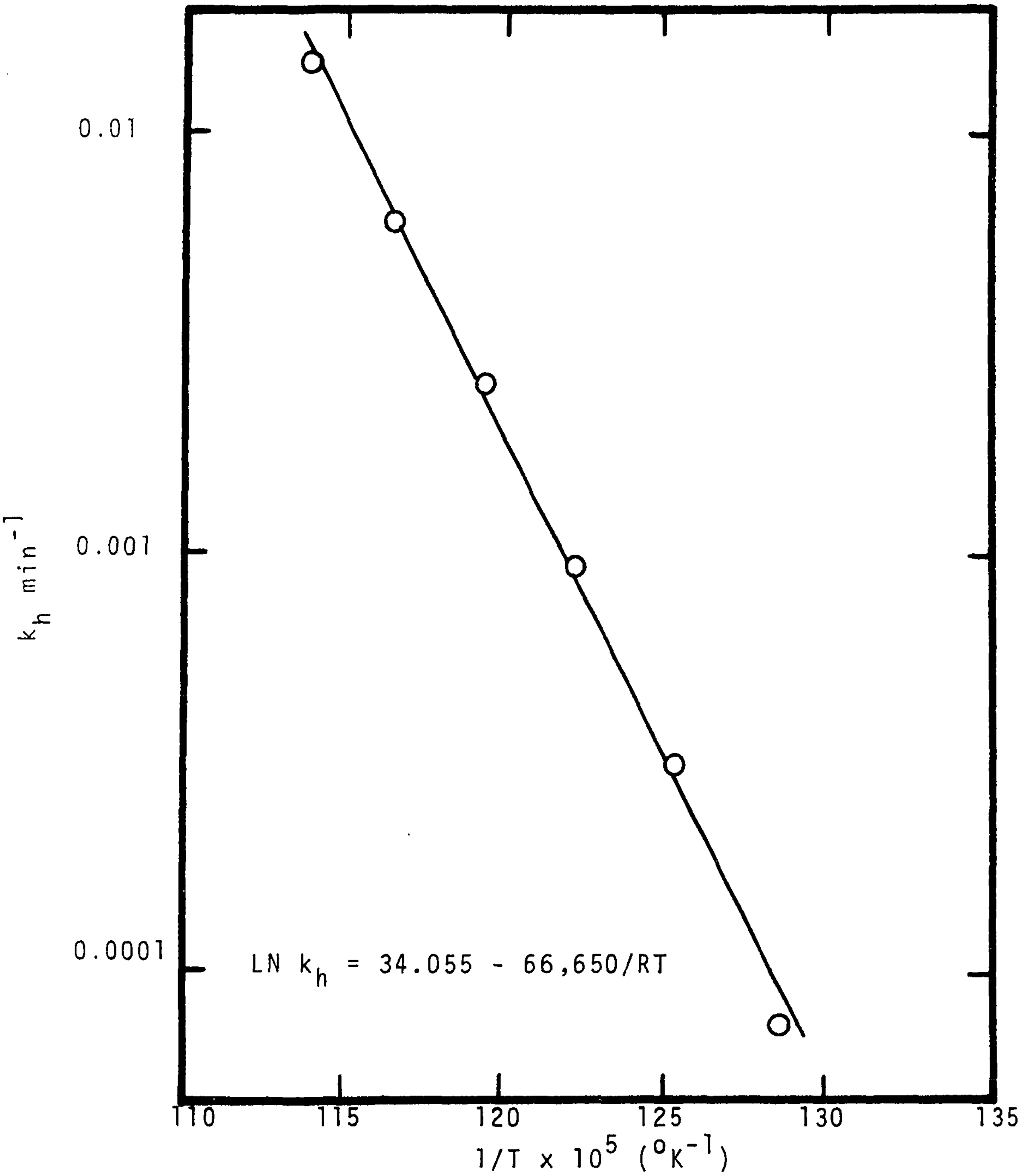

Figure 27. Arrhenius Plot of k_h at 30.3 Atmospheres.

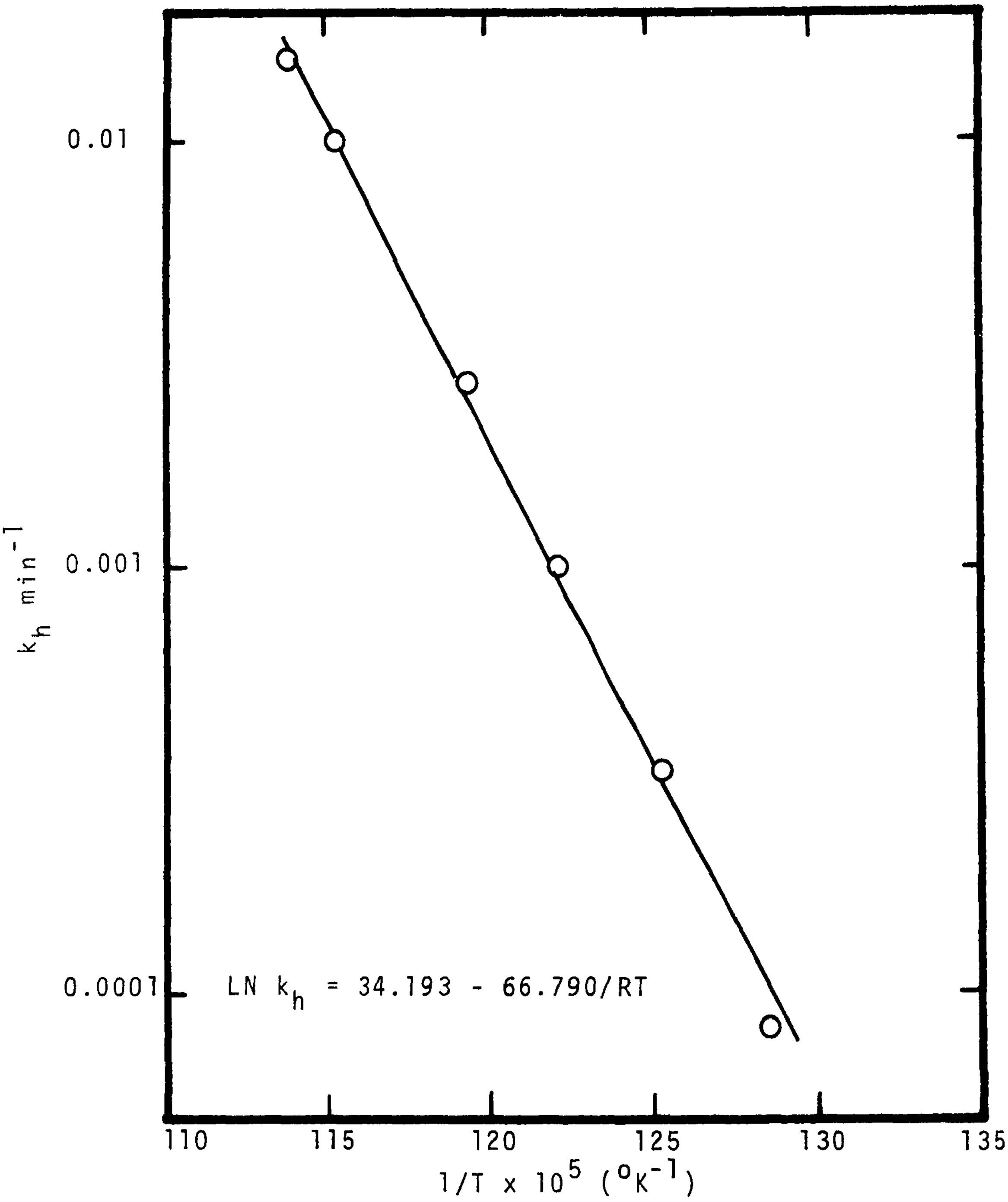

Figure 28. Arrhenius Plot of k_h at 39.1 Atmospheres.

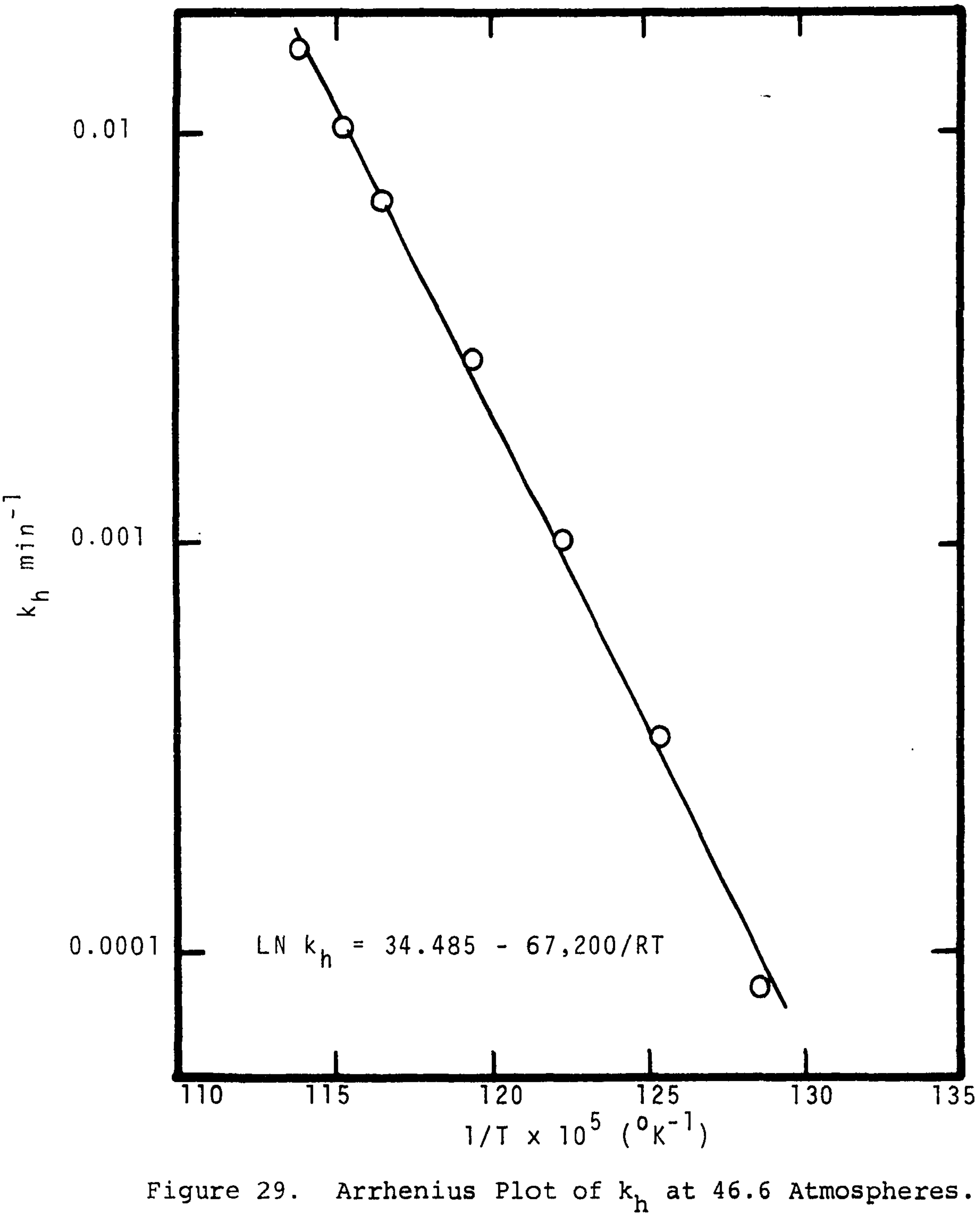

Figure 29. Arrhenius Plot of k_h at 46.6 Atmospheres.

are indicated on each figure. Deviations between values of the rate constant computed from the least-squares fits and the experimental data points averaged about 4.0 percent, which is within the range of the expected experimental error of 10.0 percent predicted in Chapter VIII.

The values of the activation energy obtained in this investigation were within the range of previously reported values for the homogeneous reaction. Hunter (29) reported values of the activation energy of 63,900 cal/gm-mole and 64,900 cal/gm-mole at pressures of 17.6 and 36.3 atm, respectively. Halladay (22) reported a value of 63,500 cal/gm-mole for the homogeneous reaction at 1 atm, although his data indicate that the reported value should actually be 74,000 cal/gm-mole, which appears to be abnormally high. The calculated activation energies from this investigation would be expected to be higher than those reported by Hunter since this investigation was conducted in the absence of any possible catalytic effect due to the glass surface.

Run 23 was made at three different residence times at a fixed temperature (585°C) and pressure (27.2 atm) to determine if there was any residence time effect upon the value of the rate constant. The values of the residence time and corresponding calculated rate constants are given below.

Residence Time, min	Rate Constant, min^{-1}
5.1	0.00610
10.2	0.00610
15.4	0.00608

These data indicate that there was no residence time effect in the decomposition of nitrous oxide under the conditions studied.

Values of Kassel's integral, represented by Equation II-38, were calculated at five temperature levels--545°C, 565°C, 585°C, 595°C, and 605°C. From these calculations, plots of log (k'/k^{∞}) versus log (p) were made. These plots are shown in Figures 30 through 34 with the curves representing the Kassel theory when s equals 2. The experimental values of k_h calculated in this investigation were related to Hunter's values for k_h corrected by Johnston and are plotted as the circles on Figures 30 to 34. At each temperature level indicated, quite good agreement between the Kassel theoretical curve and the actual experimental data can be observed until the higher pressure region is reached. In this region there is a distinct deviation in the experimental data from the theoretical curve. Since the value of the "infinite" pressure rate constant, k^{∞}, has been defined as fixed by the Kassel theory, then the observed deviation in the data seen in Figures 30 to 34 must be the result of decreases in the value of k^1 with increasing pressure.

The experimental values of the homogeneous rate constant obtained at temperature levels of 505°C, 525°C, 545°C, 565°C, 585°C, 595°C, and 602°C have been plotted as a function of pressure; these are shown in Figures 35 to 41, respectively.

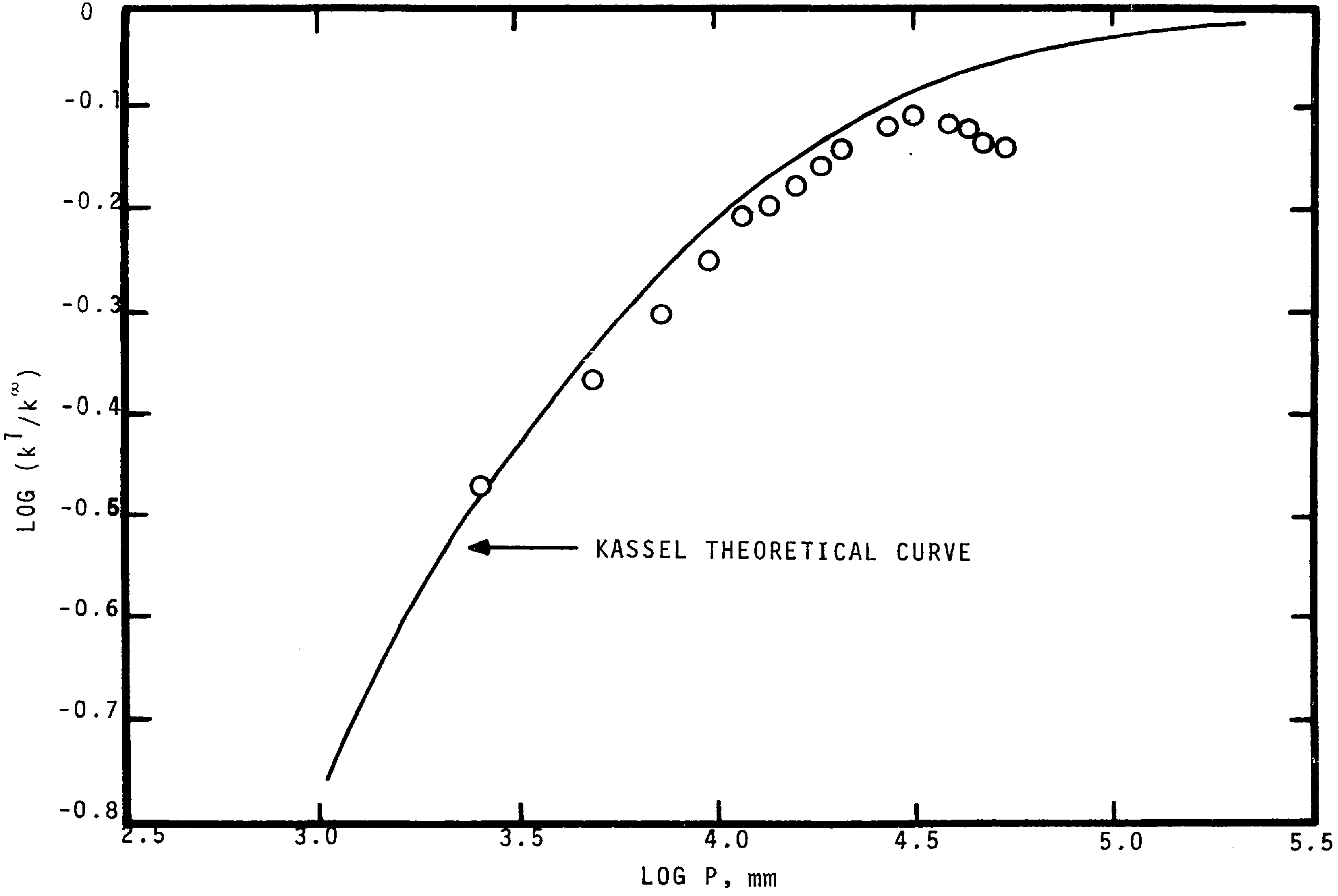

Figure 30. Kassel Theory Relating to Experimental Data at 545°C.

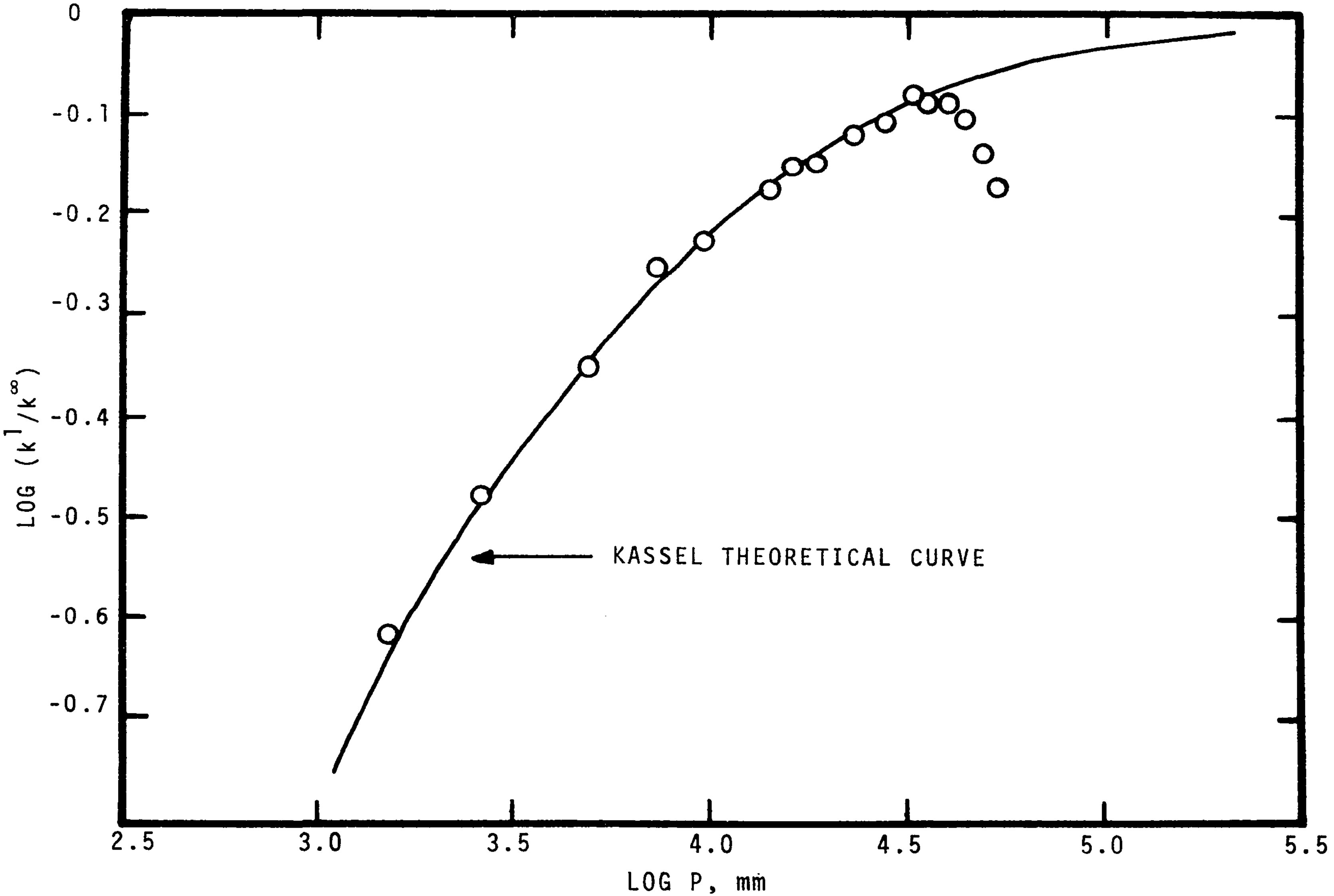

Figure 31. Kassel Theory Relating to Experimental Data at 565°C.

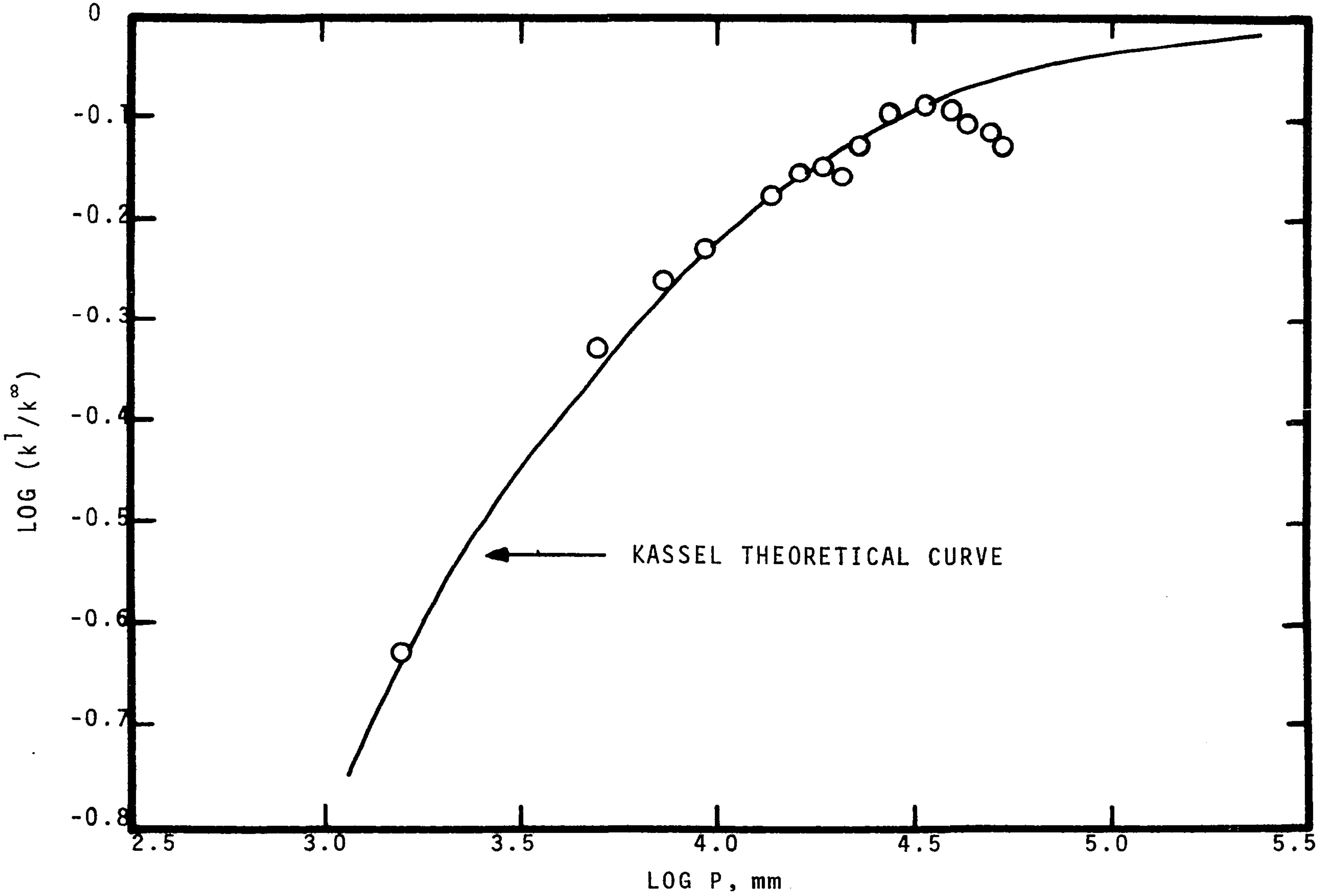

Figure 32. Kassel Theory Relating to Experimental Data at 585°C.

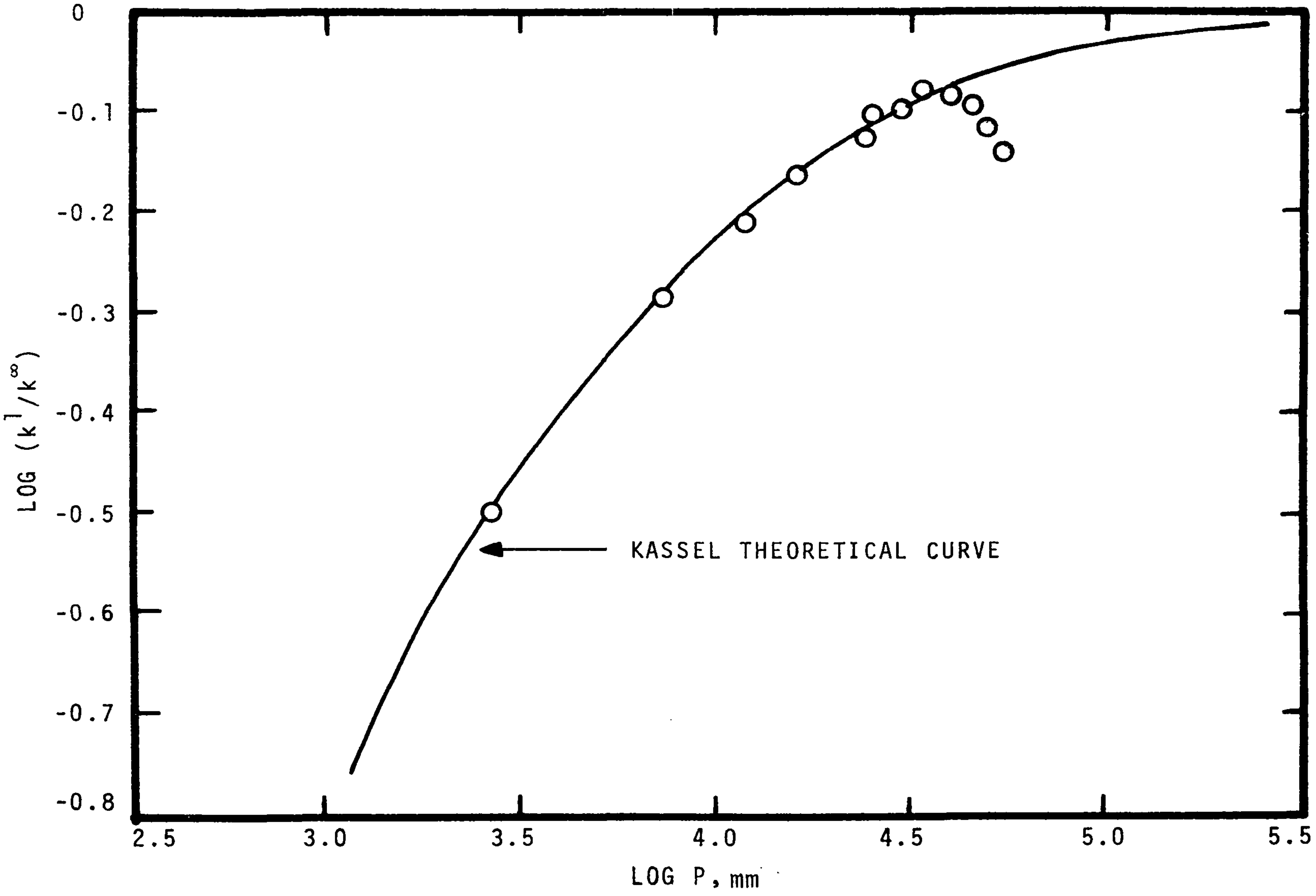

Figure 33. Kassel Theory Relating to Experimental Data at 595°C.

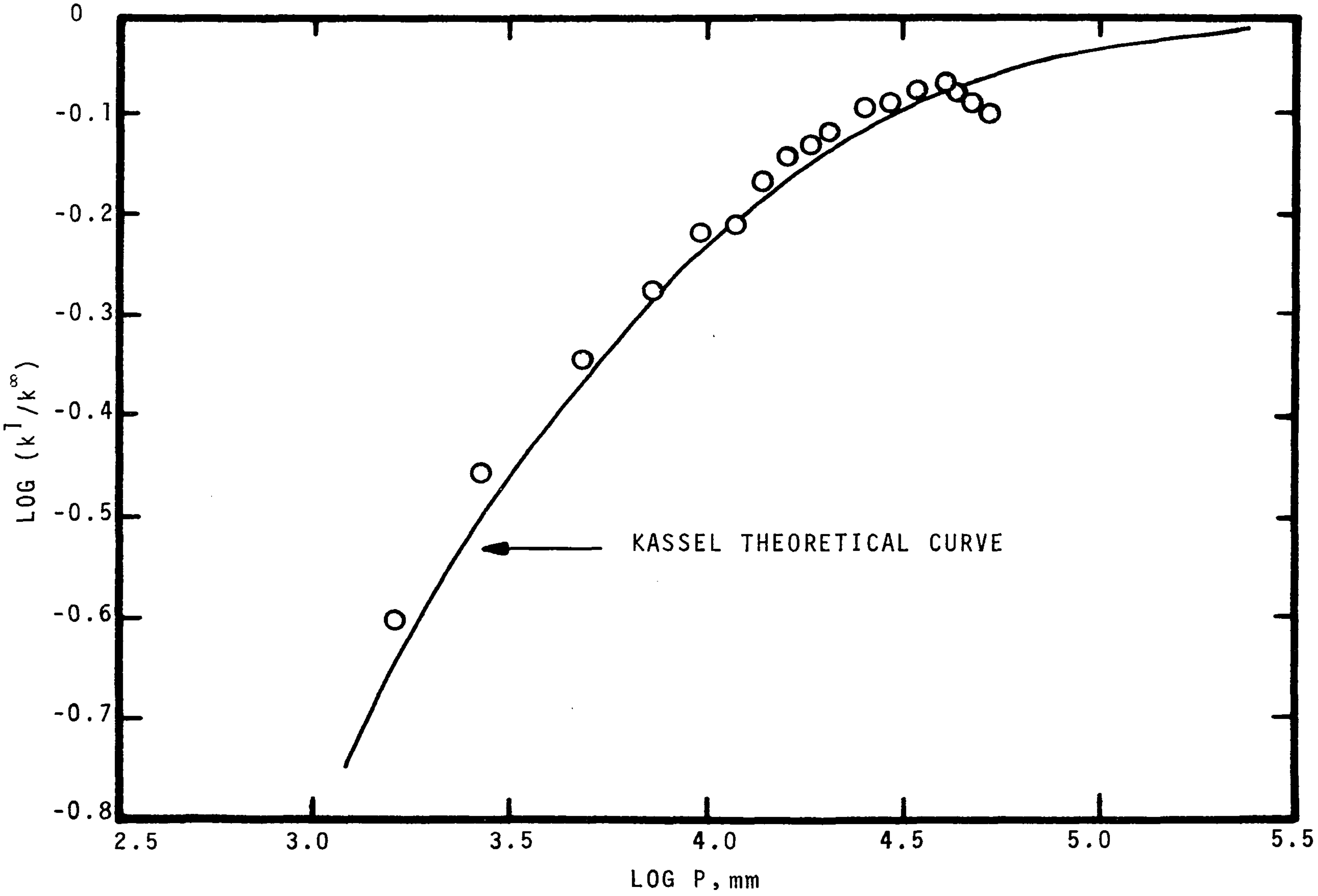

Figure 34. Kassel Theory Relating to Experimental Data at 605°C.

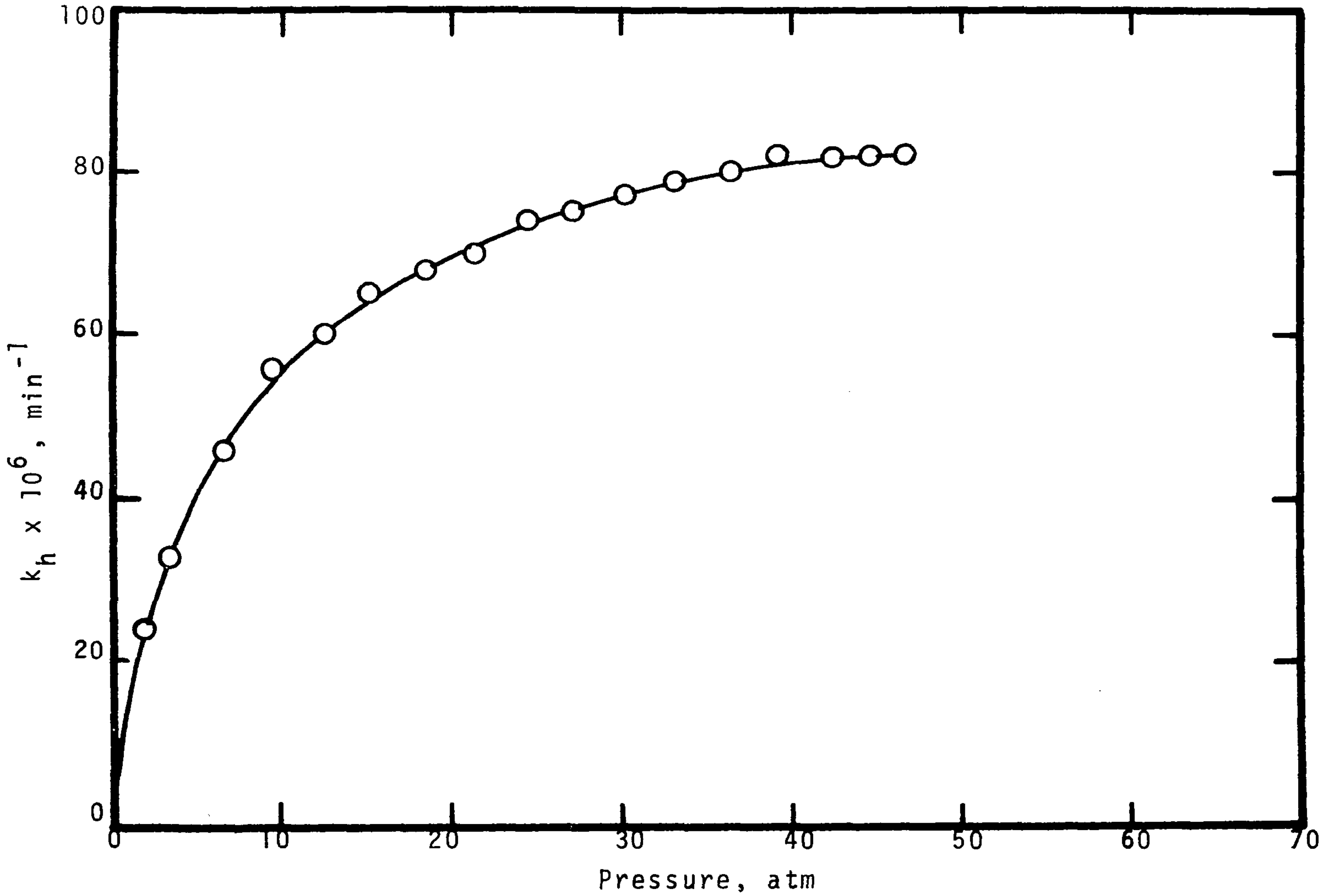

Figure 35. Variation of the Homogeneous Rate Constant with Pressure at 505°C.

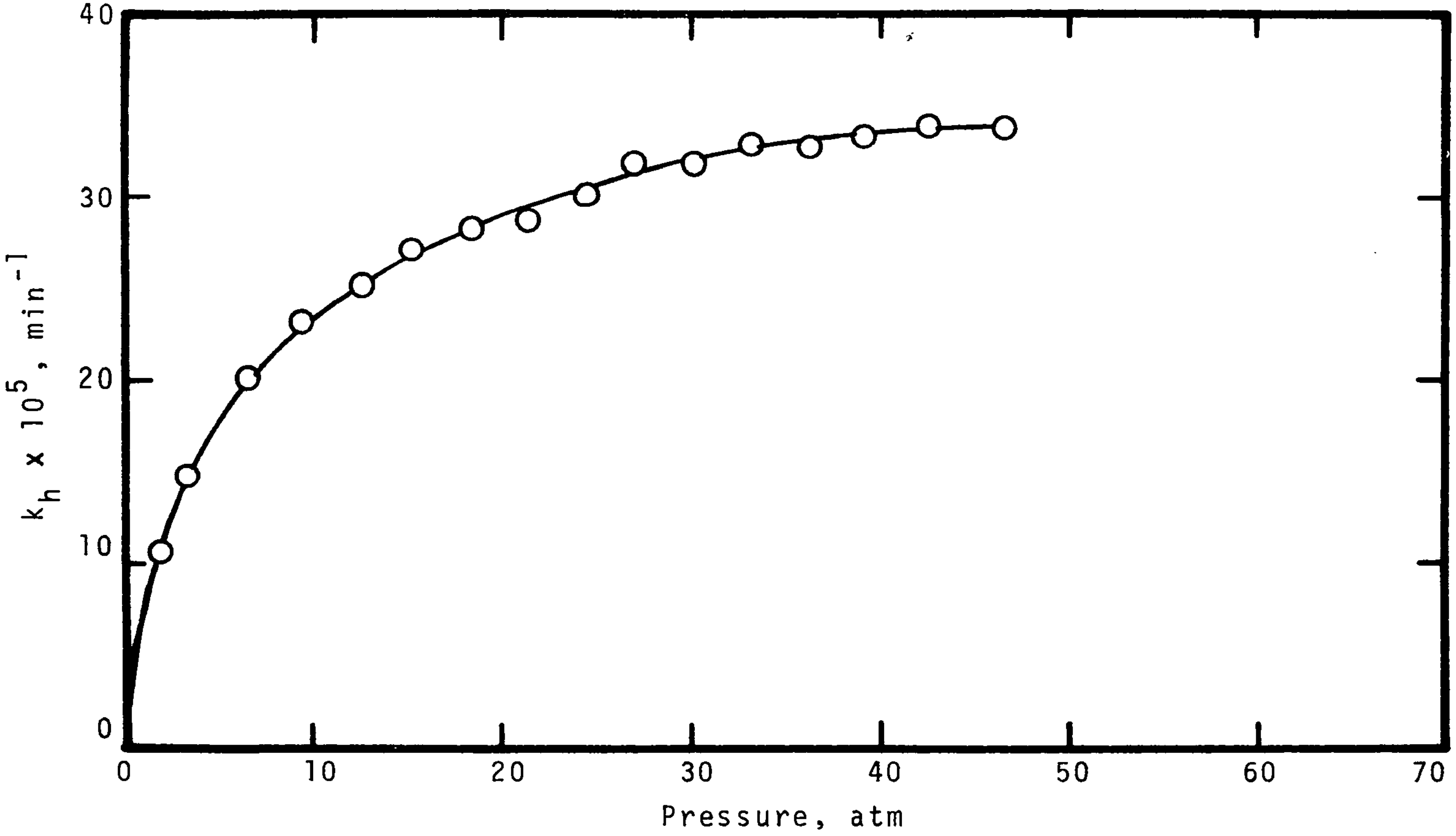

Figure 36. Variation of the Homogeneous Rate Constant with Pressure at 525°C.

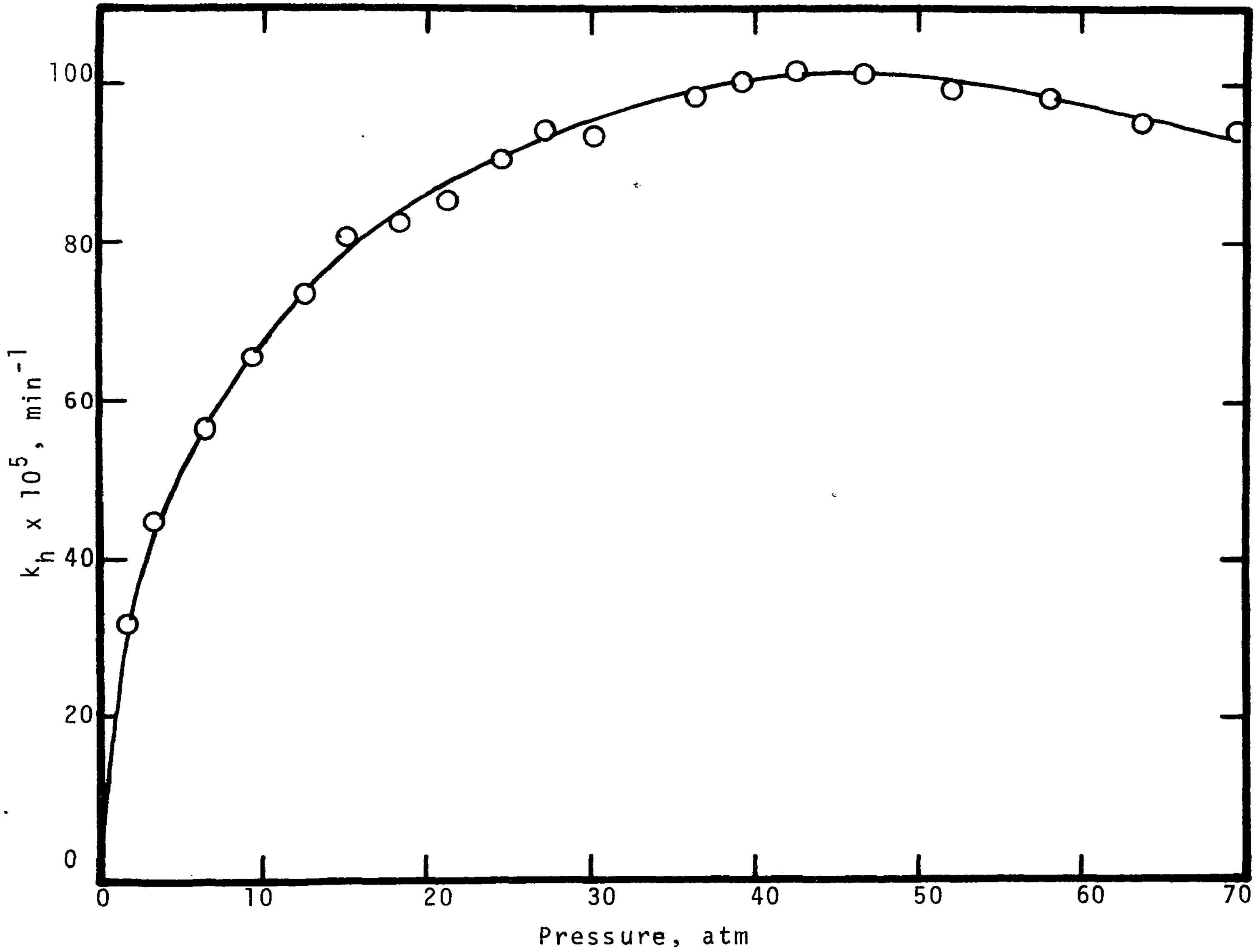

Figure 37. Variation of the Homogeneous Rate Constant with Pressure at 545°C.

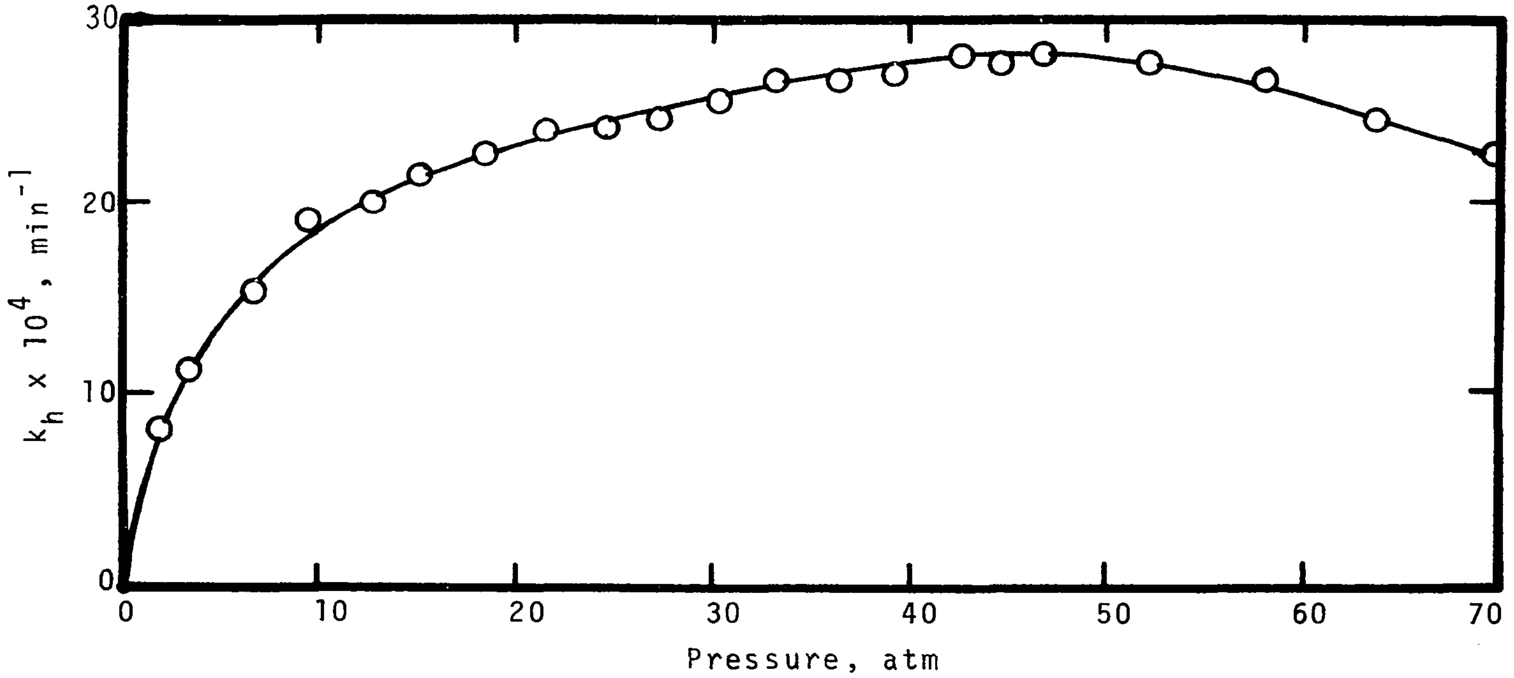

Figure 38. Variation of the Homogeneous Rate Constant with Pressure at 565°C.

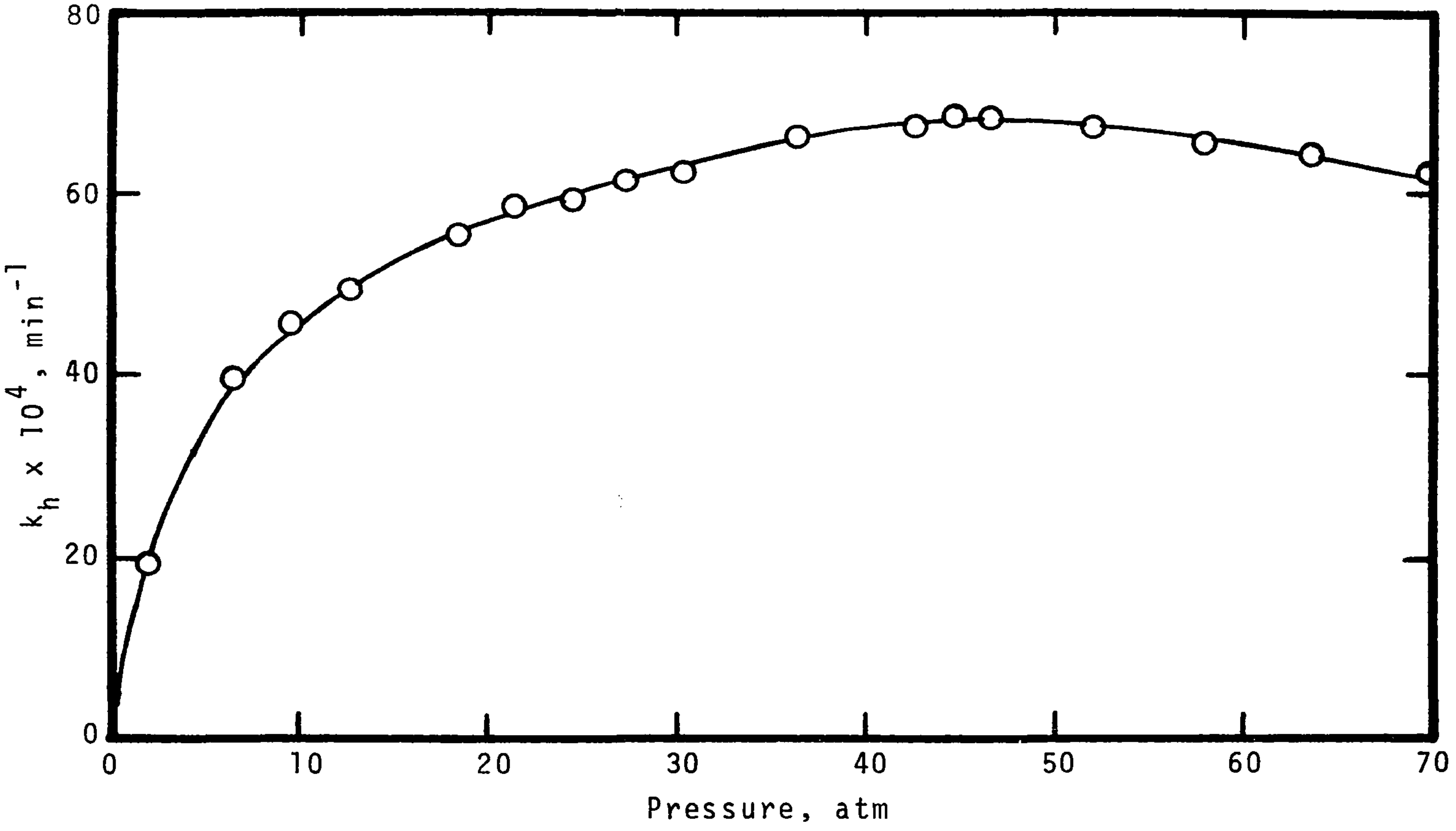

Figure 39. Variation of the Homogeneous Rate Constant with Pressure at 585°C.

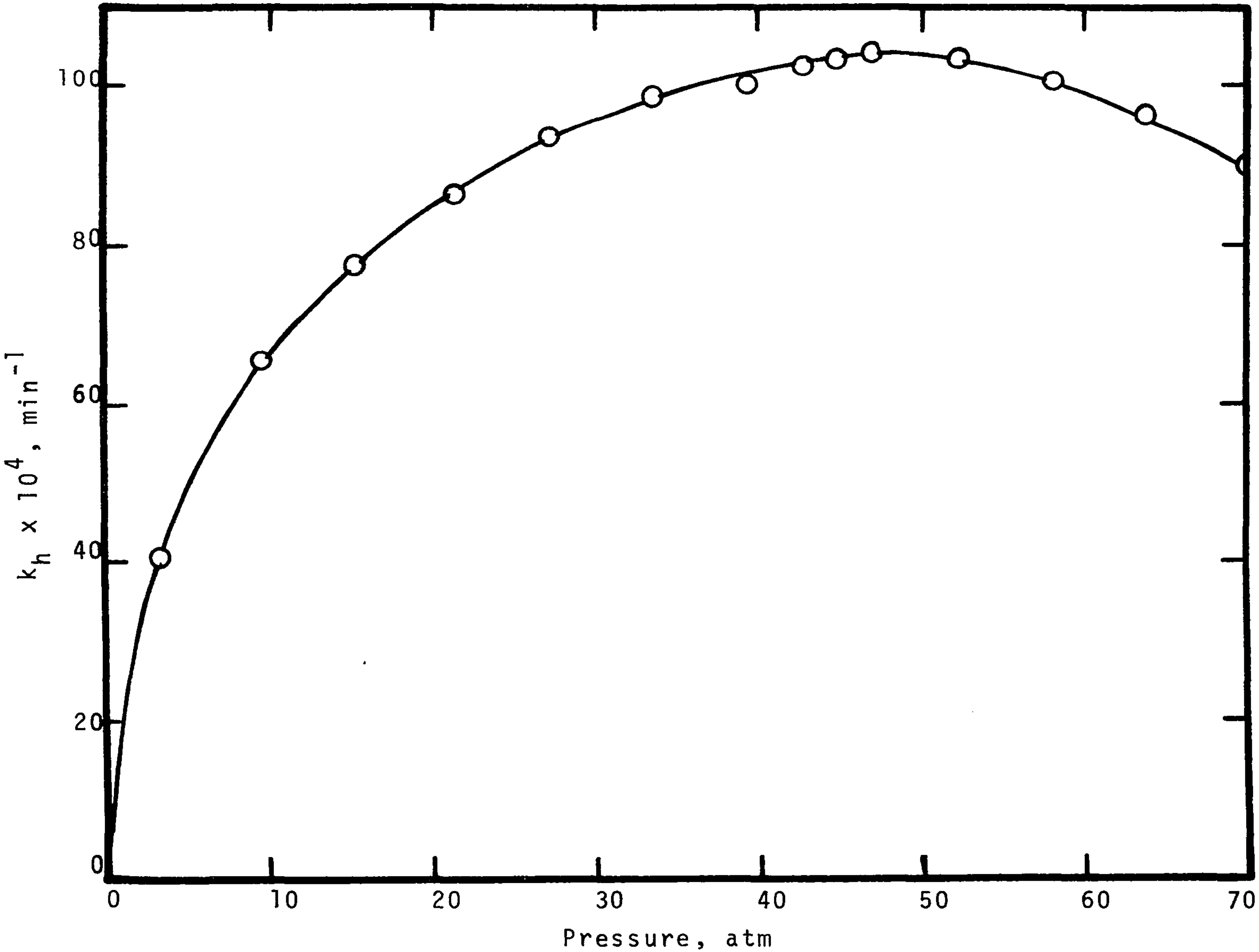

Figure 40. Variation of the Homogeneous Rate Constant with Pressure at 595°C.

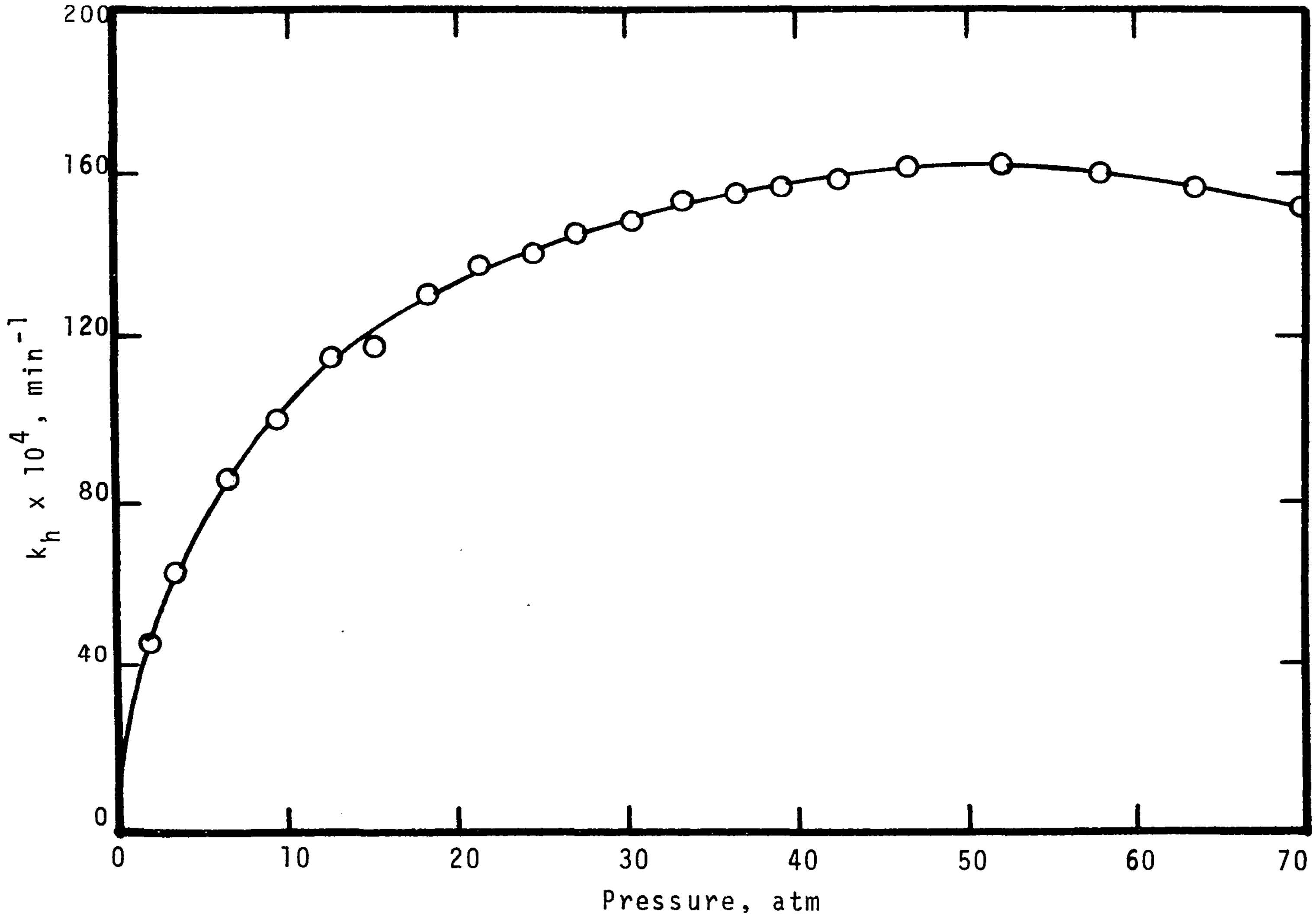

Figure 41. Variation of the Homogeneous Rate Constant with Pressure at 605°C.

The experimental data for the temperature levels from 545° to 605°, shown in Figures 37 through 41, indicate that the rate constant apparently decreases with pressure after passing through a maximum value. The line through the experimental data points in each figure represents the trend of the rate constant with pressure.

If the maximum values of the rate constant are taken from Figures 37 through 41 and compared to the infinite pressure rate constant values predicted by the Kassel theory, the observation is made that the maximum experimental values are about 0.8 of the infinite pressure values. Therefore, in any consideration of experimental high pressure rate data, the traditional concept of the infinite pressure rate constant, k_∞, should be replaced by a maximum rate constant, k_{max}. At each temperature level from 545°C to 605°C, the value of k_{max} was obtained from the plots shown in Figures 37 through 41. These values are presented as a function of temperature in Table 7 and in Figure 42. A least squares fit of these data in the Arrhenius form resulted in the expression

$$\ln k_{max} = 33.790 - 66{,}100/RT \qquad \text{(IX-7)}$$

The variation of the homogeneous rate constant, k_h, with pressure has been discussed earlier in Chapter II. The conclusions of that development were that the rate constant would increase with pressure until some maximum value of the

TABLE 7

MAXIMUM HOMOGENEOUS RATE CONSTANTS

T, °C	k_{max}, min.$^{-1}$
545	0.00101
565	0.00280
585	0.00682
595	0.01045
605	0.01620

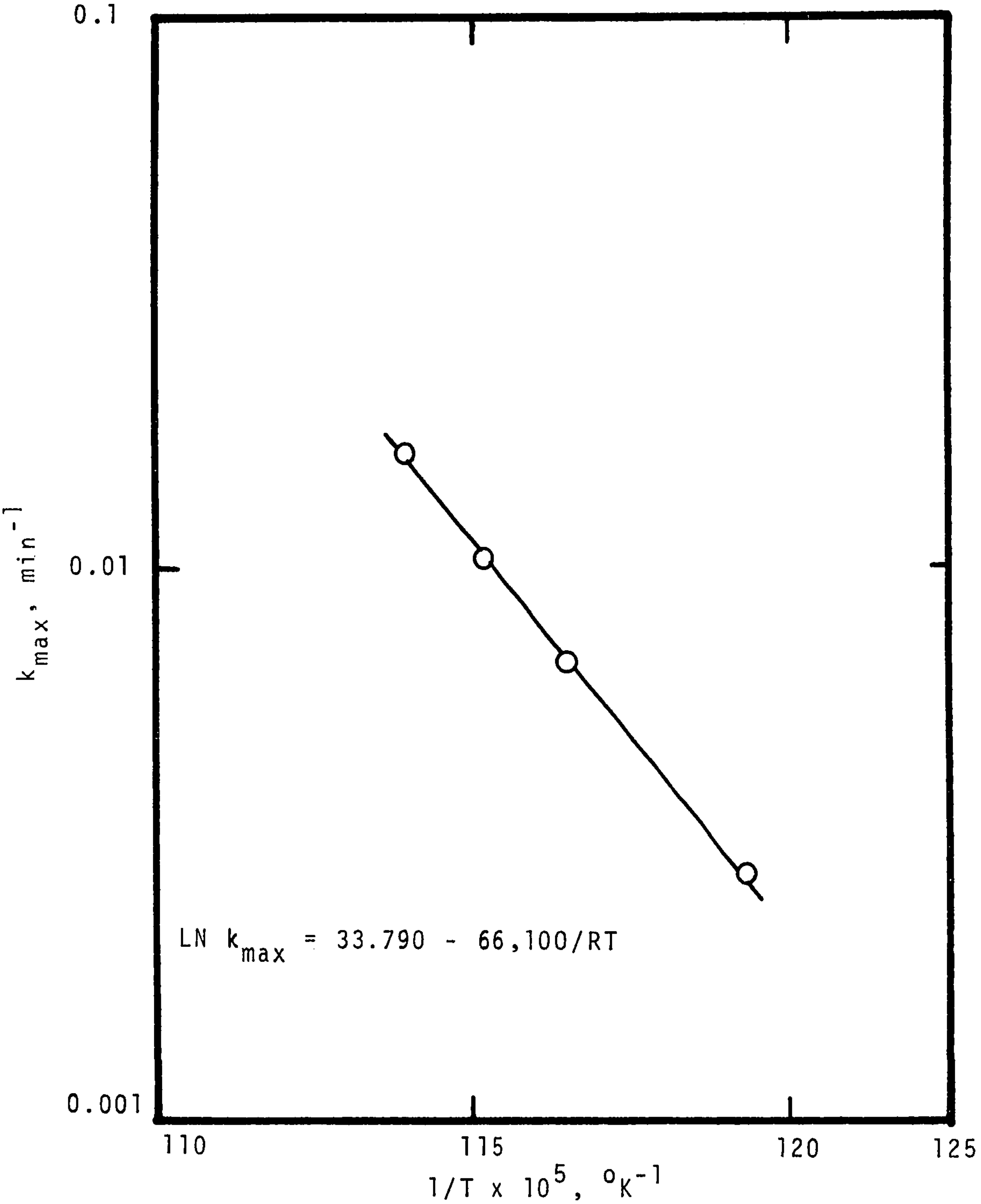

Figure 42. Arrhenius Plot of the Maximum Homogeneous Rate Constant.

rate constant, k_{max}, was reached. At pressures above the pressure corresponding to k_{max}, the rate constant would decrease with further increases in pressure. The variation in the rate constant with pressure was given by Equation II-64 as

$$\left[\frac{\partial \ln k_h}{\partial P}\right]_T = \left[\frac{\partial \ln I(T, P)}{\partial P}\right]_T - \frac{\overline{V}* - \overline{V}_A}{RT}$$

Values of $\overline{V}*$, the molar volume of the activated complex in the reaction, are not readily available since this quantity cannot be measured directly. Also, the structure of the activated complex cannot be compared to the structure of the products, since the activated complex does not rearrange structure in the product state but decomposes to form the products. The molar volume of the activated complex should be slightly larger than that of the reactant nitrous oxide since the formation of the activated complex involves the stretching of a critical bond. Thus, the quantity $(\overline{V}* - \overline{V}_A)/RT$ will be a small positive number.

In spite of the fact that $\overline{V}*$ is not determinable by direct experimental methods, the quantity $\overline{V}* - \overline{V}_A$, often known as the activation volume, has been determined for a number of reactions by past investigators. The activation volume is described in articles by McCabe and Eckert (13) and Eckert (12). These articles primarily deal with bimolecular reactions in solution, but Eckert (12) has also reported literature values of the activation volumes for bond scission reactions. His reported values range from 5 to 25 cc/mole. In all cases the activation volumes were back-calculated from values of the experimental rate constants.

In this investigation, values of $\bar{V}^* - \bar{V}_A$ were calculated using Equation II-64. The results were typically similar for the five temperature levels from 545°C to 605°C, and only the behavior at 585°C will be discussed. For pressures to 40 atmospheres, the activation volumes were between 11 and 15 cc/mole. However, over the entire pressure range studied, the calculated activation volume was as high as 350 cc/mole. This value seems abnormally large in consideration of the activation volume values presented by Eckert (12). The discrepancy is probably due to the nature of the error involved in calculating $\bar{V}^* - \bar{V}_A$ from Equation 64. Not only does the error involved with determining k_h contribute, but also the error in determining the change in ln I(T,P) with pressure. In the region of pressures surrounding the maximum rate constant value where the slopes of the ln k_h and ln I(T, P) versus pressure curves are very small, even small errors in either k_h or I(T, P) are reflected by large changes in the value of the activation volume. Nevertheless, in the temperature range from 545°C to 605°C, about 2/3 of the calculated activation volumes fell in the region between 11 and 20 cc/mole, which is consistent with the earlier reported literature values.

The concept of a high pressure limiting value of the rate constant seems to be subject to question based upon the results of this investigation and the earlier results of Pipkin (49) and Johnson (31) with cyclopropane. The results of all three investigations indicated that the rate constant apparently decreases with increasing pressure after some specific pressure value has been reached. Therefore, the value of k^{∞} developed from the theoretical curves of Kassel or Slater may be very different from the experimental value of the rate constant at high pressures. Thus, the use of k^{∞} as a high pressure value of the rate constant is incorrect since the rate constant is still changing with pressure and, in particular, appears to decrease at high pressures.

CHAPTER X

CONCLUSIONS

The conclusions developed in this investigation are presented in light of the stated objectives and include the variation in the rate constant over temperature and pressure ranges, the behavior of the rate constant at high pressures, the effect of the gold surface upon the reaction, and the feasibility of the continuous flow system for studying unimolecular reactions.

As would be expected, the rate data taken in this investigation fit the Arrhenius expression quite well at all pressure levels studied. This expression may be written as

$$\ln k = \ln A - E/RT \qquad \text{(X-1)}$$

Deviations between the Arrhenius relation and experimental data were generally less than the expected experimental error of ± 10.0 percent which was calculated for the investigation.

The rate constant was found to decrease with pressure after passing through a maximum at some pressure p_{max}. An equation was presented which indicated that such behavior should be expected at high pressures. The actual value of the rate constant at high pressures (> 45 atm) was shown to differ from the so-called "infinite" pressure rate constant, k^{∞}, which was predicted from the classical unimolecular theories of Kassel or Slater. The concept of a high pressure limit to the value of the rate constant should therefore be replaced by the consideration of a maximum rate constant value at some given pressure followed by decreasing rate constant values with further increases in pressure.

Gold was found to be catalytic to the decomposition reaction, which was first-order at the conditions studied. The activation energy for the surface reaction was found to agree quite well with the limited previous data which were available. Reaction conditions were determined at which the surface reaction was present in the absence of any homogeneous reaction contribution. Rate data obtained for the surface reaction alone permitted the determination of separate values for the heterogeneous and homogeneous rate constants whenever both reactions were occurring simultaneously.

The use of a gold-lined, tubular continuous flow reactor was found to be useful for studying a unimolecular decomposition reaction. The pressurized flow system, together with the fluidized sand heating medium, gave excellent temperature control and consistency of flow through the reactor. The high pressure construction of the entire system allowed rate data to be taken for a unimolecular decomposition at much higher pressures than were ever attainable in previous equipment.

NOMENCLATURE

A	component A in stoichiometric equation
A	frequency factor in Arrhenius equation
A_o	constant in Equation B-4
a	constant in Equation B-4
B	component B in stoichiometric equation
B_o	constant in Equation B-4
b	constant in Equation B-4
b	parameter in Kassel or Slater integral, $(\varepsilon - \varepsilon^*)/k_BT$
C	component C in stoichiometric equation
C	concentration
C_o	constant in Equation B-4
c	constant in Equation B-4
c	dimensionless concentration from Equation C-2
D	component D in stoichiometric equation
D	reactor diameter
D_{12}	diffusion coefficient
E	internal energy
E_o	energy of activation
F	partition function
F	molecular feed rate
f	fugacity

h	Plank's constant
I	integral defined by Equation II-36
K	equilibrium constant
k	specific reaction rate
k_B	Boltzman constant
k_a	specific reaction rate in terms of activities
k_c	specific reaction rate in terms of concentrations
k^1	first-order rate constant
L	length of reactor
M	molecular weight
m	adjustable parameter used in evaluation of RRK or Slater integrals
N	Avagadro's number
N	collision term in Equation II-9
N_{Re}	Reynolds number
N_i	number of moles
n	adjustable parameter in Slater integral
P	pressure
P_c	critical pressure
p	pressure
R	gas law constant
R	reactor radius
R	platinum thermometer resistance
R_t	total reaction rate
R_h	homogeneous reaction rate
R_s	surface reaction rate

r	point radius in reactor
r	rate of reaction
r_f	rate of forward reaction
r_r	rate of reverse reaction
S^o	total number of active sites available for absorption
s	adjustable parameter in RRK integral
s	degrees of freedom
s	fraction of decomposition occurring by secondary reaction
T	temperature
T_c	critical temperature
T_r	reduced temperature
t	time or residence time
V	reactor volume
$\langle v \rangle$	bulk gas velocity
X	fractional conversion
$X^{\neq}$	activated complex in the transition state theory
x	parameter in Kassel or Slater integral
z	collison frequency
ζ	compressibility factor

Greek

α	constant in Equation B-4
α	dimensionless quantity in Equation C-2
α_m	amplitude factors in Slater theory
γ	constant in Equation B-4

∂	partial derivative
ε^*	energy of activation per molecule
ε_A	fractional change in system volume with reaction
η	transmission coefficient in transition state theory
θ	absorbed fraction in Langmuir isotherm
θ	variable in Slater integral
λ	dimensionless quantity in Equation C-2
μ_m	viscosity
μ_m	normalized amplitude factors in Slater theory
μ_m	mixture viscosity at high pressures
μ_m^*	mixture viscosity at low pressures
ν	dimensionless quantity in Equation C-2
ν_m	frequencies of normal modes of vibration
$\bar{\nu}$	average vibrational frequency in Slater theory
ξ_m	quantity defined by Equation B-9
ρ	density
ρ_r	density at reaction conditions
ρ_o	density at Standard conditions
σ_{AB}	collision diameter
τ	space time
Ω_D	collision integral for diffusion
ω	term in development of Kassel or Slater integral defined by Equation A-7

Subscripts

A	species A
B	species B
X	species X
j	j-th component in a system
o	reactor inlet condition

Superscripts

$*$	specie in energized state with correct energy distribution
$'$	specie in energized state without correct energy distribution
$\neq$	specie in activated complex state
∞	high pressure limiting value
H	RRK mode of activation
S	Slater mode of activation
s	surface reaction in rate constant

BIBLIOGRAPHY

1. Ashmore, P. G. Catalysis and Inhibition of Chemical Reactions. London: Butterworth and Co., 1963.

2. Bell, T. N.; Robinson, P. L.; and Trenwith, A. B. "The Thermal Decomposition of Nitrous Oxide. The Effect of Foreign Molecules." J. Chem. Soc., 160 (1956):1474.

3. Benedict, M.; Webb, G. B.; and Rubin, L. C. "An Empirical Equation for Thermodynamic Properties of Light Hydrocarbons and Their Mixtures." J. Chem. Phys., 10 (1942):747.

4. Billeb, K. Gas Chromatography Department, Perkin-Elmer Corporation, Norwalk, Conn. Personal communication, July 8, 1971.

5. Briner, R. E.; Meiner, C.; and Rothen, A. "The Thermal Decomposition of Nitrous and Nitric Oxides." J. Chem. Phys., 23 (1926):609.

6. Burk, R. E., and Hinshelwood, C. N. "The Homogeneous Thermal Decomposition of Nitrous Oxide." Proc. Roy. Soc., A106 (1924):284.

7. Cleland, F. A., and Wilhelm, R. H. "Diffusion and Reaction in Viscous Flow Tubular Reactors." AIChE J., 2 (1956):489.

8. Cooper, H. W., and Goldfrank, J. C. "B-W-R Constants and New Correlations." Hydrocarbon Processing, 46, 12 (1967):141.

9. Danckwerts, P. V. "Continuous Flow Systems." Chem. Engr. Sci., 2 (1953):1.

10. Dean, D. E., and Stiel, L. I. "The Viscosity of Nonpolar Gas Mixtures at Moderate and High Pressures." AIChE J., 11 (1965):526.

11. Dietz, R. N. "Gas Chromatographic Determination of Nitrous Oxide on Treated Molecular Sieves." Anal. Chem., 40, 10 (1968):1576.

12. Eckert, C. A. "High Pressure Kinetics in Solution." Ann. Rev. of Phys. Chem. (1972):239.

13. Eckert, C. A.; Grieger, R. A.; and McCabe, J. R. "Solvent Effects on the Volume of a Transition State." I&EC Fund., 9, 1 (1970):156.

14. Eley, D. D., and Knights, C. F. "Decomposition of Nitrous Oxide Catalyzed by Palladium-Gold Alloy Wires." Proc. Roy. Soc., A294 (1966):1.

15. Freeman, L., and Bigeleisen, J. "Thermal Decomposition of Nitrous Oxide." J. Am. Chem. Soc., 75 (1953):2215.

16. Gardiner, W. C., Jr. Rates and Mechanisms of Chemical Reactions. New York: W. A. Benjamin, Inc., 1969.

17. Gill, E. K., and Laidler, K. J. "Some Aspects of the Theory of Unimolecular Gas Reactions." Proc. Roy. Soc., A250 (1958):121.

18. ________. "Theoretical Aspects of the Unimolecular Decomposition of Nitrous Oxide." Can. J. Chem., 36 (1958):1570.

19. Graven, W. M. "Gas Chromatograph: Gaseous Composition in the Effluent of a Flow Reactor." Anal. Chem., 31 (1959):1197.

20. ________. "Kinetics of the Decomposition of Nitrous Oxide at High Temperatures." J. Am. Chem. Soc., 81 (1959):6190.

21. Hall, K. R., and Canfield, F. B. "Optimal Recovery of Virial Coefficients from Experimental Compressibility Data." Physica, 33 (1967):481

22. Halladay, J. B. "Simultaneous Homogeneous and Heterogeneous Chemical Reaction Kinetics: Thermal Decomposition of Nitrous Oxide on a Gold Surface." Ph.D. Thesis, Oregon State University, Corvallis, Oregon, 1971.

23. Hibben, J. H. "Radiation and Collision in Gaseous Chemical Reactions." Proc. Nat. Acad. Sci., 13 (1927):626.

24. ________. "The Low Pressure Decomposition of Nitric and Nitrous Oxides." J. Am. Chem. Soc., 50 (1928):940.

25. Hinshelwood, C. N. "On the Theory of Unimolecular Reactions." Proc. Roy. Soc., A113 (1927):230.

26. Hinshelwood, C. N., and Prichard, C. R. "A Comparison Between the Homogeneous Thermal Decomposition of Nitrous Oxide and Its Heterogeneous Catalytic De-Composition on the Surface of Pt." J. Chem. Soc., 127 (1925):327.

27. ________. "The Catalytic Decomposition of Nitrous Oxide on the Surface of Gold: A Comparison with the Homogeneous Reaction." Proc. Roy. Soc., A108 (1925):211.

28. Hirschfelder, J. O.; Bird, R. B.; and Spotz, E. L. "The Transport Properties for Non-Polar Gases." J. Chem. Phys., 16 (1948):968.

29. Hunter, E. "The Thermal Decomposition of Nitrous Oxide at Pressures up to Forty Atmospheres." Proc. Roy. Soc., A144 (1934):386.

30. Hunter, M. A. "Uber die Zerfallgeschwindigkeit des Stickoxyduls." Z. Physik. Chem, 53 (1905):441.

31. Johnson, D. W. "The Thermal Isomerization of Cyclopropane." Ph.D. Thesis, University of Oklahoma, Norman, Oklahoma (1969).

32. Johnson, D. W., and Colver, C. P. "Mixture Properties by Computer. Part I: Density; Part III: Viscosity, Thermal Conductivity and Diffusivity." Hydrocarbon Process, 47, 12 (1968):79.

33. Johnston, H. S. "Interpretation of the Data on the Thermal Decomposition of Nitrous Oxide." J. Chem. Phys, 19, 6 (1951):663.

34. Kassel, L. S. Kinetics of Homogeneous Gas Reactions. New York: The Chemical Catalog Company, Inc., 1932.

35. ________. "Studies in Homogeneous Gas Reactions." J. Phys. Chem., 32 (1928):235.

36. Krisjansons, J. O.; Bollinger, L. E., and Edse, R. "Explosion Limit Studies of Nitrous Oxide and Nitrous Oxide-Nitrogen-Air Mixtures to 200 Atm. and 1800^{o}R." NASA Doc. N63-11007, ARL-62-431, The Ohio State University, Rocket Research Laboratory, September, 1962.

37. Laidler, K. J. *Chemical Kinetics*. New York: McGraw-Hill Book Company, 1965.

38. ______. *Theories of Chemical Reaction Rates*. New York: McGraw-Hill Book Company, 1969.

39. Laughrey, J. A.; Bollinger, L. E.; and Edse, R. "Detonability of Nitrous Oxide at Elevated Initial Pressures and Temperatures." NASA Doc. N63-11538, ARL-62-432, The Ohio State University, Rocket Research Laboratory, September, 1962.

40. Lewis, R. M., and Hinshelwood, C. N. "The Thermal Decomposition of Nitrous Oxide." *Proc. Roy. Soc.*, *A168* (1938):441.

41. Lindars, F. J. and Hinshelwood, C. N. "The Thermal De-Composition of Nitrous Oxide I, Secondary Catalytic and Surface Effects II, Influence of Added Gases and a Theory of the Kinetic Mechanism." *Proc. Roy. Soc.*, *A231* (1955):162.

42. Lindemann, F. A. "The Radiation Theory of Chemical Action." *Trans. Faraday Soc.*, *17* (1922):598.

43. Marcus, R. A. "Unimolecular Dissociations and Free Radical Recombination Reactions." *J. Chem. Phys.*, *20*, 3 (1951):359.

44. Musgrave, F. F. and Hinshelwood, C. N. "The Thermal Decomposition of Nitrous Oxide, and its Catalysis by Nitric Oxide." Proc. Roy. Soc., A135 (1931):23.

45. Nagasako, N. and Volmer M. "Der Thermische Zerfall des Stickoxyduls Zwischen 1 und 10 Atm." *Z. Physik. Chem.*, *B10* (1930):414.

46. Nelson, L. C. and Obert, E. F. "Generalized Compressibility Charts." *Chemical Engineering*, (July, 1954).

47. Pease, R. N. "The Experimental Basis for the Theory of Quasi-Unimolecular Reactions." *J. Chem. Phys.*, *7* (1939):749.

48. Perrin, J. *Ann. Phys.* *11*, 9 (1919):1.

49. Pipkin, O. A. "Thermal Isomerization of Cyclopropane at Elevated Pressures." Ph.D. Thesis, University of Oklahoma, Norman, Oklahoma (1964).

50. Powell, R. E. "Curve-Matching Method for Quasi-Unimolecular Reactions." J. Chem. Phys., 30, 3 (1958): 724.

51. Redmond, J. P. "Kinetics of the Low Pressure Nitrous Oxide Decomposition on a Platinum Filament." J. Phys. Chem., 67 (1963):788.

52. Reid, R. C., and Sherwood, T. K. The Properties of Gases and Liquids. New York: McGraw-Hill Book Company, 1966.

53. Rice, O. K., and Ramsperger, H. C. "Theories of Unimolecular Gas Reactions at Low Pressure." J. Am. Chem. Soc., 49 (1927):1617.

54. Slater, N. B. Theory of Unimolecular Reactions. Ithaca, New York: Cornell University Press, 1959.

55. Steacie, E. W. R., and McCubbin, J. W. "The Decomposition of Nitrous Oxide on the Surface of Platinum. I. The Retarding Effect of Oxygen." J. Chem. Phys., 2 (1934): 585.

56. Van Praagh, G., and Topley, B. "The Decomposition of Nitrous Oxide at Low Pressures Upon a Platinum Catalyst." Trans. Faraday Soc., 27 (1931):312.

57. Volmer, M., and Briske, H. "Studien über den Zerfall von Stickoxydul." Z. Physik. Chem., B25 (1934):81.

58. Volmer, M., and Froehlich, H. "Der Thermische Zerfall des Stickoxyduls." Z. Physik. Chem., B19 (1932):85.

59. Volmer, M., and Kummerow, H. "Der Thermische Zerfall des Stickoxyguls." Z. Physik. Chem., 9 (1930):141.

60. Wieder, G. M., and Marcus, R. A. "Unimolecular Reaction Rate Theory and its Application." J. Chem. Phys., 37, 8 (1962):1835.

61. Wilhite, W. F., and Hollis, O. L. "The Use of Porous Polymer Beads for Analysis of the Martian Atmosphere." J. Gas Chromatog., 6 (1968):84.

62. Yagodovskii, V., and Fontes, M. Garcia. "Kinetic Studies on Nitrous Oxide Decomposition on Granulated Gold Films." Kinet. Katal., 9, 5 (1968):1072.

APPENDICES

APPENDIX A

EVALUATION OF KASSEL AND SLATER INTEGRALS

In comparing the experimental data from any unimolecular reaction to the most widely accepted unimolecular theories (RRK theory and the Slater theory), one must be able to develop a curve representing the relationship between the ratio of the rate constant for the first-order reaction to the rate constant at high pressure. These curves may be developed by numerical integration of the integral corresponding to either Kassel's theory or Slater's theory. The equation relating the rate constant ratio and the value of the integral is

$$\log (k^1/k^\infty) = \log I_m (\Theta) \qquad \text{(A-1)}$$

or

$$(k^1/k^\infty) = I_m (\Theta) \qquad \text{(A-2)}$$

The quantity $I_m (\Theta)$ is mathematically related to log (Θ), and Θ is a function of the log of the operating pressure. Therefore, a relationship between log (k^1/k^∞) and log (p) can be developed for both the Kassel theory and the Slater theory. The exact nature of the relationship between $I_m (\Theta)$ and log (Θ) is determined by the value of <u>m</u>, the adjustable parameter in both theories. Figures 43, 44, and 45 represent the relationship between I_m (Θ) and log (Θ) for values of m equal to 1/2, 1, and 3, respectively. The Slater integral with $n = 2$ is expressed by $m = 1/2$, while the Kassel integral with $s = 2$ and $s = 4$ is represented by $m = 1$ and $m = 3$.

As previously developed in Chapter II, Kassel's equation for the ratio between the first-order rate constant and the high pressure rate constant is

$$\frac{k^1}{k^\infty} = \frac{1}{(s-1)!}\int_0^\infty \frac{x^{s-1}\,e^{-x}\,dx}{1 + (k\ /k_2[A])(x/(b+x))^{s-1}} \qquad \text{(A-3)}$$

form

$$\left(\frac{k^1}{k^\infty}\right)^s = I_{s-1}\ (\Theta') \qquad \text{(A-4)}$$

with

$$I_{s-1}\ (\Theta') = I_m\ (\Theta) \qquad \text{(A-5)}$$

and

$$\Theta^1 = (\omega/A)\ b^{s-1} \qquad \text{(A-6)}$$

Now

$$\omega = Zc \qquad \text{(A-7)}$$

and

$$Z = 4N\ \sigma^2\ (\pi RT/m^*)^{1/2} \qquad \text{(A-8)}$$

where the concentration c is in moles/cc., $N = 6.0238 \times 10^{23}$ molecule/gm-mole, $R = 8.31439 \times 10^7$ erg.deg.$^{-1}$ mole^{-1}, σ is the molecular collision diameter in centimeters, and m^* is the molecular weight. Substitution of Equation A-7 into Equation A-6 produces

$$\Theta = \frac{Zc}{A}\ b^{s-1} \qquad \text{(A-9)}$$

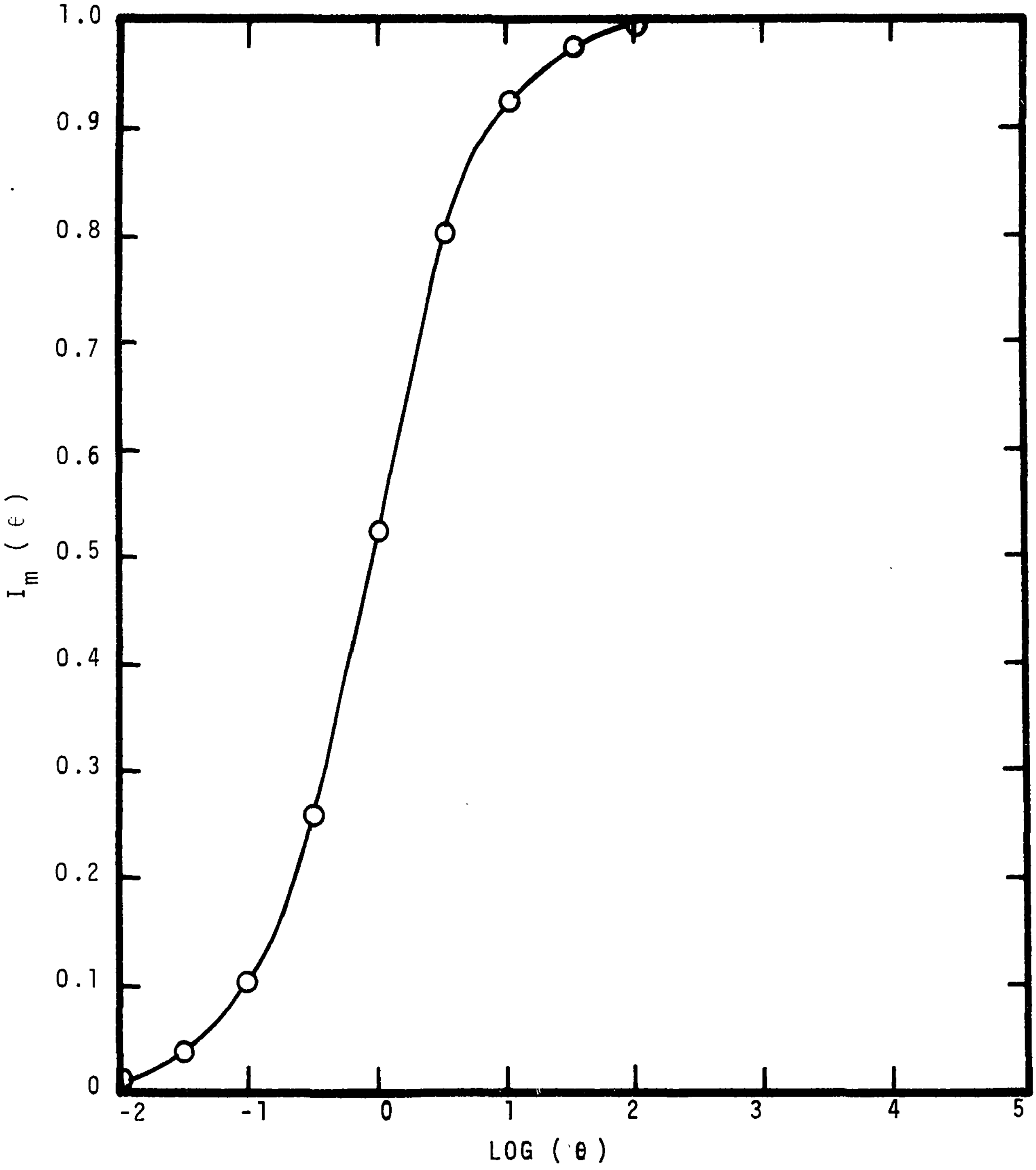

Figure 43. Kassel's or Slater's Integral with m = 1/2.

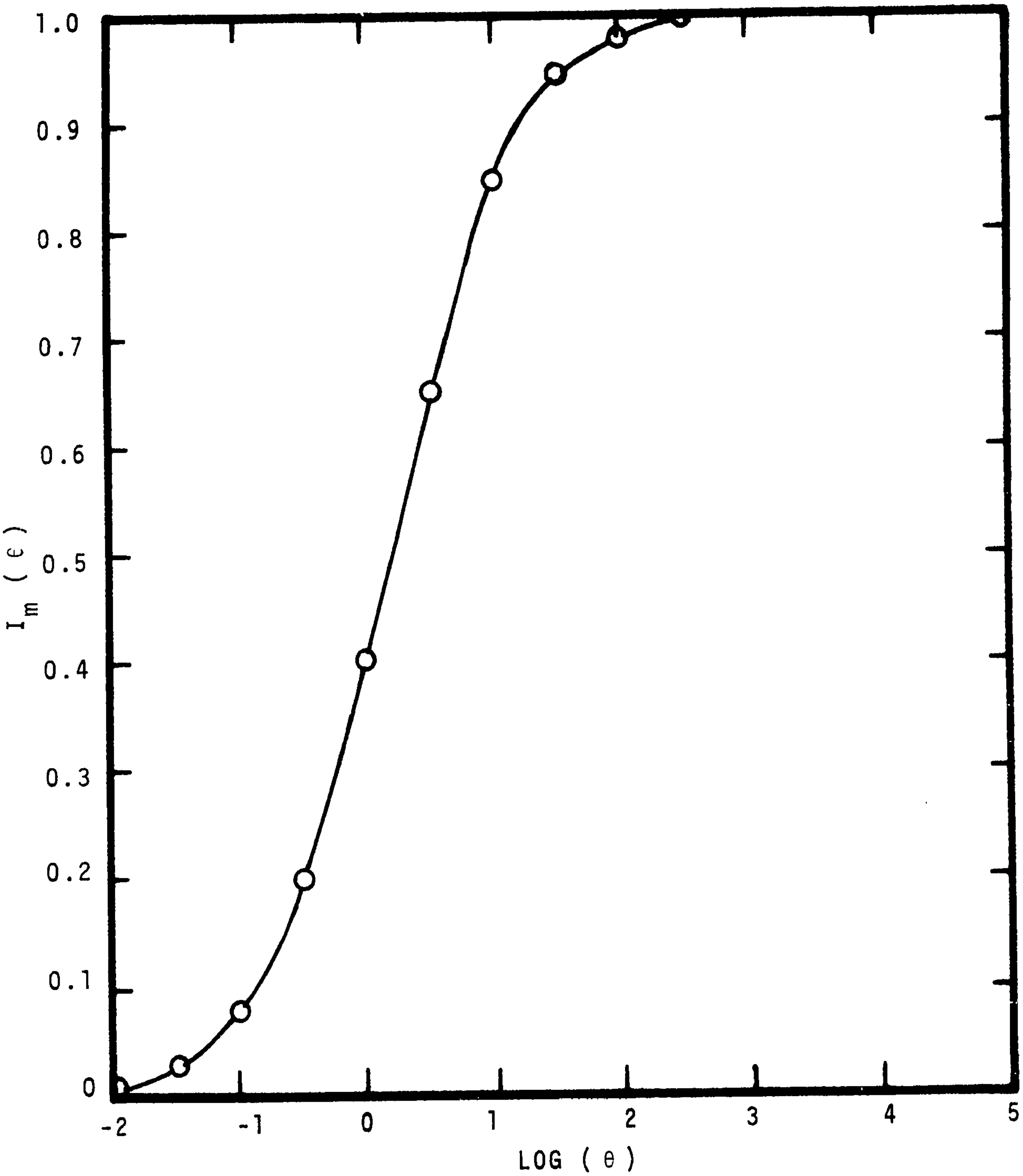

Figure 44. Kassel's or Slater's Integral with $m = 1$.

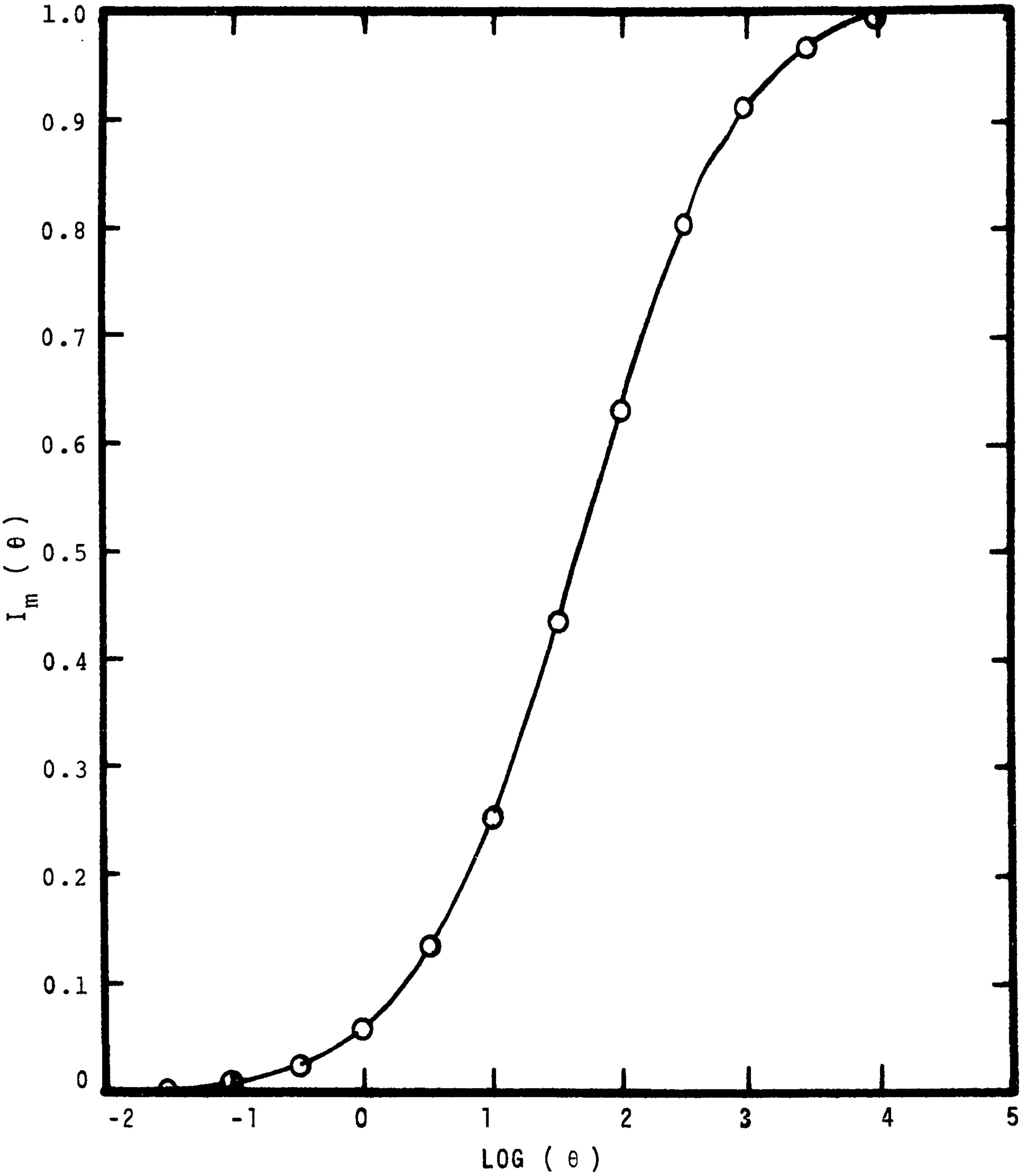

Figure 45. Kassel's or Slater's Integral with m = 3.

Further substitution of Equation A-8 gives

$$\Theta = \frac{4N\sigma^2 (\pi RT/m^*)^{1/2} c}{A} b^{s-1} \qquad \text{(A-10)}$$

We also have the expression

$$c = 1.6035 \times 10^{-5} p/T \qquad \text{(A-11)}$$

with p expressed in mm Hg and T expressed in $^{\circ}$K. Substitution of Equation A-11 into Equation A-10 gives an expression of the form

$$\Theta = \frac{6.414 \times 10^{-5} N\sigma^2 (\pi RT/m^*)^{1/2} p}{A\ T} b^{s-1} \qquad \text{(A-12)}$$

Thus, Equation A-12 relates Θ to the operating pressure in mm Hg. The values of the various quantities in Equation A-12 are as follows

$N = 6.0238 \times 10^{23}$ molecules/gm-mole
$\sigma = 3.95 \times 10^{-8}$ cm
$R = 8.31439 \times 10^{7}$ erg/deg-mole
T = operating temperature in $^{\circ}$K
$m^* = 44.016$ gm/gm-mole
p = operating pressure in mm Hg
$A = 5.01 \times 10^{11}$
$b = E^{\infty}/1.987T$
$E^{\infty} = 61,000$ cal/gm-mole

Using Equation A-12 and Figure 44 or 45, theoretical curves can be drawn for the nitrous oxide decomposition as it relates to the RRK theory.

The decline in the rate constant as predicted by the Slater theory is given in terms $I_m(\Theta)$ by

$$k^{1}/k^{\infty} = I_{1/2\ (n-1)}(\Theta) \qquad (A\text{-}13)$$

where n is the number of distinct vibration frequencies $\nu_1, \nu_2, \ldots, \nu_n$. In Equation A-13, Θ can be represented by

$$\Theta = (\omega/v)\ f_n\ b^{1/2\ (n-1)} \qquad (A\text{-}14)$$

Now

$$\omega = Zc$$

so

$$\Theta = (Zc/\bar{v})\ f_n\ b^{1/2(n-1)} \qquad (A\text{-}15)$$

Recalling from Equations A-8 and A-11 that

$$Z = 4N\ \sigma^{2}\ (\pi\ RT/m^{*})^{1/2} \qquad (A\text{-}8)$$

and

$$c = 1.6035 \times 10^{-5}\ p/T \qquad (A\text{-}10)$$

we have, upon substitution into Equation A-15, the following

$$\Theta = \frac{6.414 \times 10^{-5}\ N\sigma^{2}\ (\pi RT/m^{*})^{1/2}\ p}{\bar{v}T}\ f_n\ b^{1/2(n-1)} \qquad (A\text{-}16)$$

Thus, Equation A-16 relates Θ to the operating pressure in mm Hg. The values of the various quantities in Equation A-16 are as follows

$N = 6.0238 \times 10^{23}$ molecules/gm-mole

$\sigma = 3.95 \times 10^{-8}$ cm

$R = 8.31439 \times 10^{7}$ erg/deg-mole

T = operating temperature in ^{o}K

m^* = 44.016 gm/gm-mole

p = operating pressure in mm Hg

ν = 4.503×10^{13} sec

f_n = 1.2014

b = $E^{\infty}/1.987T$

E^{∞} = 61,000 cal/gm-mole

Using Equation A-16 and Figure 43, a theoretical curve can be drawn for the nitrous oxide decomposition as it relates to the Slater theory.

APPENDIX B

CALCULATION OF PHYSICAL PROPERTIES

Density

In making even the simplest calculations required in a study of a gaseous flow system, accurate values of certain physical properties are a necessity. The most critical property for which a value must be available is the density of the reacting gases, since calculations of space time and residence time are based upon this quantity. The basic equation relating space time to density is

$$\tau = \frac{V \rho_r}{F_o \rho_o} \qquad \text{(B-1)}$$

where V = reactor volume

ρ_r = density at reactor conditions

ρ_o = density at standard conditions

F_o = flow rate at standard conditions

Equation B-1 implies that plug flow exists in the reactor, an assumption that will be examined in more detail in Appendix C. This equation also assumes that the density remains constant throughout the length of the reactor. This assumption is not correct for the decomposition of nitrous oxide, since there is a constant volume change with conversion for this particular system. Therefore, Equation B-1 could not be used as it exists to calculate space times for this investigation.

To calculate the required densitites necessary to handle the data obtained in this investigation, pure component densities for N_2O, N_2, and O_2 were first computed at reaction conditions for each run. The following equation was used for these computations.

$$\rho = \frac{M}{0.08205\ z\ T} \qquad \text{(B-2)}$$

where ρ = density, gm-mole/liter

M = molecular weight, gm/gm-mole

p = pressure, atm

z = compressibility factor

T = temperature, $^{\circ}K$

Values of z were obtained from compressibility factor charts in Reid and Sherwood (52). The density of any product gas mixture was calculated from

$$\rho_m = X_{N_2O}\ \rho_{N_2O} + X_{N_2}\ \rho_{N_2} + X_{O_2}\ \rho_{O_2} \qquad \text{(B-3)}$$

where X_{N_2O}, X_{N_2}, X_{O_2} = the respective mole fractions

and ρ_{N_2O}, ρ_{N_2}, ρ_{O_2} = the respective pure component densities

Using Equation B-3 enables one to calculate the density at any point in the reactor as long as the conversion is known at that particular point.

An alternative method for calculating the necessary gas densities was developed from the Benedict-Webb-Rubin (BWR) equation. A computerized version of the BWR equation presented by Johnson and Colver (32) was modified and placed in the data handling program for the investigation which may be found in Appendix D. The BWR equation as proposed by Benedict, Webb, and Rubin (3) is

$$P = RT\rho + (B_oRT - A_o - C_o/T^2)\ \rho^2 + (bRT - a)\ \rho^3 + a\alpha\rho^6 + (c\rho^3/T^2)(1 + \gamma\rho^2)\ \exp\ (-\gamma\rho^2) \qquad \text{(B-4)}$$

where pressure is a function of the temperature, density, and eight constants which are specific for each pure substance. Cooper and Goldfrank (8) have tabulated values of the BWR constants for 38 pure materials which can be used in Equation B-4 to predict PVT properties. The pure component constants can be applied to gas mixtures through mixing rules. The appropriate mixture constants are developed from specific mixing rules, for example

$$A_{o_m} = (\Sigma_i\ x_i\ A_{o_i}^{1/2})^2 \qquad \text{(B-5)}$$

A complete listing of the BWR mixture constants may be found in Reid and Sherwood (52). Here again, the computerized BWR equation together with the appropriate mixing rules enables one to calculate point densities in a tubular reactor provided that the conversion is known at the point in question.

A comparison was made between the gas mixture densities calculated by Equation B-3 and by Equation B-4. This comparison revealed that the maximum difference between the two calculated densities was only 0.9%, with the majority of the differences being less that 0.4%. Densities calculated by Equations B-3 and B-4 were averaged to provide the values used in this investigation.

Viscosity

Viscosity values of the reacting gas are important in determining whether or not the assumption of plug flow is valid for a tubular reactor. These values are necessary in determining the Reynolds number of the flowing gas stream. The Reynolds number may be expressed by

$$N_{Re} = \frac{D\langle v\rangle \rho}{\mu} \qquad \text{(B-6)}$$

where D = tube diameter

$\langle v\rangle$ = bulk gas velocity

ρ = density

μ = viscosity

There is general acceptance that for Reynolds numbers below 2100 and in the absence of diffusion effects, laminar flow is prevalent in a tubular reactor. The viscosity correlation of Dean and Stiel (10) was chosen as the method to compute gas phase viscosities at the conditions used in this investigation. Dean and Stiel developed the following correlation for mixture viscosities.

$$\mu_m^* \xi_m = 34 \times 10^{-5} \, T_r^{8/9} \qquad \text{(B-7)}$$

for $T_r < 1.5$

and $$\mu_m^* \xi_m = 166.8 \times 10^{-5} \, (0.1338 \, T_r - 0.0932)^{5/9} \qquad \text{(B-8)}$$

for $T_r \geq 1.5$

where $$\xi_m = T_{c_m}^{1/6} / (M_m^{1/2} \, P_{c_m}^{2/3}) \qquad \text{(B-9)}$$

and the mixture properties are all of the form

$$T_{c_m} = \Sigma_i \, x_i \, T_{c_i} \qquad \text{(B-10)}$$

In this correlation, μ_m^* is the low pressure viscosity in centipoise. Equations B-7 and B-8 are applicable only to non-polar gas mixtures which do not contain either hydrogen or helium. Pressures are limited to under 5 atmospheres.

At the same time that Dean and Steil presented the low pressure viscosity correlation, they also introduced a method to estimate the viscosity departure for high-pressure gas mixtures. This method assumes great importance in the present investigation since most of the data were taken above 5 atmospheres pressure. The high pressure viscosity departure can be estimated with the following equation.

$$(\mu_m - \mu_m^*)\ \xi_m = 10.8 \times 10^{-5}\ [\exp\ (1.439\rho_{m_r}) - \exp\ (-1.11\rho_{m_r}^{\ 1.858})] \tag{B-11}$$

with $$\xi_m = T_{c_m}^{\ 1/6} / M_m^{\ 1/2}\ P_{c_m}^{\ 2/3} \tag{B-12}$$

and $$\rho_{m_r} = \rho_m\ V_{c_m} \tag{B-13}$$

The mixture properties are all of the form

$$V_{c_m} = \sum_i x_i\ V_{c_i} \tag{B-14}$$

By using Equation B-7, B-8, and B-11, viscosities of the gas mixtures were calculated for all runs made in this investigation.

Diffusion Coefficient

Earlier in this chapter it was mentioned that the assumption of plug flow was made for the analysis of the kinetic data. Appendix C will be devoted to justifying this assumption; presently, a method must be devised to predict diffusion coefficients. The correlation of Hirschfelder, Bird, and Spotz (28) was used to calculate diffusion coefficients in this investigation. Their equation can be represented by

$$D_{12} = \frac{0.001858\ T^{3/2}\ [(M_1 + M_2)/M_1\ M_2]^{1/2}}{P\ \sigma_{12}^{\ 2}\ \Omega\ D} \tag{B-15}$$

where T = temperature, °K

M = molecular weight

P = pressure, atm

$\sigma_{12} = (\sigma_1 + \sigma_2)/2$ collision diameter, $^{\circ}A$

Ω_D = collision integral for diffusion

It is not possible to predict the accuracy of Equation B-15 since experimental data for the nitrous oxide-nitrogen or nitrous oxide-oxygen systems are not available. In making the calculations required in this investigation, the system in all cases was considered to be a nitrous oxide-air mixture. This assumption is certainly no less accurate than other hypothetical formulations, and more logical than some of the other formulations. Table 8 of Appendix C gives the values of density, viscosity, and diffusion coefficient used to examine the effects of diffusion in this tubular reactor.

APPENDIX C

EFFECTS OF LONGITUDINAL AND AXIAL DIFFUSION IN A TUBULAR REACTOR

In most of the equations for tubular reactors that are used to analyze kinetic data, perhaps the most frequently used simplifying assumption is that of plug flow. When well-developed turbulent flow is known to exist in the reactor, this assumption is usually quite valid. In the laminar flow region, however, plug flow can be assumed to be correct only under certain conditions. Failure to meet these conditions would negate any calculations based upon the plug flow assumption. In this appendix, criteria are developed for determining when the use of the plug flow assumption is valid, and a determination is made whether these criteria have been met in the present investigation.

Without diffusion and other effects, the radial velocity distribution in a tube may be given by the Poiseuille equation, which is

$$V(r) = 2 \langle v \rangle (1 - r^2/R^2) \qquad \text{(C-1)}$$

From this equation, it can be seen that the center line fluid element (r = 0) will have a shorter residence time than any fluid element at a greater radius, thereby producing a definite distribution of residence times. This distribution becomes further complicated if radial diffusion is present. Cleland and Wilhelm (7) solved the basic partial differential equation describing the concentration field in a tube containing a fluid in laminar flow and reacting by first-order kinetics. In dimensionless form, the equation which they solved was

$$-(1 - \nu^2) \frac{\partial c}{\partial \lambda} + \alpha \frac{\partial^2 c}{\partial \nu^2} + \frac{1}{\nu} \frac{\partial c}{\partial \nu} - c = 0 \qquad \text{(C-2)}$$

with boundary conditions

$$c = 1 \text{ at } \lambda = 0 \qquad \frac{\partial c}{\partial \nu} = 0 \text{ at } \nu = 0.1$$

The dimensionless variables in the equation are

$\lambda = k_c Z/2\langle v \rangle$

$c = c/c_o$

$\alpha = D/k_c R^2$

$\nu = r/R$

Equation C-2 was developed under the assumptions of isothermal operation, fully-developed laminar flow, axial diffusion small in comparison to radial diffusion, and constant diffusivity. The solution of Equation C-2 made by Cleland and Wilhelm was limited to vllues of α and λ for which $\alpha\lambda = 1$. Johnson (31) subsequently solved the equation over larger ranges of α and λ. His results indicated that the ratio α/λ could be used as the criteria for determining the validity of the plug flow assumption. For values of α/λ greater than 10, the error in assuming plug flow will be less than 0.4 percent; for values greater than 100, the error will be less than 0.05 percent. Since the values of α/λ for this investigation were larger than 100,000, the assumption of plug flow made in analyzing the results appears to be quite valid.

Danckwerts (9) analyzed the effect of longitudinal diffusion on conversion in a tubular reactor in the absence of velocity gradients. He found that while longitudinal diffusion tends to lower the conversion below that to be expected for plug flow, this effect is negligible provided that the following expression holds

$$k_c^2 L D_{12}/\langle v\rangle^3 << 1 \qquad \text{(C-3)}$$

Calculations based upon Equation C-3 have indicated that all runs in this investigation fulfilled this criterion.

Values of the quantities α/λ and $k_c^2 L D_{12}/\langle v\rangle^3$ were computed for each run using the values of ρ, μ, and D_{12} calculated from the various correlations developed in Appendix B. These values are tabulated in Table 8. All runs in this investigation:

1. Existed in the laminar flow region.
2. Proved valid the plug flow assumption.
3. Indicated that longitudinal diffusion had a negligible effect on conversion.

TABLE 8

RESULTS OF PHYSICAL PROPERTY CALCULATIONS

Run Number	Density gm-mole/L	Viscosity micropoise	Diffusion Coefficient sq cm/sec	<v> cm/sec	Reynolds Number	α/λ	$k_c^2 D_{12}/L\langle v\rangle^3$ $\times 10^{12}$
1-50	0.048570	361.2	0.28506	7.78	18	a	--
1-100	0.09685	362.5	0.14295	9.43	43	a	--
1-225	0.21735	364.8	0.06372	12.77	128	a	--
1-400	0.38673	368.1	0.03583	9.42	162	a	--
1-545	0.52639	370.9	0.02629	18.86	429	a	--
2-50	0.04857	364.2	0.28506	5.52	12	a	--
2-225	0.21737	368.1	0.06368	7.65	73	a	--
2-400	0.38636	372.9	0.03582	13.15	209	a	--
2-545	0.52621	372.8	0.02629	14.24	313	a	--
2-575	0.55525	372.5	0.02491	14.81	347	a	--
3-50	0.05112	347.8	0.26134	5.22	14	28,941,100	1937.3
3-225	0.22825	350.5	0.05855	4.78	54	4,657,800	286.3
3-400	0.40585	351.2	0.03293	13.45	270	6,777,850	19.8
3-545	0.55273	351.8	0.02417	15.00	411	5,399,150	10.7
3-575	0.58338	351.5	0.02291	19.00	554	6,405,250	5.5
4-50	0.05241	340.7	0.25028	4.21	12	77,853,400	447.8
4-225	0.23376	342.4	0.05604	4.78	57	16,855,550	38.9
4-400	0.41633	343.6	0.03154	9.94	212	18,675,400	4.7
4-490	0.51012	344.0	0.02574	11.85	311	17,953,450	2.8
4-575	0.59853	344.5	0.02194	15.23	469	19,550,800	1.3
5-50	0.05392	333.6	0.23878	4.06	12	236,358,200	833.0
5-225	0.24035	335.2	0.05362	5.56	70	67,347,200	36.4
5-400	0.42722	336.2	0.03018	10.50	237	69,940,100	5.6
5-490	0.52347	336.9	0.02463	12.28	339	66,141,000	3.5
5-575	0.61427	337.6	0.02099	15.16	490	69,107,900	1.9
6-30	0.03117	333.4	0.41276	2.71	5	278,780,550	2710.3
6-140	0.14953	334.3	0.08619	3.94	31	78,353,200	99.0
6-315	0.33637	335.3	0.03833	9.47	169	81,697,000	7.5

TABLE 8--Continued

Run Number	Density gm-mole/L	Viscosity micropoise	Diffusion Coefficient sq cm/sec	$\langle v\rangle$ cm/sec	Reynolds Number	α/λ	$k_c^2D_{12}/L\langle v\rangle^3$ x 10^{12}
6-625	0.66794	337.9	0.01931	21.15	743	88,697,000	0.7
6-685	0.73200	338.5	0.01762	20.40	785	78,064,300	0.8
7-30	0.03070	340.0	0.42710	2.62	4	87,388,500	1607.0
7-140	0.14570	341.2	0.09008	4.24	32	25,265,450	399.6
7-315	0.32767	342.2	0.04006	8.94	151	22,124,000	20.3
7-625	0.65068	344.7	0.02018	18.10	605	21,244,700	1.3
7-685	0.71297	345.0	0.01842	20.70	759	22,177,400	0.8
8-30	0.02965	346.7	0.45045	2.62	4	27,544,300	24013.0
8-140	0.14212	348.0	0.09406	4.28	30	7,386,750	1462.5
8-315	0.31957	349.3	0.04183	8.29	134	5,592,300	101.9
8-625	0.63432	351.7	0.02108	19.93	631	6,145,350	4.1
8-685	0.69512	352.1	0.01923	19.23	668	5,487,200	4.1
9-50	0.04975	355.4	0.28345	3.84	9	7,163,500	15835.5
9-225	0.22280	357.0	0.06108	6.19	67	1,763,600	1234.4
9-400	0.39601	358.3	0.03436	10.80	205	1,568,800	144.2
9-490	0.48501	359.4	0.02805	12.97	299	1,435,200	72.9
9-575	0.56913	359.3	0.02390	15.86	433	1,481,550	34.3
10-30	0.02908	354.0	0.46760	2.42	4	8,754,900	95424.7
10-140	0.13870	356.4	0.09813	4.23	28	2,124,700	5664.8
10-315	0.31185	357.1	0.04364	9.48	143	1,788,800	264.9
10-625	0.61854	359.6	0.02199	17.81	530	1,484,700	23.0
10-685	0.67764	360.3	0.02006	17.40	562	1,323,250	22.5
11-30	0.02855	360.0	0.48502	3.86	5	4,712,200	74964.9
11-140	0.13514	365.1	0.10240	3.97	24	586,370	25379.0
11-315	0.30400	366.1	0.04549	9.86	137	518,685	917.9
11-625	0.60352	369.0	0.02293	17.95	486	411,630	88.8
11-685	0.66118	369.5	0.02092	18.98	562	390,990	69.4
12-95	0.10146	333.7	0.12695	5.53	30	165,878,300	71.1
12-185	0.19757	334.3	0.06524	6.01	63	89,618,450	29.4
12-270	0.28831	334.9	0.04469	8.67	133	86,916,400	6.8

TABLE 8--Continued

Run Number	Density gm-mole/L	Viscosity micropoise	Diffusion Coefficient sq cm/sec	$\langle v\rangle$ cm/sec	Reynolds Number	α/λ	$k_c^2 D_{12}/L\langle v\rangle^3$ x 10^{12}
12-360	0.38419	335.5	0.03353	11.57	236	85,819,600	2.2
12-445	0.47512	336.3	0.02712	13.78	346	82,100,850	1.0
12-535	0.57113	337.0	0.02256	16.42	496	80,820,350	0.5
12-655	0.69966	338.1	0.01842	19.98	737	79,928,000	0.2
13-95	0.09906	340.6	0.13248	5.00	26	45,530,650	345.0
13-185	0.19263	341.4	0.06813	6.00	60	26,369,200	109.4
13-270	0.28117	341.9	0.04668	8.65	126	25,096,800	25.9
13-360	0.37493	342.6	0.03502	11.98	233	25,447,900	7.5
13-445	0.46331	343.3	0.02834	13.75	329	23,212,500	4.1
13-535	0.55697	343.9	0.02358	16.10	463	22,345,400	2.1
14-95	0.09417	354.3	0.14455	6.40	30	5,397 850	2114.0
14-185	0.18322	356.0	0.07428	6.15	55	2,242,500	1454.9
14-270	0.26748	356.4	0.05088	8.99	117	2,063,700	347.1
14-360	0.35649	357.1	0.03817	12.50	217	2,049,700	101.7
14-445	0.44054	357.7	0.03088	14.83	317	1,875,500	51.7
14-535	0.52950	358.4	0.02569	17.74	454	1,809 000	25.9
15-95	0.09679	347.1	0.13812	6.24	31	16,749,900	654.3
15-185	0.18823	348.1	0.07120	6.51	62	8,069,250	331.5
15-270	0.27478	348.7	0.04877	9.25	129	7,413,500	83.9
15-360	0.36825	348.4	0.03659	12.40	229	7,093,600	27.5
15-445	0.45275	350.0	0.02959	15.20	347	6,903,800	12.3
15-535	0.54412	350.8	0.02463	18.45	505	6,767,350	5.9
16-95	0.09207	361.9	0.15045	5.64	25	1,387,350	11473.3
16-185	0.17885	364.6	0.07743	6.11	50	639,840	5615.3
16-270	0.26093	364.8	0.05307	9.20	111	594,060	1253.2
16-360	0.34794	365.9	0.03979	12.08	193	546,650	444.0
16-445	0.43013	366.7	0.03220	15.09	296	526,090	193.5
16-535	0.51686	367.4	0.02678	18.55	438	504,640	92.4
17-50	0.04835	363.9	0.28967	4.74	11	1,656,370	50437.2
17-225	0.21536	368.9	0.06504	7.26	70	328,790	5460.1

TABLE 8--Continued

Run Number	Density gm-mole/L	Viscosity micropoise	Diffusion Coefficient sq cm/sec	<v> cm/sec	Reynolds Number	α/λ	$k_c^2 D_{12}/L\langle v\rangle^3 \times 10^{12}$
17-400	0.38246	371.0	0.03661	13.14	221	271,675	639.3
17-490	0.46710	371.9	0.02989	14.30	293	230,480	424.1
17-575	0.55082	372.8	0.02547	21.35	511	286,630	111.1
18-30	0.02878	364.1	0.48692	3.82	5	b	--
18-140	0.13382	369.1	0.10474	4.48	27	384,290	31824.0
18-315	0.30080	371.0	0.04658	9.64	128	279,090	1871.4
18-625	0.59628	373.7	0.02347	20.50	529	247,975	118.3
18-685	0.65323	374.3	0.02142	22.33	629	241,100	85.3
19-50	0.04774	367.9	0.29520	4.65	11	874,509	103101.3
19-225	0.21248	375.0	0.06633	7.27	66	189,490	9832.5
19-400	0.37755	377.2	0.03731	12.90	203	135,715	1377.7
19-490	0.46223	3 8.4	0.03046	15.31	291	123,217	719.3
19-575	0.54350	379.4	0.02595	18.10	400	121,180	378.9
20-30	0.02859	368.2	0.49295	3.81	5	1,516,710	246896.0
20-140	0.13229	374.2	0.10656	4.58	26	203,515	59523.0
20-315	0.29731	376.1	0.04739	10.10	127	144,350	3412.0
20-625	0.58909	379.3	0.02388	19.38	470	117,530	288.5
20-685	0.64522	380.4	0.02179	21.50	561	116,225	197.6
21-95	0.0901	370.0	0.15647	5.71	24	440,565	38135.4
21-185	0.17474	374.7	0.08066	5.97	45	176,930	23087.7
21-270	0.25488	375.7	0.05528	8.64	93	153,065	5984.0
21-360	0.33985	377.3	0.04145	11.30	159	137,705	2183.9
21-445	0.41990	378.4	0.03354	14.06	242	129,735	980.5
21-535	0.50460	379.2	0.02790	16.08	344	121,890	506.2
22-445°	0.13204	313.6	0.09217	2.69	20	2,422,712,600	10.8
22-465°	0.12846	320.3	0.09662	2.65	19	734,069,750	40.5
22-485°	0.12505	327.2	0.10118	26.3	18	226,982,300	145.9
23-400A	0.38647	367.9	0.03582	9.22	159	363,440	928.6
23-400B	0.38652	366.0	0.03582	13.71	244	540,430	282.4

TABLE 8--Continued

Run Number	Density gm-mole/L	Viscosity micropoise	Diffusion Coefficient sq cm/sec	$\langle v\rangle$ cm/sec	Reynolds Number	α/λ	$k_c^2 D_{12}/L\langle v\rangle^3$ $\times 10^{12}$
23-400C	0.38653	363.9	0.03582	26.78	492	1.055,630	37.9
24-655	0.69669	351.9	0.02002	21.69	757	c	--
24-765	0.77526	352.5	0.01724	28.41	1102	c	--
25-655	0.66472	351.7	0.02011	23.40	778	6,924,450	2.4
25-765	0.77618	352.5	0.01722	28. 0	1118	7,367,850	1.1
25-850	0.86130	353.3	0.01552	31.70	1365	7,326,700	0.7
25-935	0.94888	354.1	0.01409	37.35	1763	7,980,300	0.4
25-1020	1.04095	354.9	0.01284	39.50	2040	7,737,800	0.3
26-655	0.64897	361.5	0.02095	20.09	610	d	--
26A-655	0.64964	358.9	0.02099	21.90	687	1,769,400	11.6
26A-765	0.75667	360.9	0.01797	25.90	935	1,791,500	6.0
26A-850	0.84058	361.0	0.01617	30.90	1248	1,983,350	3.1
26A-935	0.92512	362.0	0.01470	30.90	1363	1,920,300	2.6
26A-1020	1.01592	362.4	0.01338	36.20	1710	2,185,250	1.4
27-655	0.63270	368.5	0.02187	22.40	644	482,400	44.2
27-765	0.73850	370.0	0.01873	24.60	811	460,800	28.2
27-850	0.82045	370.3	0.01685	26.90	990	467,755	18.7
27-935	0.90258	370.8	0.01532	29.80	1208	478,670	12.3
27-1020	0.99090	371.6	0.01395	34.40	1524	519,570	7.1
28-655	0.61727	380.3	0.02278	19.97	497	113,370	256.3
28-765	0.72047	380.8	0.01951	24.65	718	118,390	118.2
28-850	0.78943	380.4	0.01756	25.60	856	112,395	93.7
28-935	0.88023	379.7	0.01597	31.80	1177	131,020	43.0
28-1020	0.96664	380.2	0.01455	35.45	1440	137,380	27.4
29-655	0.62516	373.7	0.02238	20.66	560	235,660	111.3
29-765	0.72914	375.1	0.01918	22.70	710	221,910	72.0
29-850	0.80966	374.2	0.01727	28.90	1024	263,080	30.4
29-935	0.89181	374.7	0.01569	32.45	1271	284,200	18.4
29-1020	0.97813	375.7	0.01430	34.75	1480	294,240	12.9

APPENDIX D

COMPUTER PROGRAM FOR EXPERIMENTAL DATA ANALYSIS

SUMMARY OF RUN DATA SHEET

20-315		Run Number
28.57	28.57	Barometric Pressure, in. Hg
25		Room Temperature, °C
977	8	Bayley Control Setting, Coarse and Fine
7.0		Barton Air Flow Indicator
10.2		Propane Rotameter
63.6678		Mueller Bridge Reading, Ohms
0.0146		Mueller Bridge Correction, Ohms
25		Mueller Bridge Temperature, °C
301		Reactor Pressure, PSIG
0	0	Flow Meter ΔP, in. Hg
35	31.5	Flow Time, sec.
100	100	Flow Range, ml.
6.5		Flow Rotameter or Metering Valve
2		Flow Meter Code, 1 = WTM 2 = SBM
12	3	Sample Number
-.15	-.15	Mercury Barometer Correction, in. Hg
Preheater	Reactor	

Figure 46. Sample Data Sheet.

```
C PROGRAM TO ANALYZE DATA FROM THE THERMAL DECOMPOSITION OF NITROUS
C OXIDE
C
C   NOMENCLATURE
C   ************
C
C         PBAR= BAROMETRIC PRESSURE, INCHES HG
C         TRM = ROOM TEMPERATURE, DEG C
C         CRSE = TEMP. CONTROLLER COARSE CONTROL SETTING
C         CFINE = TEMP. CONTROLLER FINE CONTROL SETTING
C         FLA = AIR FLOW INDICATOR
C         FLPR = PROPANE ROTAMETER
C         RMB = MUELLER BRIDGE READING, OHMS
C         TMB = MUELLER BRIDGE TEMPERATURE, DEG C
C         BCMB = MUELLER BRIDGE CORRECTION, OHMS
C         NCODE = FLOW METER CODE, 1=SBM  2=WTM
C         TFM = FLOW METER TEMPERATURE, DEG C
C         DELP = FLOW METER DELTA P, INCHES HG
C         FLT = FLOW TIME, SEC
C         RANG = FLOW METER RANGE
C         FLR = FLOW ROTAMETER READING
C         NSAMP = SAMPLE NUMBER
C         FRACI = INLET CONCENTRATION, MOLE FRACTION
C         FRACO = OUTLET CONCENTRATION, MOLE FRACTION
C         TF = REACTOR TEMPERATURE, DEG F
C         TC = REACTOR TEMPERATURE, DEG C
C         TR = REACTOR TEMPERATURE, DEG R
C         TK= REACTOR TEMPERATURE, DEG K
C         CRMB = CORRECTED MUELLER BRIDGE RESISTANCE, OHMS
C         PR = REACTOR PRESSURE, PSIG
C         CVP = CORRECTION TO MERCURY BAROMETER READING
C         CONV1 = CONVERSION OF N2O TO PRODUCTS IN PREHEATER
C         CONV2 = CONVERSION OF N2O TO PRODUCTS IN REACTOR
C         Z = COMPRESSIBILITY FACTOR
C
C
```

```
      DIMENSION X(5), AO(5), BO(5), CO(5), A(5), B(5), C(5), ALPH(5),
     1GAM(5)
   10 FORMAT(F10.3,F10.3)
   11 FORMAT(F10.3)
   15 FORMAT(F10.4)
   20 FORMAT(2I5)
   22 FORMAT(I5)
   25 FORMAT(F10.5)
   35 FORMAT(4F20.10)
  100 FORMAT(1H ,15X,'DATA ANALYSIS FOR RUN    ',F8.5)
  105 FORMAT(1H0)
  110 FORMAT(1H ,'SUMMARY OF RUN VARIABLES')
  115 FORMAT(1H ,'******* ** *** *********')
  120 FORMAT(1H ,'BAROMETRIC PRESSURE        = ',F6.2,' INCHES HG',5X,
     1F6.2,' INCHES HG')
  125 FORMAT(1H ,5X,'ROOM TEMPERATURE            = ',F6.2,' DEG C')
  130 FORMAT(1H ,5X,'BAILEY CONTROL SETTINGS  = ',F7.1,' COARSE',3X,F5.1
     1,' FINE')
  135 FORMAT(1H ,5X,'AIR FLOW INDICATOR         = ',F5.2)
  140 FORMAT(1H ,5X,'PROPANE ROTAMETER          = ',F7.2)
  142 FORMAT(1H ,5X,'FLOW ROTAMETER             = ',F6.2)
  145 FORMAT(1H ,5X,'FLOW METER CODE            = ',I2)
  150 FORMAT(1H ,5X,'FLOW METER TEMPERATURE     = ',F5.1,' DEG C',5X,
     1F5.1,' DEG C')
  155 FORMAT(1H ,5X,'FLOW METER DELTA P         = ',F6.3,' INCHES HG',5X,
     1F5.3,' INCHES HG')
  160 FORMAT(1H ,5X,'SAMPLE NUMBER FOR PREHEAT= ',I2,3X,'FOR  REACTOR  =
     1 ',I2)
  165 FORMAT(1H ,'UNCORRECTED REACTOR CONDITIONS')
  170 FORMAT(1H ,'*********** ******* **********')
  175 FORMAT(1H ,5X,'REACTOR PRESSURE           = ',F6.1,' PSIG')
  180 FORMAT(1H ,5X,'BRIDGE RESISTANCE           = ',F8.4,' OHMS')
  182 FORMAT(1H ,5X,'RESISTANCE CORRECTION       = ',F8.4, ' OHMS')
  185 FORMAT(1H ,5X,'BRIDGE TEMPERATURE         = ',F5.1,' DEG C')
  190 FORMAT(1H ,5X,'INLET CONCENTRATION        = ',F7.4)
  195 FORMAT(1H ,5X,'OUTLET CONCENTRATION       = ',F7.4)
```

```
  196 FORMAT(1H ,5X,'FLOW TIME                         = ',F7.3,' SEC',5X,
     1F7.3,' SEC')
  197 FORMAT(1H ,5X,'FLOW RANGE                        = ',F7.3,' ML',5X,
     1F7.3,' ML')
  200 FORMAT(1H ,'CORRECTED REACTOR CONDITIONS')
  205 FORMAT(1H ,'********* ******* **********')
  210 FORMAT(1H ,5X,'BRIDGE RESISTANCE             = ',F7.4,' OHMS')
  215 FORMAT(1H ,5X,'REACTOR TEMPERATURE MU BR = ',F8.2,' DEG F',3X,F8.2
     1,' DEG C')
  217 FORMAT(1H ,34X,F8.2,' DEG R',3X,F8.2,' DEG K')
  220 FORMAT(1H ,5X,'REACTOR PRESSURE              = ',F6.1,' PSIG',3X,F7.1,
     1' PSIA')
  222 FORMAT(1H ,5X,'COMPRESSIBILITY FACTOR         = ',F7.4)
  223 FORMAT(1H ,5X,'REACTOR PRESSURE              = ',F6.1,' ATM.')
  225 FORMAT(1H ,5X,'INLET CONCENTRATION           = ',F7.4)
  230 FORMAT(1H ,5X,'OUTLET CONCENTRATION          = ',F7.4)
  235 FORMAT(1H ,'SUMMARY OF RATE VARIABLES')
  240 FORMAT(1H ,'******* ** **** *********')
  245 FORMAT(1H ,5X,'TEMPERATURE              = ',F8.2,' DEG F',3X,F8.2,' DEG
     1 C')
  247 FORMAT(1H ,29X,F8.2,' DEG R',3X,F8.2,' DEG K')
  250 FORMAT(1H ,5X,'PRESSURE                 = ',F7.1,' PSIA')
  251 FORMAT(1H ,5X,'CONVERSION OF N2O P+R= ',F8.3,' PERCENT')
  252 FORMAT(1H ,5X,'CONVERSION OF N2O R-P= ',F8.3,' PERCENT')
  255 FORMAT(1H ,5X,'SPACE TIME                = ',F7.2,' MIN')
  260 FORMAT(1H ,5X,'DENSITY AT RC            = ',F7.4,' MOLES/LITER')
  270 FORMAT(1H ,5X,'FLOW RATE AT STP          = ',F9.2,' ML/MIN')
  272 FORMAT(1H ,5X,'FLOW RATE AT STP OUT = ',F9.2,' ML/MIN')
  274 FORMAT(1H ,5X,'FLOW RATE AT STP IN       ',F9.2,' ML/MIN')
  280 FORMAT(1H ,5X,'RATE CONSTANT             = ',E11.4,' PER MIN')
  282 FORMAT(1H ,5X,'RESIDENCE TIME            = ',F7.2,' MIN')
  284 FORMAT(1H ,5X,'TOTAL MOLES IN CCR        = ',F9.6,' MOLES/MIN')
  285 FORMAT(1H ,'************  END OF RUN ANALYSIS')
  900 FORMAT(1H1)
C
C                                READ INPUT DATA
```

```
  2 READ(5,11) RUN
    READ(5,10) P,T
    READ(5,10) PBAR1,PBAR2
    READ(5,11) TRM
    READ(5,10) CRSE, CFNE
    READ(5,11) FLA
    READ(5,11) FLPR
    READ(5,11) FLR
    READ(5,15) RMB
    READ(5,15) BCMB
    READ(5,11) TMB
    READ(5,11) TCALC
    READ(5,11) PR
    READ(5,10) TFM1,TFM2
    READ(5,10) DELP1,DELP2
    READ(5,10) FLT1,FLT2
    READ(5,10) RANG1,RANG2
    READ(5,22) NCODE
    READ(5,11) Z
    READ(5,20) NSAMP, NSAMP1
    READ(5,25) FRACI
    READ(5,25) FRACO
    READ(5,10) PCONV,RCONV
    READ(5,10) CVP
    READ(5,22) NCOMP
    DO 300 I= 1,NCOMP
    READ(5,25) X(I)
    READ(5,35) AO(I), BO(I), CO(I), A(I)
    READ(5,35) B(I), C(I), ALPH(I), GAM(I)
300 CONTINUE
    CRMB = RMB + BCMB
    TF = -338.5656738 + 18.0166168*CRMB + 0.0769561*CRMB*CRMB
    CP= CVP
    PFM2= PBAR2 + DELP2 - CP
    PR1= PR +(PBAR2/29.92)*14.696 -(CP/29.92)*14.696
    PA = PR1/14.696
```

```
C
C                                         CALCULATE MIXTURE CONSTANTS
      AOM= 0.0
      BOM= 0.0
      COM= 0.0
      AM= 0.0
      BM= 0.0
      CM= 0.0
      ALPHM= 0.0
      GAMM= 0.0
      DO 350 J= 1,NCOMP
      AOM = AOM + X(J)*SQRT(AO(J))
      BOM = BOM + X(J)*BO(J)
      COM = COM + X(J)*SQRT(CO(J))
      AM = AM + X(J)**0.333333
      BM = BM + X(J)**0.333333
      CM = CM + X(J)**0.333333
      ALPHM = ALPHM + X(J)*ALPH(J)*0.333333
      GAMM = GAMM + X(J)*SQRT(GAM(J))
  350 CONTINUE
      AOM = AOM*AOM
      BOM =BOM
      COM = COM*COM
      AM = AM*AM*AM
      BM = BM*BM*BM
      CM =CM*CM*CM
      ALPHM = ALPHM*ALPHM*ALPHM
      GAMM = GAMM*GAMM
      R= 0.0820567
C
C                                         GAS DENSITY CALCULATIONS
      TC= (TF-32.00)/1.8
      TK= TC + 273.16
      TR = TF + 459.69
      TV = T + 273.16
      Z1 = BOM*R*TV - AOM - COM/(TV*TV)
```

```
      Z2 = BM*R*TV - AM
      Z3= AM*ALPHM
      D= 0.0
      COR= 0.1
      DIFFE= 10.0
      ZZ= 0.0001
  401 IF(DIFFE - ZZ)412,412,402
  402 DO 406 J=1,200
      D= D + COR
      PCALC=R*TV*D+Z1*D*D+Z2*D*D*D+Z3*D**6+(CM*D*D*D/(TV*TV))*
     1(1.0 + GAMM*D*D)*EXP(-GAMM*D*D)
      DIFE= P - PCALC
      DIFFE= ABS(DIFE)
  403 IF(DIFE) 404,404,406
  404 GO TO 407
  406 CONTINUE
  407 IF(COR - 0.00001) 412,412,409
  409 D= D - COR
      COR= 0.1*COR
      GO TO 401
  412 CONTINUE
      RHO= D
C
      FLTM2 = FLT2/60.0
      FACT1 = PFM2/29.92
      FACT2 = 459.69/TCALC
      FLOO = (RANG2*FACT1*FACT2)/FLTM2
      FLOI1 = FLOO/(1.0 + 0.5*RCONV)
      FLOI = FLOI1*(1.0 + 0.5*RCONV)
      TMIN = FLOI/22414.0
C
C                                 CALCULATE SPACE TIMES
C
      TAU = (P*239.9)/(TMIN*TK*82.0567)
C
C                                 CALCULATE RATE CONSTANTS
```

```
C
      RKC = (1.5/TAU)*ALOG(1.0/(1.0-(RCONV-PCONV)))-(0.5/TAU)*(RCONV-PCO
     1NV)
C
C                               CALCULATE RESIDENCE TIMES
C
      TIME = -(1.0/RKC)*(ALOG(1.0-(RCONV-PCONV)))
      CONV = RCONV*100.0
      CCONV = (RCONV - PCONV)*100.0
C
C                               PRINT RESULTS
      WRITE(6,900)
      WRITE(6,100) RUN
      WRITE(6,105)
      WRITE(6,110)
      WRITE(6,115)
      WRITE(6,105)
      WRITE(6,120) PBAR1,PBAR2
      WRITE(6,125) TRM
      WRITE(6,130) CRSE, CFNE
      WRITE(6,135) FLA
      WRITE(6,140) FLPR
      WRITE(6,142) FLR
      WRITE(6,145) NCODE
      WRITE(6,150) TEM1,TEM2
      WRITE(6,155) DELP1,DELP2
      WRITE(6,160) NSAMP, NSAMP1
      WRITE(6,105)
      WRITE(6,165)
      WRITE(6,170)
      WRITE(6,105)
      WRITE(6,175) PR
      WRITE(6,180) RMB
      WRITE(6,182) BCMB
      WRITE(6,185) TMB
      WRITE(6,190) FRACI
```

```
WRITE(6,195) FRACC
WRITE(6,196) FLT1,FLT2
WRITE(6,197) RANG1,RANG2
WRITE(6,105)
WRITE(6,200)
WRITE(6,205)
WRITE(6,105)
WRITE(6,210) CRMB
WRITE(6,215) TF, TC
WRITE(6,217) TR, TK
WRITE(6,220) PR, PR1
WRITE(6,222) Z
WRITE(6,105)
WRITE(6,235)
WRITE(6,240)
WRITE(6,105)
WRITE(6,245) TF, TC
WRITE(6,247) TR, TK
WRITE(6,250) PR1
WRITE(6,223) PA
WRITE(6,260) RHO
WRITE(6,251) CONV
WRITE(6,252) CCONV
WRITE(6,272) FLOO
WRITE(6,274) FLOI1
WRITE(6,270) FLOI
WRITE(6,284) TMIN
WRITE(6,255) TAU
WRITE(6,280) RKC
WRITE(6,282) TIME
WRITE(6,105)
WRITE(6,285)
GO TO 2
CALL EXIT
END
```

APPENDIX E

SUMMARY OF EXPERIMENTAL DATA

Comments on Experimental Runs

a - Nitrogen leaked into the reactor from the purge system during the run period.

b - Pressure control was very erratic during run period, resulting in invalid flow rates.

c - Preheater valve was accidentally left open during the run period at this pressure.

d - Pressure control was very erratic, followed by an explosion in the gas inlet system during the second run period.

e - Pressure control was very erratic during run period, followed by failure of the Research control valve.

TABLE 9

SUMMARY OF EXPERIMENTAL RUNS

Run Number	Temperature °C	Pressure		Prod. Flow atd ml/min	τ min	t min	NO_2 Conc.		Conversion percent	k_s min^{-1}	k_h min^{-1}
		psia	atm				in	out			
1-50	585.0	50.2	3.4	119.2	--	--	--	--	a	--	--
1-100	585.0	100.2	6.8	144.5	--	--	--	--	a	--	--
1-225	585.0	224.9	15.3	195.7	--	--	--	--	a	--	--
1-400	585.0	399.9	27.2	144.4	--	--	--	--	a	--	--
1-545	585.0	544.9	37.1	289.0	--	--	--	--	a	--	--
2-50	585.0	50.3	3.4	84.6	--	--	--	--	a	--	--
2-225	585.0	225.0	15.3	117.2	--	--	--	--	a	--	--
2-400	585.0	400.0	27.2	201.5	--	--	--	--	a	--	--
2-545	585.0	545.0	37.1	218.2	--	--	--	--	a	--	--
2-575	585.0	575.0	39.1	226.9	--	--	--	--	a	--	--
3-50	545.0	50.4	3.4	80.0	3.5	3.4	0.9897	0.9785	0.95	0.00235	0.000430
3-225	545.0	225.0	15.3	73.2	17.2	17.0	0.9881	0.9128	5.20	0.00235	0.000800
3-400	545.0	400.0	27.2	206.3	10.8	10.6	0.9900	0.9404	3.43	0.00235	0.000935
3-545	545.0	545.0	37.1	229.8	13.2	13.0	0.9918	0.9303	4.24	0.00235	0.000980
3-575	545.0	575.0	39.1	291.6	11.3	10.8	0.9930	0.9415	3.56	0.00235	0.001000
4-50	525.0	50.4	3.4	64.5	4.4	4.4	0.9989	0.9895	0.65	0.00135	0.000142
4-225	525.0	225.1	15.3	73.3	17.4	17.3	0.9983	0.9618	2.76	0.00135	0.000270
4-400	525.0	400.1	27.2	152.0	14.9	14.8	0.9982	0.9629	2.43	0.00135	0.000315
4-490	525.0	490.1	33.4	182.0	15.2	15.1	0.9985	0.9625	2.50	0.00135	0.000325
4-575	525.0	575.0	39.1	234.1	13.9	13.8	0.9987	0.9657	2.29	0.00135	0.000330
5-50	505.0	50.6	3.4	62.2	4.7	4.7	0.9988	0.9931	0.38	0.00079	0.000030
5-225	505.0	225.1	15.3	85.2	15.2	15.2	0.9986	0.9800	1.29	0.00079	0.000065
5-400	505.0	400.1	27.2	160.8	14.3	14.3	0.9990	0.9813	1.23	0.00079	0.000075
5-490	505.0	490.1	33.4	188.1	15.0	15.0	0.9989	0.9803	1.29	0.00079	0.000079
5-575	505.0	575.1	39.1	232.3	14.3	14.3	0.9991	0.9813	1.24	0.00079	0.000083
6-30	505.0	29.3	2.0	41.5	4.1	4.1	0.9992	0.9945	0.33	0.00079	0.000024
6-140	505.0	140.0	9.5	60.4	13.3	13.3	0.9992	0.9829	1.12	0.00079	0.000056
6-315	505.0	315.0	21.4	145.1	12.5	12.5	0.9991	0.9838	1.07	0.00079	0.000070
6-625	505.0	625.0	42.5	323.7	11.1	11.1	0.9990	0.9854	0.96	0.00079	0.000082
6-685	505.0	685.0	46.6	312.8	12.6	12.6	0.9989	0.9835	1.09	0.00079	0.000082
7-30	525.0	29.6	2.0	40.1	4.1	4.1	0.9993	0.9904	0.60	0.00135	0.000110
7-140	525.0	140.0	9.5	65.1	12.1	12.1	0.9988	0.9715	1.89	0.00135	0.000230
7-315	525.0	315.0	21.4	136.9	13.0	12.9	0.9989	0.9685	2.09	0.00135	0.000285
7-625	525.0	625.0	42.5	276.9	12.7	12.7	0.9991	0.9687	2.11	0.00135	0.000330
7-685	525.0	685.0	46.6	317.3	12.2	12.1	0.9992	0.9699	2.02	0.00135	0.000335
8-30	545.0	29.3	2.0	40.1	4.0	4.0	0.9982	0.9814	1.06	0.00235	0.000320
8-140	545.0	140.1	9.5	65.6	11.8	11.7	0.9980	0.9480	3.46	0.00235	0.000650
8-315	545.0	315.0	21.4	127.1	13.8	13.6	0.9981	0.9363	4.27	0.00235	0.000850
8-625	545.0	625.0	42.5	305.1	11.4	11.3	0.9980	0.9441	3.72	0.00235	0.001020
8-685	545.0	685.0	46.6	294.8	--	--	--	--	b	--	--

TABLE 9--Continued

Run Number	Temperature °C	Pressure psia	Pressure atm	Prod. Flow std ml/min	τ min	t min	NO_2 Conc. in	NO_2 Conc. out	Conversion percent	k_s min^{-1}	k_h min^{-1}
9-50	565.0	50.3	3.4	58.9	4.6	4.6	0.9967	0.9644	2.22	0.00380	0.00112
9-225	565.0	225.0	15.3	95.1	13.0	12.8	0.9961	0.8906	7.35	0.00380	0.00215
9-400	565.0	400.0	27.2	165.5	13.4	13.1	0.9945	0.8820	7.85	0.00380	0.00244
9-490	565.0	490.0	33.3	198.4	13.6	13.4	0.9931	0.8742	8.30	0.00380	0.00267
9-575	565.0	575.0	39.1	243.0	13.1	12.9	0.9960	0.8813	8.00	0.00380	0.00270
10-30	565.0	29.4	2.0	37.1	4.3	4.2	0.9975	0.9691	1.95	0.00380	0.00085
10-140	565.0	140.0	9.5	58.8	13.1	12.9	0.9960	0.8947	7.05	0.00380	0.00188
10-315	565.0	315.0	21.4	145.4	11.9	11.7	0.9959	0.8953	7.00	0.00380	0.00240
10-625	565.0	625.0	42.5	273.5	12.6	12.4	0.9953	0.8827	7.85	0.00380	0.00281
10-685	565.0	685.0	46.6	266.6	14.3	14.0	0.9958	0.8699	8.80	0.00380	0.00280
11-30	585.0	29.6	2.0	59.1	2.6	2.6	0.9960	0.9655	2.10	0.00615	0.00195
11-140	585.0	139.9	9.5	60.8	12.7	12.3	0.9829	0.8100	12.35	0.00615	0.00455
11-315	585.0	314.9	21.4	151.3	11.5	11.1	0.9838	0.8095	12.45	0.00615	0.00580
11-625	585.0	624.9	42.5	275.0	12.6	12.1	0.9844	0.7848	14.40	0.00615	0.00670
11-685	585.0	684.9	46.6	290.8	13.2	12.7	0.9821	0.7734	15.15	0.00615	0.00680
12-95	505.0	95.1	6.5	84.8	6.4	6.5	0.9992	0.9914	0.54	0.00079	0.000047
12-185	505.0	185.1	12.6	92.2	11.6	11.6	0.9990	0.9850	0.98	0.00079	0.000062
12-270	505.0	270.1	18.4	133.1	11.7	11.6	0.9990	0.9850	0.99	0.00079	0.000067
12-360	505.0	360.1	24.5	177.5	11.7	11.6	0.9992	0.9848	1.00	0.00079	0.000074
12-445	505.0	445.1	30.3	211.1	12.1	12.1	0.9993	0.9842	1.05	0.00079	0.000078
12-535	505.0	535.1	36.4	251.7	12.3	12.3	0.9991	0.9840	1.06	0.00079	0.000080
12-655	505.0	655.1	44.6	306.4	12.3	12.3	0.9992	0.9838	1.07	0.00079	0.000083
13-95	525.0	95.2	6.5	76.6	7.0	7.0	0.9992	0.9833	1.07	0.00135	0.000195
13-185	525.0	185.2	12.6	92.0	11.3	11.3	0.9988	0.9729	1.79	0.00135	0.000250
13-270	525.0	270.2	18.4	132.4	11.5	11.4	0.9989	0.9722	1.85	0.00135	0.000280
13-360	525.0	360.2	24.5	183.6	11.1	11.0	0.9990	0.9735	1.80	0.00135	0.000300
13-445	525.0	445.1	30.3	210.8	11.9	11.9	0.9990	0.9701	1.96	0.00135	0.000315
13-535	525.0	535.1	36.4	247.2	12.2	12.1	0.9989	0.9698	2.00	0.00135	0.000325
14-95	565.0	95.1	6.5	98.2	5.2	5.2	0.9968	0.9572	2.72	0.00380	0.00152
14-185	565.0	185.1	12.6	94.4	10.0	10.6	0.9960	0.9103	5.95	0.00380	0.00200
14-270	565.0	270.1	18.4	137.9	10.8	10.6	0.9967	0.9073	6.20	0.00380	0.00225
14-360	565.0	360.0	24.5	191.8	10.3	10.1	0.9965	0.9087	6.10	0.00380	0.00241
14-445	565.0	445.0	30.3	227.2	10.8	10.6	0.9966	0.9030	6.50	0.00380	0.00225
14-535	565.0	535.0	36.4	271.9	10.8	10.7	0.9965	0.9013	6.63	0.00380	0.00265
15-95	545.0	95.4	6.5	95.5	5.5	5.5	0.9986	0.9758	1.58	0.00235	0.000565
15-185	545.0	185.1	12.6	99.9	10.3	10.2	0.9982	0.9535	3.08	0.00235	0.000730
15-270	545.0	270.1	18.4	141.9	10.6	10.4	0.9981	0.9509	3.25	0.00235	0.000810
15-360	545.0	360.1	24.5	190.2	10.5	10.4	0.9982	0.9494	3.32	0.00235	0.000900
15-445	545.0	445.1	30.3	233.1	10.6	10.5	0.9980	0.9492	3.37	0.00235	0.000930
15-535	545.0	535.0	36.4	283.3	10.5	10.3	0.9979	0.9100	5.65	0.00235	0.000980

TABLE 9--Continued

Run Number	Temperature °C	Pressure		Prod. Flow std ml/min	τ min	t min	NO_2		Conversion percent	k_s min^{-1}	k_h min^{-1}
		psia	atm				in	out			
16-95	585.0	95.2	6.5	86.5	5.9	5.8	0.9919	0.9100	5.65	0.00615	0.00390
16-185	585.0	185.0	12.6	93.7	10.8	10.5	0.9879	0.8335	10.95	0.00615	0.00490
16-270	585.0	270.0	18.4	141.2	10.5	10.9	0.9858	0.8288	11.15	0.00615	0.00550
16-360	585.0	360.0	24.5	185.3	10.7	10.3	0.9850	0.8209	11.70	0.00615	0.00590
16-445	585.0	445.0	30.3	231.3	10.6	10.3	0.9830	0.8162	11.90	0.00615	0.00620
16-535	585.0	535.0	36.4	284.9	10.3	10.0	0.9822	0.8141	12.00	0.00615	0.00660
17-50	594.5	50.6	3.4	72.7	3.6	3.6	0.9909	0.9309	4.14	0.00770	0.00400
17-225	594.5	225.1	15.3	111.3	11.2	10.8	0.9850	0.7740	15.30	0.00770	0.00770
17-400	594.5	400.0	27.2	201.5	11.0	10.6	0.9793	0.7539	16.45	0.00770	0.00930
17-490	594.5	490.0	33.3	257.4	10.6	11.3	0.9720	0.7288	17.95	0.00770	0.00980
17-575	594.5	575.0	39.1	277.9	11.5	11.0	0.9722	0.7312	17.75	0.00770	0.0100
18-30	595.0	30.2	2.1	58.6	--	--	--	--	c	--	--
18-140	595.0	140.1	9.5	68.6	11.2	10.9	0.9735	0.7767	14.30	0.00770	0.00650
18-315	595.0	315.0	21.4	147.7	11.9	11.4	0.9757	0.7449	16.93	0.00770	0.00860
18-625	595.0	625.0	42.5	314.1	11.1	10.6	0.9625	0.7281	17.35	0.00770	0.01020
18-685	595.0	685.0	46.6	342.2	11.2	10.7	0.9539	0.7178	17.60	0.00770	0.01040
19-50	605.0	50.6	3.4	71.3	3.7	3.6	0.9889	0.9067	5.70	0.00970	0.0064
19-225	605.0	225.0	15.3	111.4	11.3	10.7	0.9599	0.6861	20.60	0.00970	0.0118
19-400	605.0	400.0	27.2	197.4	11.5	10.8	0.9518	0.6505	23.05	0.00970	0.0145
19-490	605.0	490.0	33.3	234.6	11.9	11.2	0.9395	0.6255	24.40	0.00970	0.0153
19-575	605.0	575.0	39.1	277.6	11.6	9.3	0.8805	0.6175	20.95	0.00970	0.0156
20-30	605.0	30.0	2.1	58.3	2.7	2.7	0.9885	0.9350	3.72	0.00970	0.0046
20-140	605.0	140.0	99.5	70.1	11.1	10.5	0.9620	0.7085	18.90	0.00970	0.0102
20-315	605.0	315.0	21.4	154.7	11.5	10.8	0.9604	0.6654	22.40	0.00970	0.0137
20-625	605.0	624.9	42.5	298.4	11.9	11.2	0.9439	0.6245	24.80	0.00970	0.0158
20-685	605.0	684.9	46.6	329.5	11.8	11.1	0.9073	0.5945	24.85	0.00970	0.0161
21-95	605.0	95.4	6.5	87.5	5.8	5.7	0.9809	0.8415	9.85	0.00970	0.0086
21-185	605.0	185.0	12.6	91.5	11.3	10.8	0.9619	0.6903	20.40	0.00970	0.0115
21-270	605.0	270.0	18.4	132.6	11.5	10.9	0.9618	0.6733	21.85	0.00970	0.0130
21-360	605.0	360.0	24.5	173.1	11.8	11.1	0.9445	0.6433	23.20	0.00970	0.0140
21-445	605.0	445.0	30.3	215.4	11.7	11.0	0.9185	0.6189	23.55	0.00970	0.0148
21-535	605.0	535.0	36.4	257.2	11.6	11.1	0.9115	0.6030	24.40	0.00970	0.01550
22-445°	445.0	114.0	7.8	41.3	17.2	17.4	1.0000	0.9962	0.23	0.000132	0.0
22-465°	465.0	114.0	7.8	40.6	17.0	16.8	1.0000	0.9965	0.42	0.00025	0.0
22-485°	485.0	114.0	7.8	40.3	16.7	16.7	0.9995	0.9892	0.71	0.00042	0.0
23-400A	585.0	400.1	27.2	141.4	15.9	15.4	0.9764	0.7550	17.15	0.00615	0.00608
23-400B	585.0	400.1	27.2	210.1	10.4	10.2	0.9850	0.8209	11.70	0.00615	0.00610
23-400C	585.0	400.1	27.2	410.3	5.2	5.1	0.9931	0.8053	6.10	0.00615	0.00610
24-655	545.0	658.0	44.8	332.4	--	--	--	--	d	--	--
24-765	545.0	764.0	52.0	435.3	--	--	--	--	d	--	--

TABLE 9--Continued

Run Number	Temperature °C	Pressure		Prod. Flow std ml/min	τ min	t min	NO_2 Conc.		Conversion percent	k_s min^{-1}	k_h min^{-1}
		psia	atm				in	out			
25-655	545.0	655.0	44.6	358.4	10.1	10.0	0.9982	0.9502	3.30	0.00235	0.00100
25-765	545.0	765.0	52.1	440.8	9.6	9.6	0.9980	0.9525	3.14	0.00235	0.00099
25-850	545.0	849.0	57.8	486.3	9.7	9.6	0.9981	0.9528	3.13	0.00235	0.00098
25-935	545.0	935.0	63.6	572.4	9.0	9.0	0.9980	0.9558	2.92	0.00235	0.00096
25-1020	545.0	1026.0	69.8	604.8	9.4	9.3	0.9980	0.9544	3.01	0.00235	0.00093
26-655	565.0	656.0	44.6	307.8	--	--	--	--	e	--	--
26A-655	565.0	654.9	44.6	335.6	10.7	10.6	0.9960	0.8999	6.68	0.00380	0.00274
26A-765	565.0	764.9	52.1	397.2	10.6	10.4	0.9953	0.9005	6.59	0.00380	0.00275
26A-850	565.0	849.9	57.8	474.2	9.8	9.7	0.9961	0.9087	6.05	0.00380	0.00265
26A-935	565.0	934.9	63.6	473.6	10.8	10.7	0.9953	0.9024	6.45	0.00380	0.00245
26A-1020	565.0	1026.9	69.9	538.7	10.5	10.3	0.9955	0.9090	6.03	0.00380	0.00225
27-655	585.0	655.1	44.6	344.1	10.5	10.2	0.9808	0.8082	12.35	0.00615	0.00680
27-765	585.0	765.1	52.1	376.4	11.3	10.8	0.9750	0.7942	13.00	0.00615	0.00670
27-850	585.0	850.1	57.9	411.9	11.4	11.1	0.9772	0.7957	13.05	0.00615	0.00650
27-935	585.0	935.1	63.6	456.6	11.3	11.0	0.9792	0.7999	12.85	0.00615	0.00640
27-1020	585.0	1026.6	69.9	527.2	10.7	10.4	0.9765	0.8080	12.05	0.00615	0.00620
28-655	605.0	655.0	44.6	305.9	12.2	11.4	0.9129	0.5929	25.40	0.00970	0.01600
28-765	605.0	765.0	52.1	378.0	11.5	10.8	0.9002	0.5945	24.35	0.00790	0.01620
28-850	605.0	850.0	57.8	392.5	12.3	11.6	0.9617	0.6273	25.80	0.00970	0.01600
28-935	605.0	934.5	63.6	488.0	10.8	10.0	0.9575	0.6625	22.45	0.00790	0.01560
28-1020	605.0	1026.0	69.8	543.0	10.6	9.9	0.9590	0.6700	21.90	0.00970	0.01520
29-655	595.0	655.5	44.6	316.6	11.6	11.1	0.9707	0.7264	18.05	0.00770	0.0103
29-765	595.0	765.0	52.1	348.7	12.3	11.8	0.9692	0.7115	19.15	0.00770	0.0103
29-850	595.0	849.5	57.8	442.4	10.8	10.3	0.9735	0.7335	16.65	0.00770	0.0100
29-935	595.0	935.0	63.6	497.6	10.4	10.0	0.9750	0.7583	15.80	0.00770	0.0095
29-1020	595.0	1026.0	69.8	532.0	10.7	10.3	0.9736	0.7577	15.75	0.00770	0.0090

APPENDIX F

SAND BATH DIAGRAMS

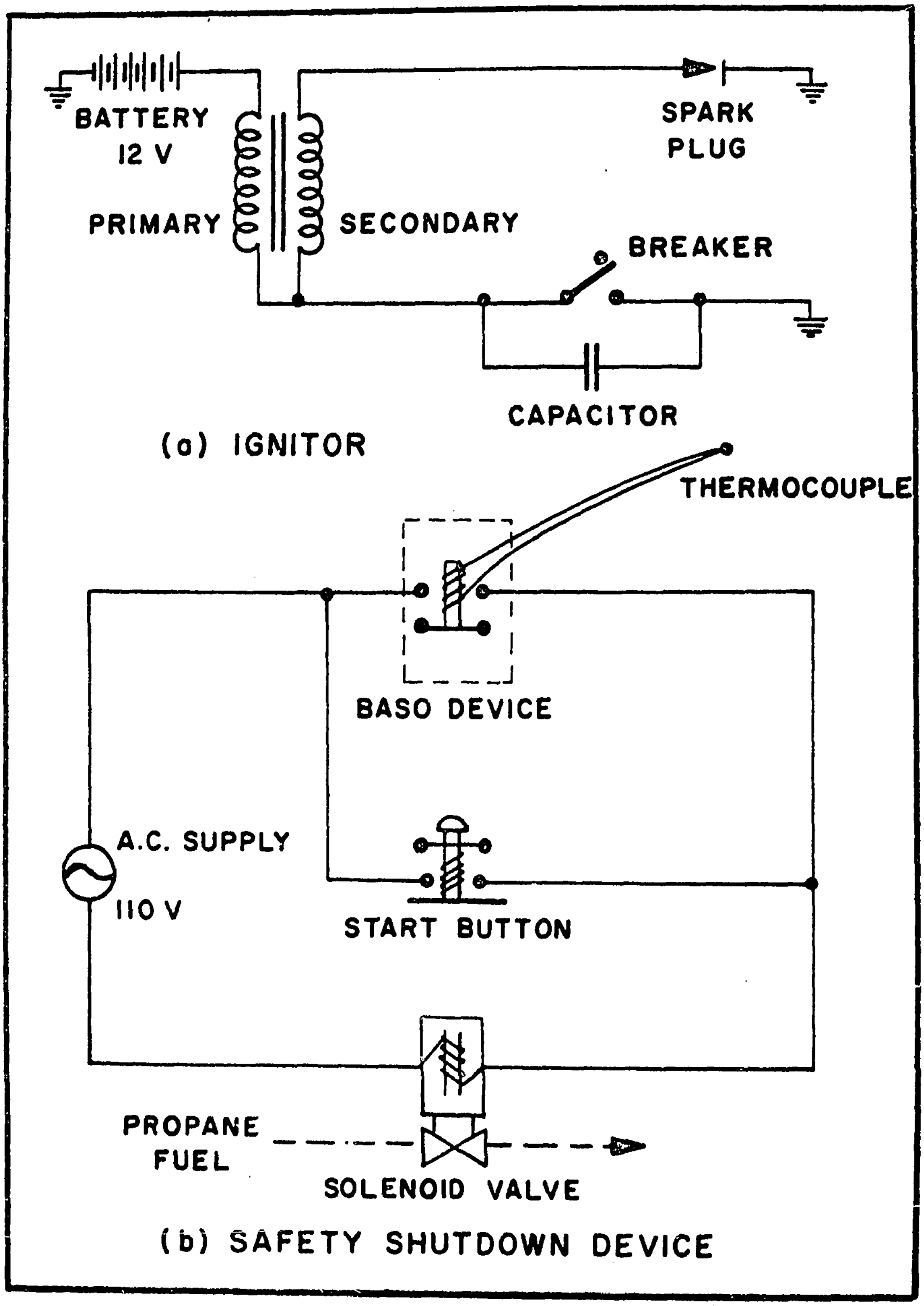

Figure 47. Burner Ignition System Electrical Circuit Diagrams.

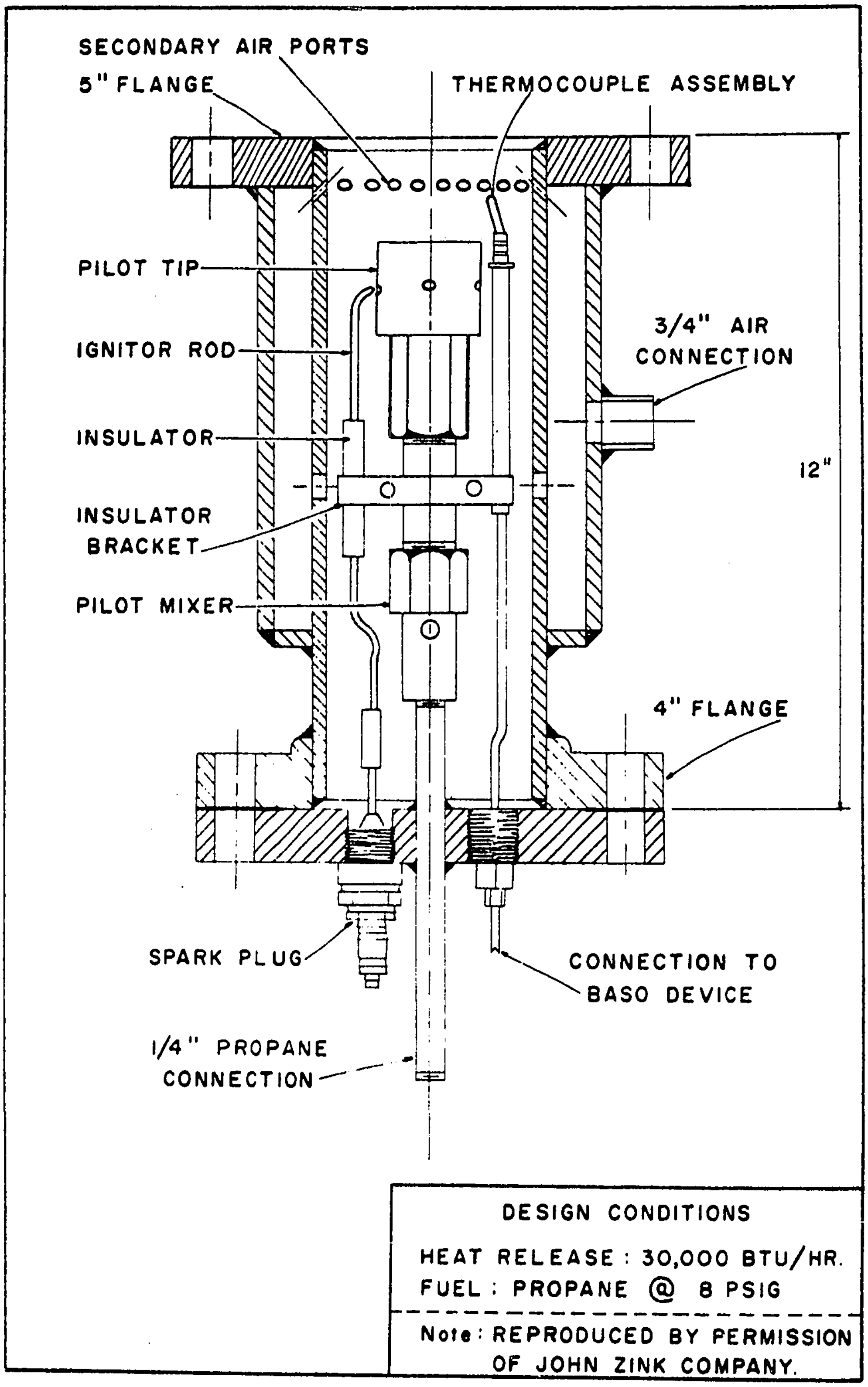

Figure 48. Sectional Elevation of Burner for Sand Bath Heater.

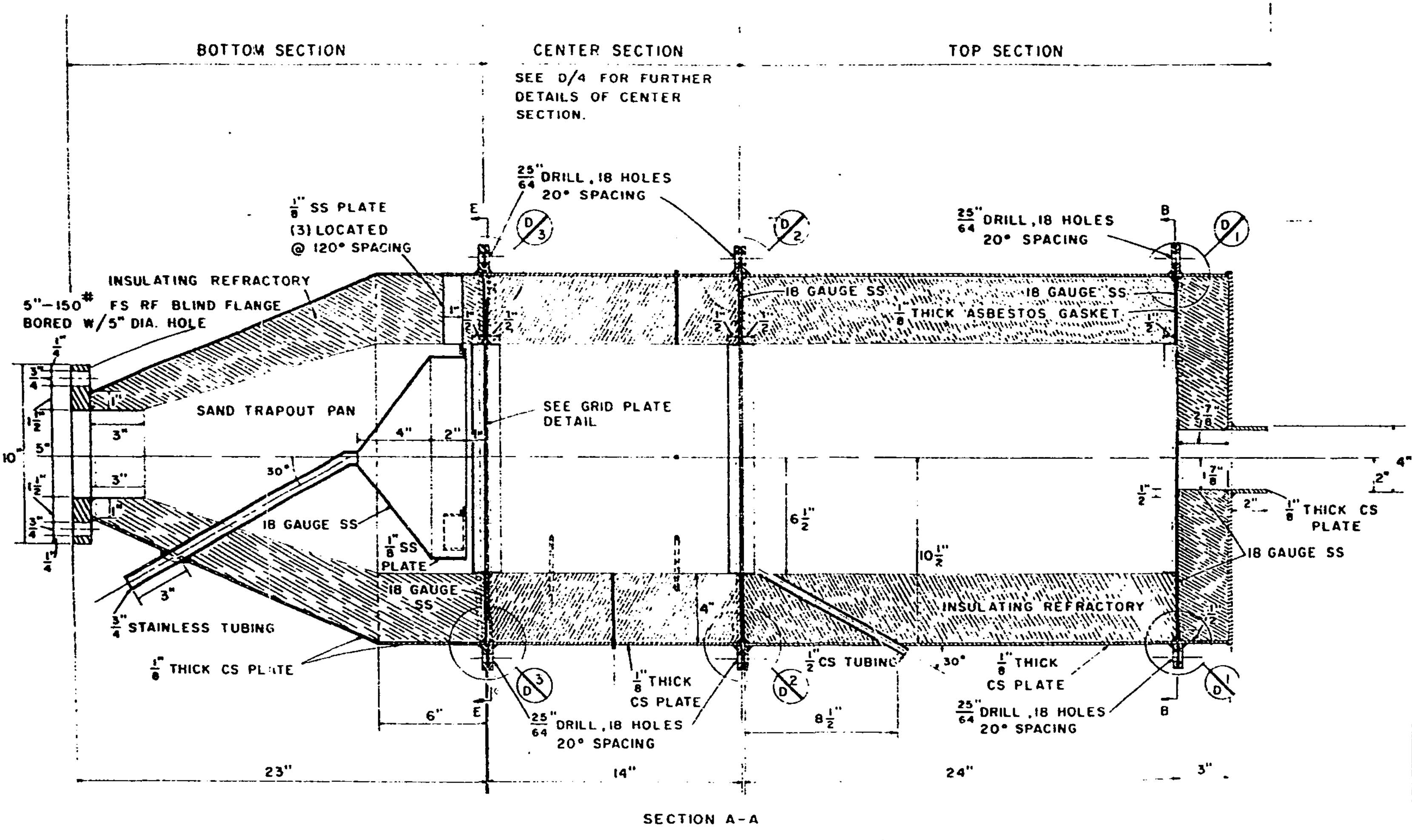

Figure 49.
REACTOR FLUIDIZED SAND HEATER

1 OF 3

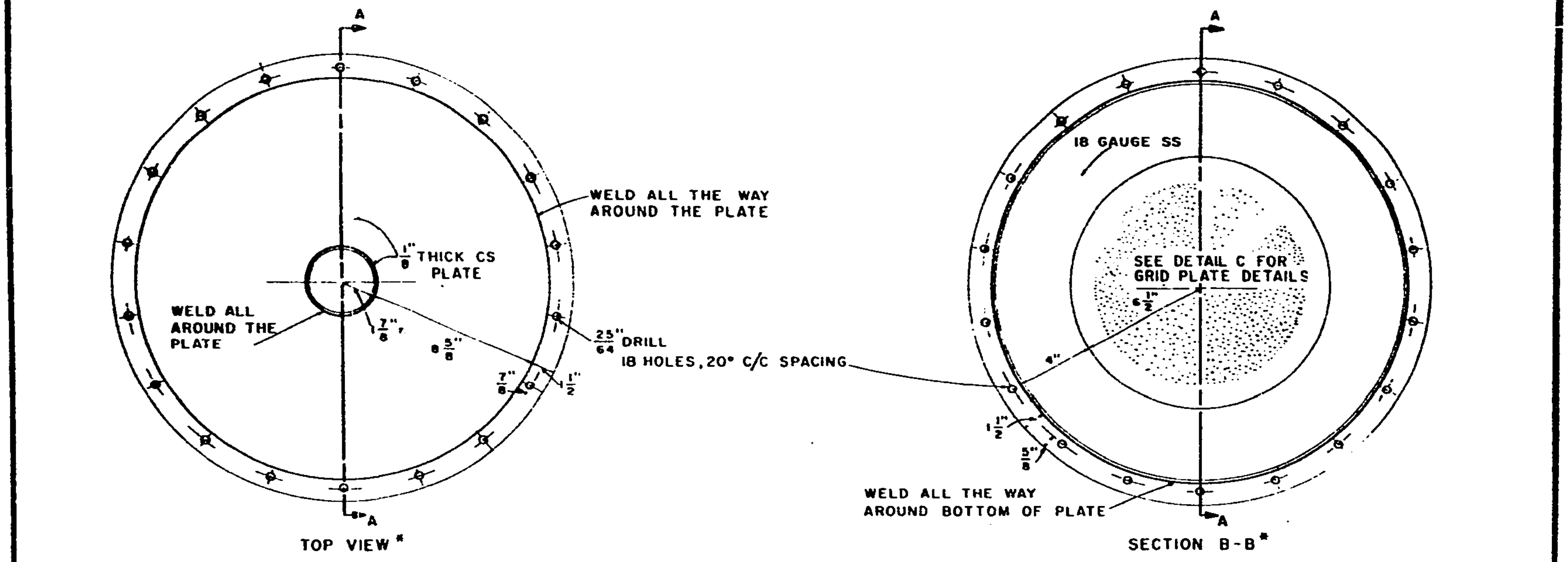

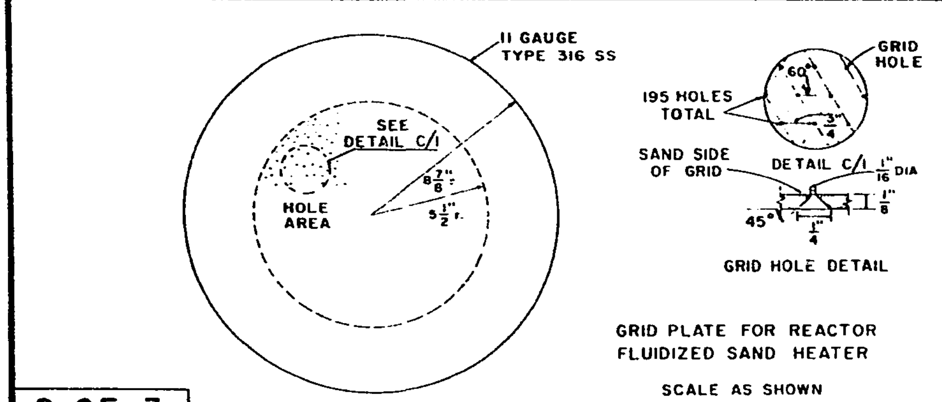

GRID PLATE FOR REACTOR FLUIDIZED SAND HEATER

SCALE AS SHOWN

2 OF 3

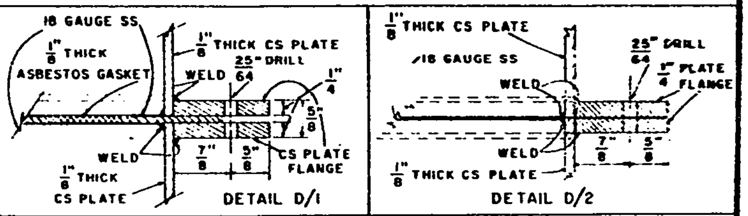

* NOTE

NO HIDDEN LINES ARE SHOWN ON SECTION DRAWINGS, WITH THE EXCEPTION OF SECTION A-A. THIS WAS DONE TO FACILIATE VIEWING OF DETAIL DRAWINGS.

SCALE 0 1 2 3 4 5 6

Figure 50.
REACTOR FLUIDIZED SAND HEATER

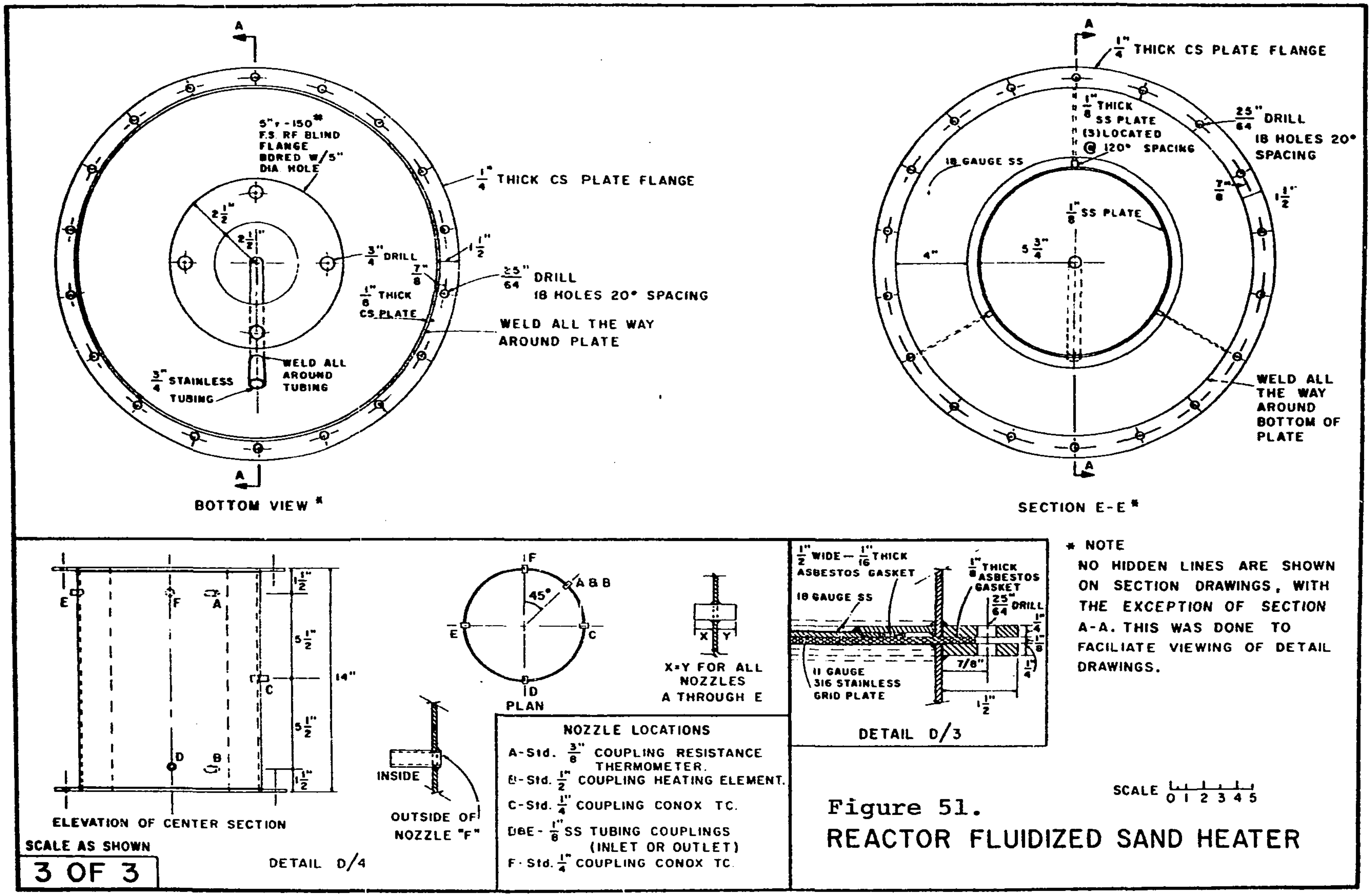

NOZZLE LOCATIONS

A-Std. 3/8" COUPLING RESISTANCE THERMOMETER.
B-Std. 1/2" COUPLING HEATING ELEMENT.
C-Std. 1/4" COUPLING CONOX TC.
DBE- 1/8" SS TUBING COUPLINGS (INLET OR OUTLET)
F-Std. 1/4" COUPLING CONOX TC.

* NOTE

NO HIDDEN LINES ARE SHOWN ON SECTION DRAWINGS, WITH THE EXCEPTION OF SECTION A-A. THIS WAS DONE TO FACILIATE VIEWING OF DETAIL DRAWINGS.

Figure 51.
REACTOR FLUIDIZED SAND HEATER